**Application of Hydrogel-based Materials for Vascular Targeted Drug Delivery**

by

Jonathan Lee

A dissertation submitted in partial fulfillment
of the requirements for the degree of
Doctor of Philosophy
(Chemical Engineering)
in the University of Michigan
2024

Doctoral Committee:

Professor Omolola Eniola-Adefeso, Chair
Professor Joerg Lahann
Professor Andrew Putnam
Associate Professor Greg Thurber

Jonathan Lee

leejkh@umich.edu

ORCID iD: 0009-0003-5041-8579

## Dedication

To Mom, Dad, Genevieve, Ethan, and Adam, my biggest cheerleaders and supporters I could ever ask for.

**Acknowledgements**

My PhD was a long journey with many, many ups and downs. Without the support of my community, I surely would not have made it to the dissertation finish line.

First, I have to thank my advisor, Professor Omolola Eniola-Adefeso, for welcoming me into her lab nearly 6.5 years ago. Her guidance and expertise led me down so many scientific journeys throughout my time at Michigan, and she held me to higher standards that made me the scientist I am today. Someone at the beginning of my PhD said, "When you don't believe in yourself, believe in the people that do," and when I had doubts, I could always rely on Lola to reassure me. Thank you for always pushing me to be a better researcher and inspiring my science, and for supporting me throughout this PhD.

Thank you to my dissertation committee members, Professors Joerg Lahann, Andrew Putnam, and Greg Thurber. I appreciate time taken out of your very busy schedules to attend my thesis proposal, data meeting, and dissertation defense as well as your feedback and advice during this process.

I would also like to acknowledge the funding generously provided by the National Science Foundation and their NSF-GRFP program. Without their support, I would not have had the flexibility to explore my research projects and the directions I had chosen to take them in.

Next, I want to acknowledge all of the lab members, both past and present, who have helped me throughout my PhD journey. To Dr. Billy Kelly, Dr. Hanieh Safari, and Dr. Mario Gutierrez, thank you for guiding me during the early graduate school years, when I was a new

lab member and had no idea what I was doing. Dr. Korie Grayson, thank you for joining the lab and offering me your expertise and support as a post-doc assuring me there was light at the end of the tunnel. Special thanks go to Dr. Genesis Lopez and Dr. Alison Banka, who graciously offered their advice, support, and sympathy as I pushed through these very tough last months. To the current members of the lab, thank you for putting up with all of my shenanigans over the last 6 long years; there are many moments I think about fondly, but some specific ones come to mind for each one of you. Valentina Guevara, I enjoyed gossiping and spilling tea with you on days when we couldn't be (or didn't want to be) productive. Logan Piegols, thank you for always keeping rod hydrogel production fabrication days interesting and discussing the finer details of D&D. Daniel Kupor, I appreciate you for the occasional long conversations in your office and the late nights we spent in lab together. Seun Akanbi, you complimented me on my eyebrows one time and I'm still riding that high every now and then. Shivanie and Sumukh, you both just joined the lab, but I have thoroughly enjoyed working alongside you for the past couple of months. To my office mate, Rue Felder, thank you for continuing to deal with my antics and shared roasting of each other; I doubt I'll find anyone else to have this kind of rapport with. Finally, thank you to Dr. Emma Brannon, who just recently defended, for being the exit buddy I needed as we pulled each other past the finish line. The time I have spent in the lab would not be the same without you all in it.

Thank you to all of the friends I made during my PhD that gave me support and encouragement throughout my degree. Specifically, I want to thank Brittany Rupp, Anjali Mittal, Zeqi Niu, and Carlos Rodriguez for pulling me out of my lab every now and then to be a social person. I would not have made it through without you all pushing me along.

Thank you to the oSTEM and GoSTEM community for the comradery you gave me throughout my PhD. Doing a PhD as a queer person is difficult, but the triumphs, failures, and laughs shared made it bearable on the hardest days. I couldn't ask to be a part of a better group of LGBTQ+ scientists and engineers who understand the unique struggles we go through in life, and they made me feel like a part of something bigger than myself. oSTEM gave me purpose and drive outside of research, and I'm proud to be a part of this organization.

To my very close friends from undergrad, Abigail Anderson, Tim Anderson, Thomas Janssen, and Gregory Nathan, thank you for always providing the escape I needed from my sometimes very busy and hectic research. It's crazy to me that we've known each other for over 10 years at this point, but I look forward to playing games with you all every chance I get, whether it be League of Legends, Pathfinder, or any other of a variety of games we've played over the years. You have all been a consistent presence anchoring me in life, and I greatly appreciated every chance we had to spend late nights playing silly PC games.

To Adam, the man I've spent the last 8 years complaining to, thank you for being the stable force to my very long and winding PhD journey. Whether it was grabbing food for me on days I was too busy to make time to eat, doing the dishes after I finished cooking dinner, or just laying next to me after a rough day of research, I know that without your love and support, I would not be where I am today. You have been with me through my best and my worst days, and somehow, you've decided that you still want to be my partner. I can't thank you enough for being one of my biggest supporters and the best boyfriend I could ever hope for.

Finally, I want to thank my family – Mom, Dad, Genevieve, and Ethan. You all gave me the love and support to push through my PhD, and even though you didn't always understand

everything that was going on, you were always there for me, throughout the past 28 years of my life.

## Table of Contents

## List of Figures

## List of Abbreviations

| | |
|---|---|
| AEM | 2-Aminoethylmethacrylate hydrochloride |
| ANOVA | Analysis of Variance |
| APC | Allophycocyanin |
| AR | Aspect Ratio |
| $Ca$ | Capillary Number |
| CAD | Coronary Artery Disease |
| CAM | Cellular Adhesion Molecule |
| CEA | 2-Carboxyethylacrylate |
| CVD | Cardiovascular Disease |
| DMEM | Dulbecco's Modified Eagle Media |
| DMF | Dimethylformamide |
| DMSO | Dimethylsulfoxide |
| ECM | Extracellular Matrix |
| EDC | 1-Ethyl-3-(3-dimethylaminopropyl)carbodiimide |
| EDTA | Ethylenediaminetetraacetic |
| ESD | Equivalent Spherical Diameter |
| FACS | Flow Activated Cell Sorting |
| HA | Hyaluronic Acid |
| HAMA | Hyaluronic Acid Methacrylate |

| | |
|---|---|
| HLB | Hydrophilic Lipophilic Balance |
| HUVEC | Human Umbilical Vein Endothelial Cell |
| ICAM | Intercellular Adhesion Molecule |
| IL-1β | Interleukin-1β |
| IRB-MED | Medical School Internal Review Board |
| LAP | Lithium phenyl-2,4,6-trimethylbenzoylphosphinate |
| LDL | Low Density Lipoproteins |
| MES | 2-(N-morpholino)ethanesulfonic acid |
| MMP | Matrix Metalloproteinase |
| MP | Microparticle |
| MW | Molecular Weight |
| NP | Nanoparticle |
| PBS | Phosphate Buffered Saline |
| PE | Phycoerythrin |
| PEG | Polyethylene Glycol |
| PEGDA | Polyethylene Glycol Diacrylate |
| PEGVS | Polyethylene Glycol Vinyl Sulfone |
| PI | Photoinitiator |
| PLGA | Poly(lactic-co-glycolic acid) |
| PS | Polystyrene |
| PVA | Polyvinyl Alcohol |
| RBC | Red Blood Cell |
| RES | Reticuloendothelial System |

| | |
|---|---|
| SDS-PAGE | Sodium Dodecyl Sulfate Polyacrylamide Gel Electrophoresis |
| SEM | Scanning Electron Microscopy |
| TEOA | Triethanolamine |
| UV | Ultraviolet |
| VTC | Vascular Targeted Carrier |
| WBC | White Blood Cell |
| WGA | Wheat Germ Agglutinin |

## Abstract

The design of vascular targeted carriers (VTCs) has continually been optimized in terms of size and shape, and recently, attention has also shifted to carrier elasticity, which has been shown to have significant impact on circulation time and immune cell clearance. Notably, soft materials such as hydrogels have been of interest because of their high water content and biocompatibility. In this thesis, we develop an enzyme-degradable hydrogel material suitable for use as a VTC and characterize its use as a carrier for NPs, followed by an in-depth investigation of interactions between elastic particles and human neutrophils. Finally, we developed a scalable, high-throughput technique to produce rod-shaped hydrogel particles.

We first developed multiple reaction schemes to incorporate enzyme-sensitive peptides (VPM) into a polyethylene-glycol hydrogel (PEG) matrix and selected for a material that degraded completely in the presence of trypsin and MMP-2. Thiol-ene photopolymerization did not allow for reaction specificity of thiol to acrylate groups. Nucleophilic Michael addition instead allowed for greatly increased peptide incorporation (up to 95%), generating high-MW PEG-VPM macromers, yielding a hydrogel material capable of degrading completely in the presence of trypsin in the span of two hours. We pivoted to a multifunctional PEGVS molecule to increase crosslinking density, successfully developing an enzyme-degradable hydrogel material with physical properties suitable for vascular drug delivery.

Using this material, we fabricated hydrogel particles for use as VTCs, and successfully demonstrated that they could degrade enzymatically, be functionalized with targeting ligands, be

loaded with non-degradable PS NPs, and adhere to an inflamed monolayer of endothelial cells. 2 – 4 μm particles were generated using a water-in-oil emulsion and characterized using SEM. These particles were degraded using MMP-2, a more physiologically relevant enzyme compared to trypsin, and were found to degrade completely within 6 hours. Next, to demonstrate their utility as VTCs, we conjugated particles with avidin and biotin-anti-ICAM1 using a thiolated avidin protein to react with residual vinyl sulfone groups. We confirmed successful conjugation by staining with fluorescent tags and analyzing with flow cytometry. Finally, we perfused targeted particles over a layer of activated HUVEC and demonstrated that enzyme-degradable hydrogels had an 8-fold increase in particle adhesion compared to an untargeted particle control.

We found neutrophils effectively phagocytose particles of various moduli, despite macrophages exhibiting a lowered ability to uptake soft particles compared to stiff particles. 2 μm and 500 nm PEG particles were taken up at an equivalent or greater rate by primary human neutrophils as compared to PS. We similarly saw equivalent uptake of HA-based particles (50 – 700 kPa) by human neutrophils. These trends were visually confirmed using optical tweezer assays. Surface conjugation of the particle resulted in notable reduced uptake, likely due to increased albumin adsorption, based on SDS-PAGE analysis of the protein corona of the particle.

Finally, we successfully developed a novel fabrication technique for the shearing of polymer droplets and *in situ* crosslinking of deformed droplets to generate rod-shaped hydrogel particles. The displacement-flow driven shear system allowed us to fabricate elongated hydrogel particles with an average ESD of 5 μm and an AR between 1 – 3.5 from a shear rate of 0 – 1400 $^{s-}$1. Overall, in this dissertation, we seek to demonstrate the utility of hydrogels specifically within the context of vascular targeted drug delivery and showcase the potential of soft materials for tissue engineering.

# Chapter 1 : Introduction

## 1.1 Background and significance

Cardiovascular disease (CVD) remains the leading cause of mortality in the US, accounting for approximately 30% of all deaths, surpassing cancer and chronic lower respiratory disease combined, the second and third leading causes of mortality, respectively, in non-COVID years[1,2]. The most prevalent form of CVD is coronary artery disease (CAD), which comprises nearly half of all deaths caused by CVD[2]. Nearly half of all Americans are projected to have some form of CVD by 2035, with a total health care cost of $1.1 trillion globally; in fact, CAD alone is projected to cost $400 billion[1]. Thus, CVD, and especially CAD, remains a significant health concern with an unmet clinical need for improved treatment.

CAD is characterized by a buildup of atherosclerotic plaques in arteries that constrict blood flow to crucial parts of the body. Atherosclerosis in early stages is largely dictated by the inflammatory cascade, which recruits leukocytes to the area and causes the release of pro-inflammatory cytokines, followed by subsequent accumulation of lipids, macrophages, foam cells, smooth muscle cells, and several other components that contribute to plaque formation[3,4]. Further development of these plaques over time leads to thinning of the fibrous cap, the layer of smooth muscles cells beneath the plaque endothelium, eventually leading to plaque rupture, the main cause of sudden and severe health complications, including heart attacks and strokes. Plaque formation and development are typically asymptomatic until rupture, and the variability of atherosclerosis makes detection and treatment difficult until such complications arise. Typically, treatments for CAD include invasive surgeries and the administration of lipid-

lowering statins, which tend to be reactive rather than preventative treatment, and tend to be impermanent solutions, unable to prevent restenosis or the development of plaques elsewhere in the body. Specifically, vein grafts for bypass and the use of stents are common to help treat CAD and plaque formation. However, while vein grafts are successful in bypassing the affected vessel and preventing plaque rupture by alleviating the blood flow to the plaque, they are prone to failure due to the mismatches in size and blood flow rate between artery and vein[5]. Stents work to prevent blood vessel constriction by expanding the vessel in which it is placed, but can come with risks of calcification and in-stent restenosis, leading to stent failure[6]. While statins indeed help to lower levels of low-density lipoproteins (LDLs) in the blood, aggressive use of statins have been shown to have diminishing returns on lowering LDLs and are associated with adverse side effects such as hepatotoxicity and myalgia[7]. These treatments, while useful as temporary solutions, lack the ability to halt and reverse the accumulation and development of plaques in diseased blood vessels. Thus, there is an unmet clinical need for accurate, early detection of CAD and noninvasive treatment.

### 1.2 Vascular Targeted Carriers

The use of vascular targeted carriers (VTCs) has gained increasing interest as a possible route for site-specific drug delivery, presenting a significantly less invasive method of treatment for CAD and atherosclerosis[8,9]. VTCs are drug-loaded carriers designed to accumulate at regions of diseased vascular tissue and locally release their payload to the vascular endothelium,

typically fabricated with a wide range of materials, including lipids, polymeric materials, and proteins[10–12]. A schematic of general VTC design is outlined in Figure 1.1.

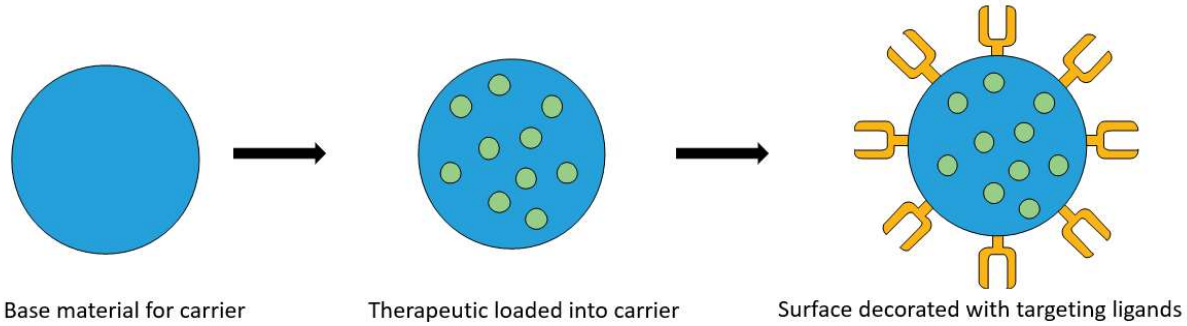


Figure 1.1: General VTC design, where a carrier is loaded with therapeutics and surface conjugated with targeting ligands to target areas of inflamed and diseased tissue.

### *1.2.1 Lipid- and Protein-based Particles*

Lipid-based carriers, such as liposomes and micelles, are the most common and well-researched type of drug carrier, seeing use in the clinic to delivery therapeutics such as doxorubicin[13,14]. The amphiphilic nature of lipid-based carriers provides great utility, as they can be used to carry both hydrophobic and hydrophilic therapeutics, and are commonly used on the nanoscale for delivery of cancer treatments[10,15]. Similarly, protein-based VTCs are composed of proteins found in the body, such as mucin, albumin, and collagen[11,16–18]. Because of their naturally derived origins, these particles and their associated degradation products pose little risk of toxicity, given their high biocompatibility. These types of particles have already been demonstrated to have utility in delivery therapeutics and imaging agents[19,20]. However, one significant drawback to both lipid-based and protein-based carriers is the lack of tunability and control over physical properties such as surface charge, density, and Young's modulus that polymer-based VTCs possess.

### *1.2.2 Polymer-Based Particles*

Polymeric particles can be based on naturally derived polymers, such as chitosan, hyaluronan, and alginate, or synthetic polymers such as poly-(lactic-co-glycolic acid) (PLGA), polycapralactone, and polystyrene (PS)[21–27]. With a wide variety of materials, polymeric particles, especially those made from synthetic polymers, provide more design flexibility than the types of carriers mentioned previously, allowing for selection of an appropriate material for a specific application. Indeed, there are many design parameters that need to be considered for a VTC to be successful.

### 1.3 VTC Design

For a VTC to be successful, it must be able to first navigate the entirety of the vasculature after intravenous injection, then localize and bind to the targeted area of interest, typically an area of diseased or inflamed vascular tissue. Site-specific adhesion in the case of vascular delivery is typically achieved via active targeting with the use of ligands to bind to inflammation markers on the endothelium, such as selectins and cellular adhesion markers (CAMs)[28–30].

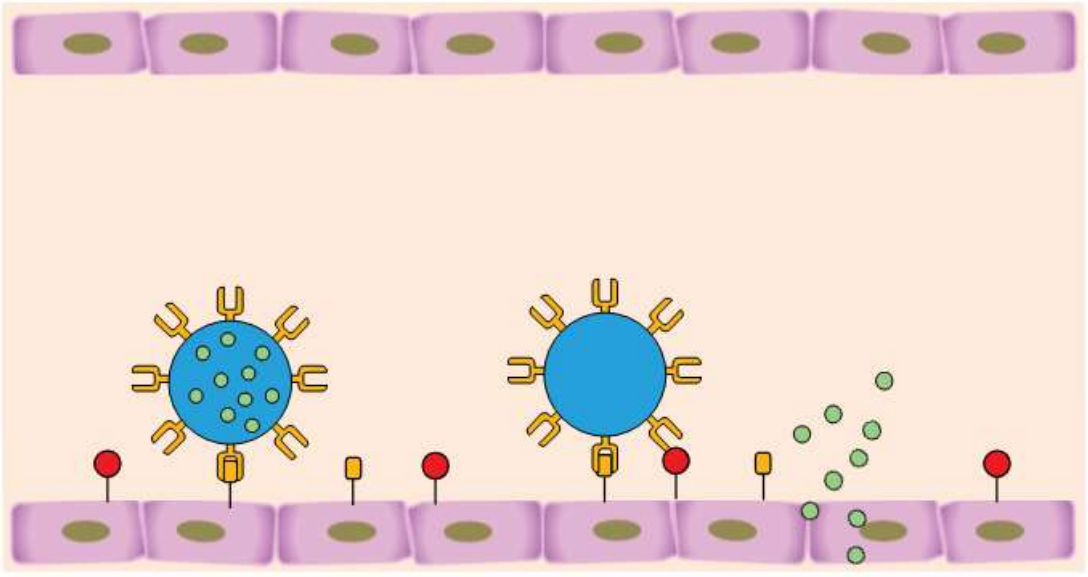

Figure 1.2: Visual depiction of success transport of a therapeutic loaded into a VTC, shown from left to right. First, the VTC needs to navigate the bloodstream and marginate to the endothelium to bind to inflammation markers present on the cells. Next, the therapeutic needs to be released from the interior of the carrier and enter the tissue space for there to be any therapeutic benefit.

Following adhesion to the endothelium, VTCs also need to under intracellular delivery and enter the tissue space for their loaded cargo to have any therapeutic benefit. Thus, when designing VTCs, they must be designed such that all of these transport obstacles are addressed. Figure 1.2 visually outlines the successful transport of the therapeutic encapsulated within a VTC from blood flow into the tissue space.

### *1.3.1 Particle Size*

Size is a significant parameter that greatly affects the performance of a VTC. Nano-sized carriers have long been of particular interest for the various advantages they provide over larger, micron-sizes particles. For example, previous studies have demonstrated that nanoparticles (NPs) have a longer circulation time than microparticles (MPs), providing more opportunities to find and adhere to their target location[31]. Due to their smaller size, they also more effectively avoid clearance via macrophages and are capable of easily navigating the vasculature, being much smaller than the smallest capillaries in the body[32,33]. One of the most important reasons for the prevalence of NPs in particle formulation is their ease of internalization by multiple types of cells; multiple studies have shown that the upper size limit on cell internalization tends to be on the order of 100 nm by endothelial and epithelial cells[34–36]. Because of the numerous advantages that NPs possess, they have been widely regarded as a useful approach to localized drug delivery.

However, aside from entry into the tissue space, VTCs must also reach and adhere to the vascular endothelium to begin the internalization process. From this perspective, research has instead shown that nano-sized particles are largely unable to navigate the complexity of blood flow and reach the endothelium[27,37]. Due to interference from red blood cells (RBCs), NPs tend to localize in the center of blood flow and exhibit minimal adhesion to the cell wall, limiting

their use as VTCs[38]. The optimal size for margination has been found to be on the order of 2 – 5 μm, markedly different than the size needed for intracellular delivery. Particles of this size range, while much more effective at margination than NPs, also exhibit shorter circulation times and are more likely to be cleared by immune cells, preventing them from reaching their target[39]. Notably, a longer circulation time has not been directly shown to translate to increased adhesion, and thus the enhanced margination of MPs may prove more beneficial.

### *1.3.2 Particle Rigidity*

One of the major limitations to the use of MPs is the concern for their high probability to occlude smaller blood vessels, especially capillaries having a diameter as small as 4 μm, when delivered intravenously[40]. Interestingly, however, other components of blood, such as RBCs and white blood cells (WBCs), are approximately 8 and 10 μm respectively and deform as they navigate blood vessels of a smaller diamter[40–42]. This phenomenon suggests the necessity of a deformable aspect for MPs to successfully and safely navigate the vasculature. Indeed, recent studies exploring microbubbles for the delivery of imaging agents as well as liposomal-based carriers for vascular drug delivery indicate the success of soft carriers to traverse all types of blood vessels[10,43]. However, as previously mentioned, a large drawback of these soft carriers is their lack of tunability, and furthermore, they also lack stability on a microscale to withstand larger shear forces present in blood flow, and thus are largely unfeasible for vascular drug delivery[44,45].

Instead, hydrogels, a class of highly water absorbent polymeric materials, may provide more utility in being able to navigate the vasculature while benefiting from enhanced margination effects. Being polymeric in nature, hydrogels possess a high degree of tunability not found in other deformable materials and can absorb up to many times their own weight in water.

Because of this, hydrogels have seen a great amount of use in tissue engineering, possessing mechanical properties close to that of many types of tissue in the body, including blood cells, muscle tissue, and even bone. Furthermore, because of the high water content of hydrogels, they are able to more closely mimic the aqueous environment of these tissues and are considered more biocompatible than other hydrophobic polymeric materials[46]. Thus, hydrogel-based MPs may prove more useful than their rigid counterparts as VTCs, as demonstrated by their maintained ability to bind to an inflamed endothelium *in vitro*[47]. However, the use of a deformable MP still does not address the deficiency of being unable to enter the tissue space as compared to NPs.

### *1.3.3 NP-Loaded MP Design*

Considering the unique advantages that MPs and NPs both offer as a VTC, there is a size mismatch with regards to designing a VTC that can effectively localize and bind to the endothelium and one that can undergo intracellular uptake and enter the tissue space. In order to address this dilemma, studies have begun exploring the potential of using NP-loaded hydrogel MPs to facilitate NP transport to the vascular wall in a dual-delivery approach. Indeed, NP-loaded hydrogels have already been demonstrated to delivery NPs at a greater rate than free NPs in flow, yet did not show NP release from the hydrogel and adhesion to the endothelium[48]. In order to demonstrate that NPs loaded into hydrogel MPs can bind to the endothelium at a higher rate than free NPs, a degradation pathway needs to be built into the hydrogel particle such that it will degrade near sites of inflammation to achieve site-specific release of NPs. While there have been many different hydrogel degradation pathways explored previously, such as hydrolysis, photodegradation, and pH-mediate degradation, these stimuli would likely not result in site-specific degradation; from the perspective of the disease microenvironment, there are few

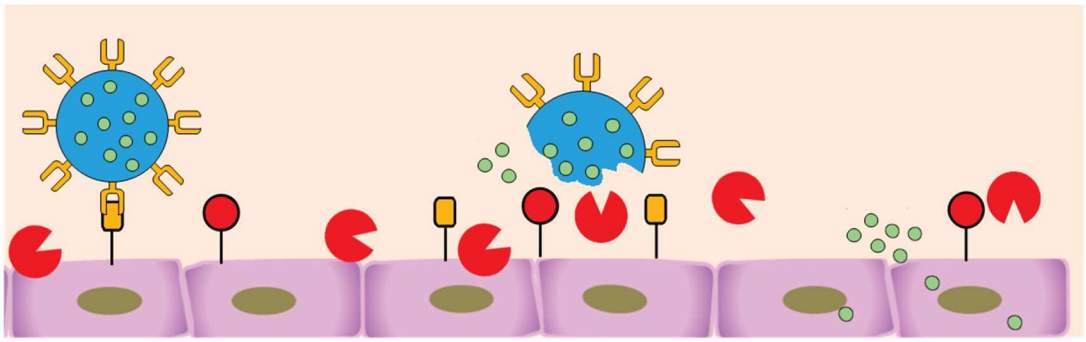

Figure 1.3: A schematic of the NP-loaded MP system, which would leverage the presence of inflammatory enzymes to degrade the hydrogel MP and release NPs. This dual delivery approach would allow for site-specific degradation of the MP and facilitate the transport of NPs to the vascular wall.

meaningful differences between that of diseased and healthy tissue, since temperature and pH are typically tightly regulated within the body[49]. However, one major difference lies in the varying levels of inflammatory enzymes that are upregulated near areas of inflamed and diseased tissue. Specifically, matrix metalloproteinases (MMPs) are of interest because of their well-documented overexpression near regions of atherosclerotic plaques compared to healthy tissue[50–52]. MMPs are zinc-dependent enzymes responsible for cleavage of extracellular matrix (ECM) components and linked to vessel remodeling[50]. Numerous studies have previously explored the use of enzyme-degradable hydrogel systems by crosslinking polyethylene-glycol (PEG) with various peptides sensitive to MMPs and demonstrated their potential for applications such as cell scaffolding, tissue regeneration, and pulmonary delivery[53–56]. While previous work has explored the reaction kinetics of various peptide sequences cleavable by MMPs, selection of an appropriate peptide sequence would likely depend on the timescale of degradation desired, which would likely be within 4 – 6 hours based on the circulation time of deformable particles[53,57,58]. A schematic of the proposed NP-loaded MP design is shown in Figure 1.3. Designing an NP-loaded hydrogel MP instead for vascular targeted drug delivery will need to incorporate different aspects of previous work to address the shortcomings of MPs and NPs alone while addressing

the transport obstacles to overcome, including first margination and binding, followed by intracellular delivery.

### 1.4 Phagocytosis and Circulation Time

A major issue regarding VTC design is their inability to avoid rapid removal from circulation by filtration via RES organs and clearance by phagocytic leukocytes[59–61]. Efforts to design VTCs to avoid phagocytic uptake and achieve extended circulation times have been an active area of biomedical research for several decades. Many solutions have been explored, typically focusing on exploiting non-fouling surface coatings to avoid accumulation of opsonins on the surface, such as PEG, cell-membrane-derived, and zwitterionic coatings[62–64].

In recent years, particle elasticity has emerged as a design parameter for polymeric particles for intravenous drug delivery applications due to favorable effects on phagocytosis. Research has shown that softer particles have a lower propensity to be phagocytosed by macrophages and monocytes[58,65,66]. For example, one study involving PEG-based NPs showed significant differences between soft and hard NPs regarding cellular uptake by J774 macrophages, where stiffer particles were taken up at a greater rate than their softer counterparts[58]. Other work involving polyacrylamide MPs exposed to mouse bone marrow-derived macrophages supported these findings, where softer particles more readily avoided cellular internalization[67]. Furthermore, *in vivo* experiments also point to particle elasticity as an important factor in extending circulation time, where soft nanoparticles were shown to have a longer circulation time, attributed to their ability to avoid filtration by RES organs in addition to avoiding immune cell recognition[58,68,69]. Indeed, many *in vivo* studies confirm that softer particles can more effectively circulate throughout the body for longer, increasing the likelihood of successful delivery to sites of interest[70,71]. However, most of the work evaluating particle

deformability as a viable approach to minimize or avoid particle phagocytosis has focused on *in vitro* assays with macrophages, which reside in tissues, and monocytic cell lines. Furthermore, *in vivo* experiments, primarily in murine models, may not fully represent the phagocytic phenotype of primary cells in a human system.

### 1.5 Neutrophil Interactions with Particle Carriers

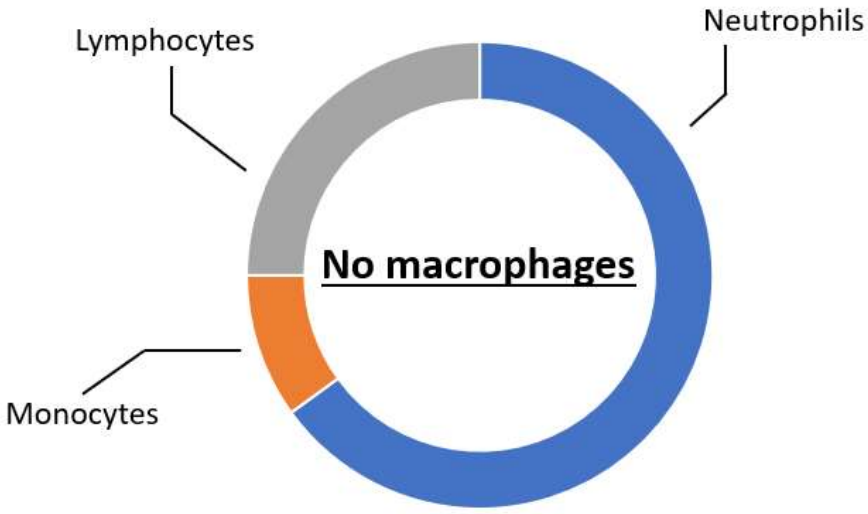


Figure 1.4: Composition of circulating leukocytes in human blood. Neutrophils compose 50 – 70% of all circulating white blood cells, lymphocytes about 25 – 33%, and monocytes < 10%. Notably, macrophages are tissue-resident macrophages and are typically not present in circulation.

Neutrophils are highly efficient phagocytes that comprise 50 – 70% of all immune cells circulating in human blood, with monocytes and lymphocytes at 25 – 33% and <10%, respectively[72] (shown in Figure 1.4). VTCs are delivered intravenously due to the desired function of delivering drugs to the vascular wall; thus, neutrophils are likely the primary phagocyte with which VTCs will interact. However, little is known about how neutrophils engage with soft particles and whether the trends relating elasticity to phagocytosis will hold in human blood flow, largely due to a lack of cell lines to model neutrophil behavior along with

difficulties in working with fresh neutrophils. The few studies that have explored the interactions between neutrophils and particle carriers highlight that neutrophils may not behave the same as typical phagocytes. For example, one notable study found that in the presence of human plasma, neutrophils more readily phagocytosed PEGylated polystyrene particles than non-PEGylated particles, a departure from trends seen in macrophages, where PEGylation typically acts as a stealth coating[73]. A separate study found neutrophils unexpectedly phagocytosed rods at a significantly greater rate than spheres while macrophages exhibited lower phagocytosis of rod-shaped particles as expected[74]. Given the differences in particle interactions between neutrophils and other model phagocytes like macrophages and monocytes, there is the possibility that trends seen regarding deformable particles and macrophages may not necessarily hold true for neutrophils, and the characterization of these interactions would be crucial to gain more insight into how VTCs might behave in a human system in blood flow.

### 1.6 Dissertation Outline

Overall, there is an unmet need for more effective detection and treatment of CVD, especially CAD. While current treatment options can be effective at mitigating the complications of atherosclerosis, they fail to reverse or otherwise prevent formation of plaques within affected blood vessels. While VTCs have been explored as a non-invasive alternative to invasive surgeries and statin administration, they have largely failed to reach clinical relevance due to obstacles in particle transport that are not fully addressed by either NPs or MPs. While a degradable hydrogel particle has the potential to address these shortcomings, we have yet to develop a degradable material suitable for vascular drug delivery. Furthermore, interactions between neutrophils and deformable materials have been uncharacterized thus far and would be crucial to understanding how deformable VTCs might perform in human blood flow. Therefore,

the main focus of this thesis will be on developing and characterizing hydrogel-based materials within the context of vascular targeted drug delivery.

Chapter 1 provides an overview of CVD and current treatments in the clinic, with an emphasis on the potential for VTCs as a novel treatment for CVD and specifically, CAD. In addition, the chapter discusses the utility of hydrogels and their potential impact on VTC design.

Chapter 2 discusses the materials and methods used to collect the data collected here in this thesis, including the particle fabrication and characterization techniques as well as cellular assays used to characterize interactions between particles and immune cells.

Chapter 3 investigates various reaction schemes used to incorporate VPM peptide into a PEG hydrogel matrix using either thiol-ene photopolymerization or nucleophilic Michael addition click chemistry using various PEG molecules. The material developed in this chapter is useful for fabricating hydrogel MPs suitable for vascular targeted drug delivery.

Chapter 4 builds off of the previous chapter and explores the fabrication of hydrogel MPs using the material developed in chapter 3 and characterizes their potential as a VTC for carrying and delivering NPs to the vascular wall to facilitate NP adhesion to an inflamed endothelium. Here, we successfully developed a hydrogel MP capable of degrading in the presence of MMP-2 and binding to an endothelium following ligand conjugation.

Chapter 5 examines the interactions between immune cells and particles composed of deformable materials, including PEG and HA. We explored the impacts of surface charge and conjugation on the phagocytosis of hydrogel particles and found that neutrophils phagocytose particles indiscriminately of particle elasticity, while macrophages were less likely to phagocytose softer materials.

Chapter 6 outlines the development of a novel fabrication technique for the production of rod-shaped and fibrous hydrogel particles, which could provide more utility than spherical particles, especially in the context of muscular tissue regeneration.

Chapter 7 concludes the thesis and discusses potential future directions for this research.

# Chapter 2 : Materials and Methods

## 2.1 Introduction

This chapter describes in detail the materials and methods used to collect the experimental data presented in the data chapters of this thesis. The protocols for both bulk and particle fabrication of various hydrogel-based materials are detailed here, including fabrication of PEGDA, PEGVS, and HA-based hydrogels using different reaction schemes. We also detail the various phagocytosis assays using both primary human neutrophils and J774 macrophages as well as imaging assays performed with an optical tweezer system. Finally, we discuss the different types of shear designs for the fabrication of rod-shaped particles and the various methods of characterization for these particles. Materials and details on their sources are listed within the subsection where that material was used.

## 2.2 Thiol-ene Photoclick Polymerization of PEG and VPM

700 Da polyethylene-glycol diacrylate (PEGDA) (Sigma Aldrich), lithium phenyl-2,4,6-trimethylbenzoylphosphinate (LAP) (TCI Chemicals), and the MMP-sensitive peptide GCRDVPMSMRGGDRCG (VPM) (Genscript) were first mixed together in methanol at a 15 wt% concentration, as described previously[47]. 10 μL of the polymer solution was then placed between two hydrophobic coverslips spaced 1 mm apart and polymerized using a UV lamp for 10 minutes at a wavelength of 365 nm to created disk-shaped samples. Afterwards, hydrogel samples were swelled in PBS -/- for 24 for further use.

## 2.3 PEG-VPM Macromer synthesis

PEGDA and VPM peptide were first dissolved in 0.1M sodium phosphate buffer (pH 8) at a concentration of 1 mM and 1.6 mM respectively and allowed to react for 1.5 hours to create PEG-VPM macromers, as described previously[75]. The excess of PEGDA was used to ensure that the resulting macromers were acrylate terminated for subsequent photopolymerization. Next, the polymer solution was dialyzed against DI water for 24 hours using snakeskin dialysis tubing with a MW cutoff of 3500 Da (Thermofisher Scientific) to remove any residual unreacted PEGDA and VPM as well as the sodium phosphate. Finally, the solution was flash frozen in liquid nitrogen and lyophilized to yield purified PEG-VPM macromers. To fabricate hydrogel samples, PEG-VPM macromer was dissolved in PBS -/- at a concentration of 25 wt% with 1% LAP PI. Next, 10 μL of polymer solution was placed between two hydrophobic coverslips spaced 1 mm apart and exposed to UV at a wavelength of 365 nm for 10 minutes. After polymerization, hydrogel samples were swelled in PBS -/- for further use.

## 2.4 Fabrication of Bulk Hydrogels from VPM and PEGVS

4-armed polyethylene-glycol vinyl sulfone (PEGVS) (Jenkem Technologies) was dissolved in 0.3M triethanolamine (TEOA) (Sigma Aldrich) at a pH of 9 at varying concentrations. Separately, VPM was dissolved in 0.3M TEOA at a pH of 9 at an equimolar ratio of thiol to vinyl sulfone groups. To polymerize the PEGVS and the VPM, the two solutions were first mixed together in stoichiometric ratios of reactive groups to yield 10 μL of precursor solution, and the resulting solution was quickly placed between two hydrophobic coverslips spaced 1 mm apart and allowed to crosslink for 10 minutes. After polymerization, hydrogel samples were swelled in PBS -/- for 24 hours prior to further use.

### 2.5 Shear Rheometry of Bulk Hydrogel Samples

To determine the Young's modulus of our hydrogel materials, we placed our disk samples on the heated stage of an AR-G2 Rheometer (TA Instruments) held at 37 °C and used an 8-mm plate geometry for the purposes of rheometry. The normal force during each measurement was kept at 0.5 N, and a time sweep was performed using a 1% strain and an angular frequency of 1 rad/s. These assays yielded a storage modulus, which was then converted to Young's modulus according to the following relationship:

$$E = 2G(1 + v)$$

where $E$ is the Young's modulus of the material, $G$ is the shear modulus of the material, and $v$ is the Poisson's ratio of the material. Here, we assumed a Poisson's ratio of 0.5 for elastic materials.

### 2.6 Bulk Enzyme Degradation Assays

Bulk hydrogels were made as described above, and after swelling, hydrogel samples were placed in either 500 μL of a control buffer or an enzyme solution. For trypsin assays, hydrogels were placed in 2 μM trypsin in PBS -/-, and for MMP-2 assays, hydrogels were placed in 20 nM MMP-2 in a tricine buffer, comprised of 100 mM tricine (Sigma Aldrich), 50 μM $ZnCl_2$ (Sigma Aldrich), 50 mM $CaCl_2$ (Sigma Aldrich), 50 mM NaCl (Sigma Aldrich), 0.05% Brij-35 (Thermofisher Scientific). To monitor degradation, the surrounding solution of hydrogels was sampled periodically by taking 10 μL of the solution, and after the assay was complete, collected samples were analyzed using a fluorescamine assay. Each sample was incubated with 40 μL of 3 mg/mL fluorescamine (Acros Organics) in dimethyl sulfoxide (DMSO) for 45 minutes under foil. Finally, the fluorescence of each sample was measured using a Biotek plate reader using an excitation wavelength of 365 nm and an emission wavelength of 470 nm.

## 2.7 Ellman's Assay to Characterize Extent of Thiol Conversion

For PEG-VPM photoclick reactions, samples were collected by first incubating crosslinked photopolymerized gels in PBS -/- overnight to allow any unreacted VPM to diffuse into the surrounding liquid. Similarly, for the synthesis of PEG-VPM macromers, samples of the PEGDA and VPM mixture were collected over designated time points.

To perform the Ellman's assay, reaction buffer was first made by making a solution of 0.1M sodium phosphate (pH 8) with 1 mM ethylenediaminetetraacetic (EDTA), and Ellman's buffer was made by adding 4 mg of Ellman's reagent (Sigma Aldrich) to 1 mL of reaction buffer. Next, for each sample, we mixed together 6.25 μL of Ellman's buffer, 312.5 μL of reaction buffer, and 31.25 μL of sample (350 μL total). Each sample was then incubated for 15 minutes at room temperature under foil, and the absorbance at 414 nm was measured on a 96-well plate using a Biotek plate reader.

## 2.8 PEGVS Hydrogel Particle Fabrication

Precursor solutions of PEGVS and VPM were prepared as previously described in bulk PEGVS hydrogel fabrication. To encapsulate PS NPs into the hydrogels, 50 nm yellow-green PS NPs (Polysciences) were directly added to the PEGVS precursor solution. After mixing the PEGVS and VPM to form the polymer solution, it was quickly placed in paraffin oil (Sigma Aldrich) with 1% surfactant, comprised of Span 80 (Sigma Aldrich) and Tween 80 (Thermofisher Scientific) for an HLB of 5, and sonicated at 20% intensity to form a water-in-oil emulsion using a probe sonicator. After emulsion formation, particles were allowed to polymerize for at least two hours. Particles were purified with successive centrifugal washes in hexanes, ethanol, and tricine buffer. To obtain particles approximately in the 2 μm range, they

were filtered through a 2 μm filter tip and then spun down at 1500 x g to remove smaller particles. Particle size and surface morphology were then assessed via SEM imaging.

### 2.9 HUVEC culture and activation

Umbilical cords were acquired from Mott Children's Hospital in Ann Arbor under a Medical School Internal Review Board (IRB-MED) approved human transfer protocol. Human umbilical vein endothelial cells (HUVEC) were isolated using a collagenase perfusion method from three or more umbilical cords and pooled, as described elsewhere[76]. HUVEC were then cultured in T75 flasks pretreated with 0.2% gelatin at 37 °C and 5% $CO_2$ until confluent. Confluent HUVEC flasks were trypsinized and seeded onto 30 mm coverslips pretreated with glutaraldehyde-crosslinked gelatin and grown for 48 – 72 hours at 37 °C and 5% $CO_2$ until confluent on the coverslip. To induce HUVEC inflammation, cells were activated with 2 mL of 1 ng/mL interleukin-1β (IL-1β) for 24 hours to induce maximal expression of intercellular cell adhesion molecule-1 (ICAM1)[77].

### 2.10 PEGVS Particle Degradation

First, 5E7 particles per sample were placed in an Eppendorf tube, centrifuged at 20000 x g, and the supernatant was removed via aspiration. Particles were then resuspended in either 20 nM MMP-2 or a tricine buffer control. At given time intervals, samples were centrifuged to pellet the particles, and 10 μL of the supernatant was taken, followed by resuspension of the particles via brief sonication. After the degradation assay was complete, samples were analyzed using a fluorescamine assay as described earlier.

### 2.11 Particle Conjugation and Characterization

Neutravidin protein (Thermofisher Scientific) was conjugated to the surface of PEGDA-based particles using 1-ethyl-3-(3-dimethylaminopropyl)carbodiimide hydrochloride (EDC) chemistry to covalently link carboxylic acid groups on the particle surface to primary amines on the Neutravidin protein. First, 1E9 particles were resuspended in 400 μL of 2-morpholinoethanesulfonic acid (MES) buffer at a pH of 7 containing 5 mg/mL Neutravidin protein and rotated under foil for 15 minutes. Afterwards, 400 μL of 100 mg/mL EDC in MES buffer was added to the particle solution and allowed to react overnight, after which the reaction was quenched with the addition of 20 mg of glycine and washed once with PBS -/-.

PEGVS particles were instead conjugated with the use of thiolated avidin. 2E8 particles were added to 1 mL of 1 mg/mL avidin-SH in 0.3M TEOA, pH 9, and rotated overnight to link surface vinyl sulfone groups with the thiol groups present on the avidin protein. After washing with tricine buffer, 1E8 particles were conjugated with biotin-PE (Thermofisher Scientific) and subsequently analyzed using an Attune flow cytometer to characterize the avidin reaction. To instead characterize the conjugation of targeting ligands to the particle surface, avidin-coated PEGVS particles were first reacted with biotinylated anti-ICAM1 (Biolegend) followed by IgG-APC (Biolegend) to characterize the ligand conjugation via flow cytometry.

### 2.12 PEGVS Particle Adhesion Assays

For static adhesion assays, HUVEC were cultured onto glass coverslips with gelatin and grown to confluency as described previously. After 24-hour activation with IL-1B in complete M199 media, 1E8 particles coated with a saturating amount of anti-ICAM1 were added to the media and allowed to incubate for 4 hours. Coverslips were then washed with 10% bovine serum albumin in PBS and imaged for adherent particles.

For adhesion-degradation assays, fixed HUVEC was first incubated with 5 µg/mL of FITC-conjugated wheat germ agglutinin (WGA) to stain the cells. Next, 1 mL of 5E7 particles/mL in PBS -/- were perfused through a parallel plate flow chamber lined with the stained HUVEC at a shear rate of 500 $s^{-1}$ according to the equation:

$$\gamma_W = \frac{6Q}{h^2 w}$$

where $\gamma_W$ is the shear rate in the channel, $h$ is the channel height (0.0127 cm), $w$ is the channel width (0.25 cm), and $Q$ is the volumetric flow rate. After the particle adhesion step, the channel was flushed with fresh PBS -/- to remove any unbound particles, then either a 2 µM trypsin solution or just PBS -/- was perfused through the channel and was flowed back and forth using a syringe pump to simulate continuous flow for 2 hours. After the degradation step was complete, the coverslip was imaged using confocal microscopy to detect the presence of PEGVS particles and released NPs adherent to the HUVEC.

**2.13 NP Conjugation**

7E13 50 nm PS NPs (Polysciences) were added to 400 µL of 1 mg/mL Neutravidin protein in MES buffer (pH 10) and rotated under foil for 15 minutes, followed by addition of 400 µL of 100 mg/mL EDC and allowed to react for 2 hours. After the reaction was complete, the reaction was quenched with 20 mg of glycine and diluted up to 4 mL using DI water. To wash the particles, the NP solution was subjected to ultracentrifugation via a Sorvall MX120 ultracentrifuge for 3 hours at 150,000 x g, and the supernatant was aspirated. Particles were then resuspended in PBS -/- with 1% Brij-35, and to characterize the avidin reaction, 5E12 particles were stained with biotin-PE (Thermofisher Scientific) for 30 minutes, and following a second ultracentrifugation step, particles were visually inspected for successful conjugation. For

conjugation of targeting ligands, 5E12 particles were incubated with a saturating amount of biotinylated anti-ICAM1 (Biolegend) and subjected to ultracentrifugation to wash away any unreacted antibody.

### 2.14 PEGDA Particle Fabrication

PEG particles were fabricated as previously described[47]. We first mixed together PEGDA, 2-carboxyethyl acrylate (CEA) (Sigma Aldrich), LAP, acryloxyethyl thiocarbamoyl Rhodamine B (Rhod) (Polysciences), and methanol to form a precursor solution, with PEGDA in quantities to form 50 and 15 wt% solutions. Precursor solution was then added to an oil phase of silicone oil in a one to ten volumetric ratio, briefly sonicated to form a water-in-oil emulsion and placed under a UV lamp to allow particles to crosslink. Particles were subsequently washed in hexanes and ethanol and filtered using 2 μm filters and centrifuged at 1500 x g to remove smaller particles. To alter the zeta potential of the PEG particles, an equivalent mass of 2-aminoethyl methacrylate hydrochloride (AEM) was added in lieu of the CEA. Neutrally charged particles were fabricated using an equivalent mass of a 50-50 mixture of CEA and AEM. Successful AEM incorporation into the particle backbone was demonstrated using a fluorescamine assay, and zeta potential was measured using a Malvern Zetasizer.

### 2.15 Hyaluronic Acid Methacrylate Particle Fabrication

A precursor solution of rhodamine, LAP, and HAMA in 50 vol.% methanol solution in water was first made, adjusting the amount of HAMA to achieve 5, 10, and 20% wt/vol solutions. The HAMA precursor solution was added to an oil phase of silicone oil and sonicated to form a water-in-oil emulsion and placed under a UV lamp for particles to crosslink. Particles were

subsequently washed in hexanes and ethanol and filtered using 2 μm filters and centrifuged at 1500 x g to obtain 2 μm-sized particles.

### 2.16 Human Blood Preparation

Informed, written consent was first obtained by all healthy blood donors according to a protocol approved by the IRB-MED, and blood was then obtained from blood donors via venipuncture. First, a tourniquet was placed around the donor's arm, and the skin over the vein was sterilized with a sterile alcohol pad. A sterile butterfly needle was attached to a syringe filled with heparin anticoagulant such that the total concentration was 7 mL of anticoagulant per 50 mL of blood, and the needle was then inserted into the vein. Blood was slowly drawn up to the desired amount of blood, and after the blood draw was complete, the tourniquet was first removed, followed by removal of the needle and placement of gauze over the puncture site. After clot formation, the clot was covered with additional clean gauge and a bandage. Blood was stored at 37 °C for further use.

### 2.17 Isolation of Primary Human Neutrophils

20 mL of fresh human blood was first drawn from a healthy human donor, layered onto a Lymphoprep density gradient (STEMCELL Technologies) in a 1:1 volume ratio, and centrifuged at 400 x g for 20 minutes at an acceleration of 3 and brake of 0. The plasma layer was collected for future use and the rest of the supernatant (buffy coat and gradient layer) were discarded. 20% dextran (Sigma Aldrich) with 0.15M NaCl was then added to the RBC and neutrophil layer at a 1:2 volume ratio and mixed by gently rotating the tube. PBS -/- was added up to 25 mL total volume and gently rotating the tube, and the RBCs were allowed to settle for 30 minutes. The supernatant (neutrophils and residual RBCs) was collected and PBS -/- was added up to 50 mL

and centrifuged at 500g for 5 minutes. The supernatant was then aspirated and to lyse remaining RBCs, 20 mL of 0.2% NaCl solution was first added and mixed by inverting. After 45 seconds, 30 mL of 1.8% NaCl solution was added to the tube and centrifuged at 500g for 5 minutes. Cells were washed once with PBS -/-, counted, and resuspended in plasma or RPMI media for particle uptake studies.

### 2.18 Neutrophil Phagocytosis Assays

Fresh blood was drawn from a healthy human donor as described previously, and 100 µL of whole blood each was placed into FACS tubes for particle uptake assays. To each tube, $10^6$ particles were added for a final concentration of $10^7$ particles/mL of whole blood and incubated at 37 °C and 5% $CO_2$ for two hours. Afterwards, neutrophils were stained with APC-CD45 (Biolegend) and APC-Cy7-CD11b (Biolegend) for 30 minutes on ice before cell fixing with Fix-Lyse buffer (Thermofisher Scientific) to remove red blood cells. Samples were subjected to centrifugal washes before analysis using flow cytometry. Neutrophils were comprised of events that were positive for CD45 and CD11b, and particle positive cells were those that were positive for FITC and rhodamine for PS and PEG respectively. For isolated neutrophils, $2x10^5$ cells in 100 µL of either RPMI media or human plasma were placed in FACS tubes per sample, and $10^6$ particles were placed in each sample for a cell:particle ratio of 1:5. The uptake study was then run as with whole blood samples.

### 2.19 J774 Macrophage Culture

J774 macrophages were purchased from the American Type Culture Collection (ATCC) and cultured according to a protocol by ATCC. The cell vial was first thawed and resuspended in 10 mL of Dulbecco's modified Eagle media (DMEM) supplemented with 10% fetal bovine serum

(FBS) and then centrifuged at 500 x g for 5 minutes. After removing the supernatant, the cells were resuspended in 10 mL of fresh DMEM and transferred to a T75 flask and incubated at 37 °C and 5% $CO_2$. Media was replaced every 2 days, and every 5 days, cells were subcultured by first removing spent media from the flask via aspiration and adding 10 mL of fresh media. Next, cells were detached from the flask using a cell scraper, and the cell suspension was transferred to new T75 flasks at a 1:3 dilution of cells to fresh media. For particle uptake studies, cells were first detached from T75 flasks and counted using a hemocytometer. Cells were then centrifuged at 500g and reconstituted with fresh media to a concentration of 107 cells/mL for future use.

### 2.20 Macrophage Phagocytosis Assays

Cells were first detached from T75 flasks via scraping, followed by counting cells using a hemocytometer to determine cell concentration. Cells were centrifuged at 500g and resuspended at a concentration of $10^6$ cells/mL of DMEM media with 10% FBS. Next, $10^5$ cells per sample were placed in the wells of a 96-well plate and incubated at 37 °C and 5% $CO_2$ for one hour to allow the cells to adhere to the plate. Afterwards, $10^6$ particles were added per sample and then incubated for 2 hours. Macrophages were detached by gently pipetting the media up and down, and cells were transferred to FACS tubes for staining with APC-Cy7-CD11b on ice, followed by cell fixation with 2% paraformaldehyde. Samples were analyzed with flow cytometry, and results were represented as a percentage of particle-positive neutrophils out of the whole population of macrophages.

### 2.21 Optical Tweezer

First, 1 mg/mL of poly-L-lysine was adsorbed to coverglass-bottom cell culture dishes (Bioptechs) for 5 minutes before rinsing with DI H2O. 1 mL of cells (either primary human

neutrophils or J774 macrophages) were added (diluted in plasma to approximately 1.6E6 cells/mL) and allowed 15 minutes to adhere. 100 µL of particles were added to the dish, and the dish was mounted on a temperature-controlled stage (Bioptechs) to maintain the sample at 37 °C over the course of the experiment.

Particles were manipulated using a bespoke optical tweezer system. Briefly, a 1064nm laser (IPG Photonics) was expanded to slightly overfill the back aperture of an objective (Nikon MRD01602, 60x, 1.45NA) then focused to a diffraction-limited spot at the image plane. Particles were optically trapped and brought into contact with a cell. Images of the cells were acquired with brightfield images at approximately 1 Hz, and the cell was then observed over a 5-minute period to assess particle engulfment.

**2.22 SDS-PAGE**

Characterization of plasma protein adsorption onto particles was done via sodium dodecyl sulfate polyacrylamide gel electrophoresis (SDS-PAGE). First, 5E7 PEG particles were added to 1 mL of heparinized human plasma and incubated at 37 °C for five minutes to allow a protein corona to form. Following incubation, particles were washed three times with PBS -/- to remove residual plasma, and then particles were resuspended in 50 µL of lane marker non-reducing buffer (Thermofisher Scientific, Pierce) and heated to 95 °C for five minutes using a thermocycler to denature and detach proteins adsorbed to the particle surface. Finally, the solution was centrifuged once more to pellet particles remaining in the samples. 20 µL of each sample, along with 5 µL of a standard dual stain protein ladder (Bio-Rad) were loaded into the lanes of a Tris-Glycine protein gel (Invitrogen), and the gel was run at 200 mV for two hours to separate proteins by molecular weight. The gel was then removed from the cast and stained with

Coomassie blue (Invitrogen) overnight, followed by destaining with DI water. The gel was then imaged to visualize protein bands from each sample.

### 2.23 Rod-Shaped Hydrogel Fabrication from Rotational Shear

A cup-and-bob or cone-and-plate geometry was first designed and 3D-printed in curable resin. Next, a PEGDA solution was made as previously described, and emulsified in silicone oil (AP 10000, Sigma Aldrich) using an overhead Caframo mixer. The emulsion was then placed between the gap of the stationary and rotating sections of the shear geometries, and the emulsion was sheared using the mixer at a rotational speed of 5000 rpm and crosslinked using a UV lamp at a wavelength of 365 nm. After particles were polymerized, the particles and silicone oil were moved to Eppendorf tubes and washed with hexanes and ethanol and stored in a 1% PVA solution. Further characterization of the particles was done using fluorescent microscopy and SEM.

### 2.24 Rod-Shaped Hydrogel Fabrication from Tube Shear

A PEGDA solution was made as previously described and emulsified into silicone oil (AP 10000). Next, the emulsion was pumped through a 1 mm in-diameter tubing with two syringe pumps; one syringe pump was used to push the solution through the tube, and the other was used to pull the solution. A range of flow rates was used to vary the shear rate from 0 to 1400 $^{s-}$1. As the emulsion traveled through the tube, it was pumped past a bespoke UV array to crosslink particles while in shear, and after polymerization, particles in oil were collected into Eppendorf tubes and washed with hexanes and ethanol before being stored in a 1% PVA solution for further characterization.

Fabrication of HAMA-based rod hydrogels was done by first making a 1 wt% HAMA solution in a 10% methanol in water, along with 1% Rhod and 1% LAP photoinitiator. Otherwise, the fabrication process was unchanged from PEG rod fabrication.

### 2.25 Characterization of Rod-Shaped Hydrogels

A dilute sample of PEG rods was added to resin and placed into the wells of a 96-well plate. To anchor particles to the bottom of the wells, the plate was centrifuged at 1000 x g for 5 minutes, and the resin was then crosslinked with a UV lamp to immobilize the particles. Fluorescent microscopy was used to image particles, and image processing was performed to determine the aspect ratio (AR) and equivalent spherical diameter of the particles.

### 2.26 Differential Centrifugation

Particle samples generated from tube flow fabrication at different shear rates were subjected to centrifugation steps at increasing speeds, from 50 x g up to 1500 x g. Particles that pelleted were collected after every centrifugation step, and particle fractions were washed with DI $H_2O$ to remove residual PVA. Particle samples were then imaged using SEM, and image analysis was performed using ImageJ software to determine AR and ESD of each particle fraction.

### 2.27 HA Synthesis

Hyaluronic acid from rooster comb (HA) (Sigma Aldrich) was first dissolved into a 50/50 solution of dimethyl formamide (DMF) at a concentration of 10 mg/mL. Next, methacrylic anhydride (MA) was added dropwise to the HA solution while stirring vigorously until a 20x stoichiometric excess of MA to hydroxyl group of HA was reached, and sodium hydroxide was also incrementally added to keep the pH of the reaction between 8 and 9. The reaction was then

incubated at 4 °C overnight to allow for the formation of HA methacrylate (HAMA). To precipitate the HAMA, the polymer mixture was added to ethanol at a ratio of 1000 mL ethanol per 50 mL of polymer, centrifuged to pellet the HAMA, and washed once more with fresh ethanol. To purify the HAMA, the polymer was then dissolved in DI water and dialyzed against DI water using snakeskin dialysis tubing (MW cutoff of 3500 Da) for at least 24 hours. Finally, the HAMA was lyophilized and stored at -20 °C for future use.

# Chapter 3 : Evaluation of Techniques for the Fabrication of Peptide-crosslinked Hydrogels for Enzyme Degradation

## 3.1 Abstract

PEG, a hydrophilic polymer, is a material of great interest for its biocompatibility and non-fouling properties. While its potential as a vascular targeted carrier has been explored in multiple studies for its ability to both navigate the vasculature and marginate to an inflamed endothelium, they do not explore site-specific release of therapeutics, a critical aspect of a successful VTC. In this work, we explored the incorporation of VPM into PEG hydrogel networks via both thiol-ene photoclick chemistry and Michael addition reactions to both PEGDA and PEGVS. Photoclick hydrogels fabricated from PEGDA and VPM exhibited incomplete peptide incorporation and degradation by trypsin, thus limiting their use as a material for vascular delivery. PEGDA-VPM macromers synthesized via Michael addition reactions successfully formed hydrogels capable of complete enzymatic degradation by trypsin within two hours, yet were found to have a Young's modulus too low to be feasible as a VTC (200 Pa). Finally, by using a 4-armed PEGVS instead of a linear PEG molecule, we showed that bulk hydrogels formed from PEGVS and VPM were demonstrably more rigid than PEGDA-VPM hydrogels (15 – 30 kPa), while retaining their ability to undergo complete enzymatic degradation. These PEGVS hydrogels were degraded by trypsin within 6 hours and by MMP-2 within 48 hours. Overall, this work demonstrates the utility of a peptide conjugated PEG hydrogel material that responds to enzymatic stimuli with properties suitable for vascular targeted drug delivery.

## 3.2 Introduction

The field of smart biomaterials continues to advance towards increasingly complex materials capable of responding to external and environmental stimuli for a wide range of applications, including cell scaffolding, tissue regeneration, and delivery of bioactive therapeutics to treat diseases[46,78,79]. Smart materials have traditionally been selected for use based on their ability to interact with various biological systems and mimic tissue responses while avoiding immune response and cytotoxicity[78,80,81]. Common biodegradable macromolecules, such as collagen, hyaluronic acid, chitosan, and protein-derived materials have been demonstrated to be successful in tissue engineering, yet without chemical modification, lack the structural stability and tunability that synthetic polymeric materials typically exhibit[78,82–85]. Conversely, synthetic materials such as polycapralactone and PLGA typically do not contain biological moieties necessary for interaction with many biological systems and are more likely to elicit immune responses, being recognized as foreign material[26,86].

Hydrogels are a class of material composed of polymer networks with the ability to swell up to 90% water content[87]. This type of material has been of great interest due to its hydrophilicity and elasticity compared to other traditional polymeric networks, thus making it attractive as a material for tissue engineering. Indeed, hydrogels composed of crosslinked PEG and HA have been shown to be useful as biodegradable materials, being used for cell-responsive cell scaffolds, tissue analogs, and injectable biomaterials for drug release[54,88–91]. PEG is particularly attractive material due to its high degree of tunability and non-fouling properties; many aspects of PEG can be modified for specific applications, including molecular weight, branching structure, and incorporation of terminal functional groups confer greater complexity and bioactivity, such as by including antibodies, enzyme-sensitive peptides, and fluorescent

tags[92]. Furthermore, its hydrophilicity allows it to avoid protein adsorption that other hydrophobic polymeric materials suffer from, thus more effectively avoiding immune responses[93,94].

Aside from bulk hydrogel applications, PEG has also seen use as a particle drug carrier for treatment of cardiovascular disease, where PEG particles have been shown to both effectively evade immune cell clearance while exhibiting a long circulation time[58]. Furthermore, PEG particles have been demonstrated to bind to an inflamed endothelium model, thus exemplifying its potential as a VTC[47]. However, while work in this space has investigated its utility as a carrier, the feasibility of use in terms of site-specific drug release has yet to be determined, as these studies used non-degradable materials unable to release cargo via biological stimuli. In this chapter, we explore the incorporation of VPM, an MMP-sensitive peptide, into PEG hydrogels using various reaction schemes to develop and characterize an enzyme-degradable hydrogel material suitable for vascular targeted drug delivery and capable of degrading in the presence of both trypsin, a model enzyme, and MMP-2, an enzyme shown to be upregulated in inflamed endothelia[51].

## 3.3 Results

### *3.3.1 Synthesis Scheme 1 – Photoinitiator-mediated thiol-ene Michael addition*

To incorporate peptide bonds into the polymer network of our hydrogels, we first developed a synthesis reaction based off of previous hydrogel fabrication protocols[47,48], using the terminal functional groups already present on both polyethylene glycol diacrylate (PEGDA) and the MMP-sensitive peptide GCRDVPMSMRGGDRCG (VPM). As outlined in reaction 1 of

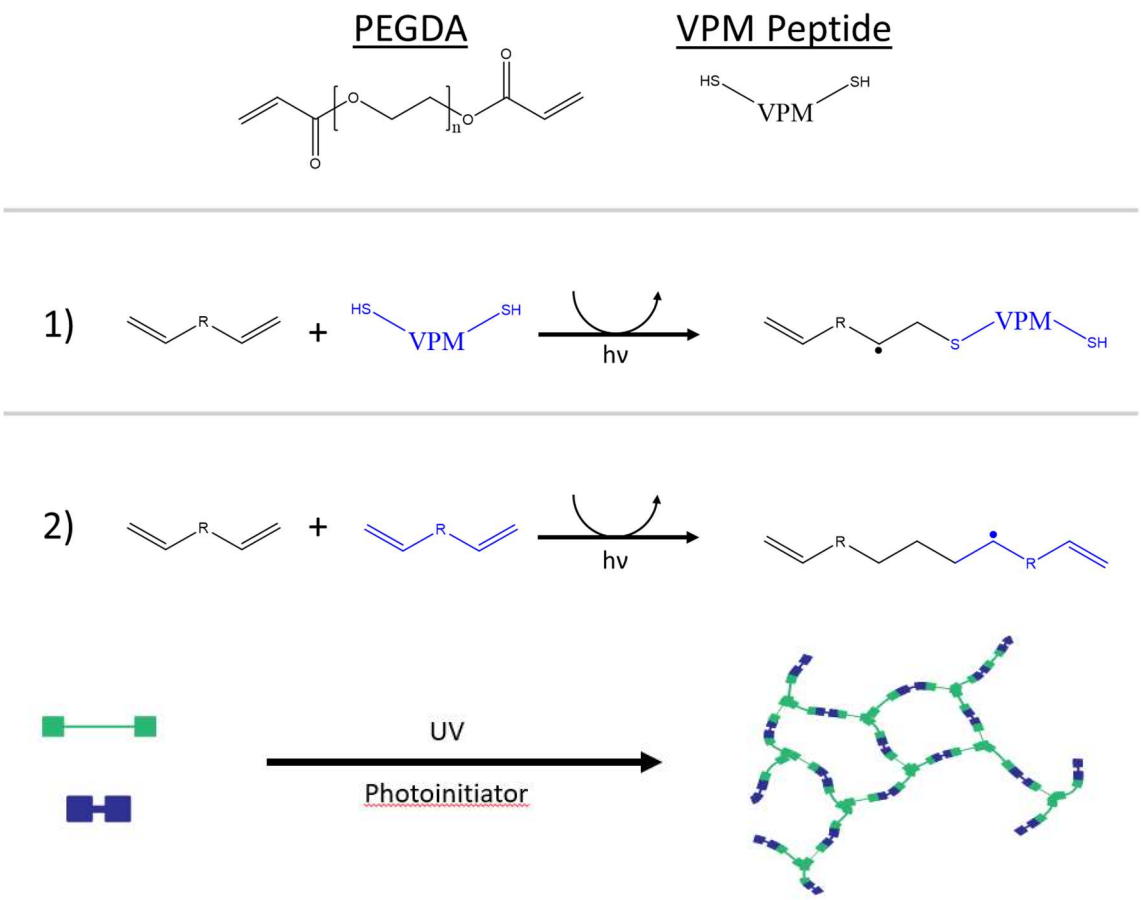


Figure 3.1: Reaction scheme of thiol-ene photoclick chemistry using PEGDA and VPM. Reaction 1 outlines the radical-mediated addition of PEGDA to VPM via reaction of the diacrylate group on PEGDA to the thiol group on VPM, which occurs via a step growth mechanism followed by a chain transfer step. Reaction 2 depicts the radical-mediated addition of two PEGDA molecules, which propagates via the alkene bonds on each PEGDA molecule. A schematic of the reaction between the two reagents is outlined on the lower part of the figure, demonstrating the incorporation of peptide bonds into the hydrogel matrix.

Figure 3.1, the acrylate groups on PEGDA and the thiol groups from the residual cysteines of VPM participate in radical-mediated propagation. The acrylate group first reacts with a radical generated from the photoinitiator, which subsequently reacts with the thiol group on the VPM molecule, transferring the hydrogen from the thiol to the carbon chain. Next, the radical on the thiol group undergoes a propagation step, covalently connecting it to another PEGDA molecule. Finally, the resulting radical on the carbon activates another thiol group on a VPM molecule, thus allowing the chain to participate in further radical reactions and incorporate the peptide into

the hydrogel network. In addition to thiol-ene Michael additions, PEGDA will also react with itself via a radical-mediated propagation, in which the radical from one acrylate group reacts with another on a separate PEG molecule, which then allow for crosslinking of the polymer into a mechanically stable hydrogel.

To optimize the incorporation of VPM into the PEG hydrogel, we varied the molar ratio of VPM to PEG, using either a 1:4 or 1:2 ratio in a 15 wt% formulation as described previously. After fabricating the bulk VPM-conjugated PEG hydrogels using thiol-ene click chemistry, we next quantified the conversion of VPM using an Ellman's assay to detect the presence of residual thiols in solution. As shown in Figure 3.2 (A), hydrogels fabricated using both molar ratios tested

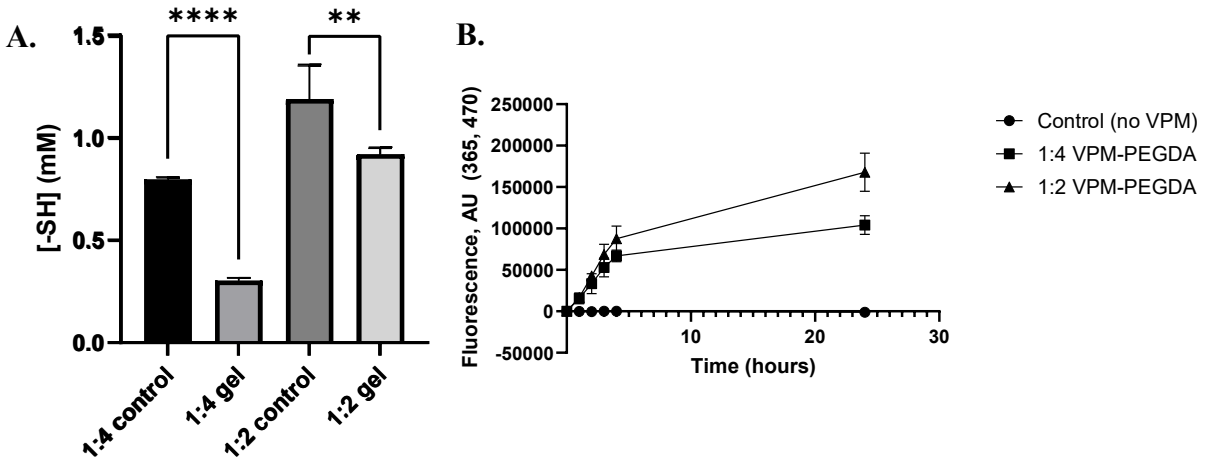


Figure 3.2: (A) PEG polymer formulations of 1:4 or 1:2 VPM to PEG were used to fabricate 15 wt% hydrogels, and residual thiol groups were quantified using an Ellman's assay. (B) 15 wt% PEG hydrogels crosslinked with VPM were subjected to 2 μM trypsin solutions and enzyme activity was tracked using a fluorescamine reaction over 24 hours. Statistics on thiol conversion were performed using an unpaired t test on the 1:4 and 1:2 formulation. (**, $P < 0.01$; ****, $P < 0.0001$).

indicated a significant reduction in the concentration of thiol groups as compared to an uncrosslinked control. While a 1:4 ratio of VPM to PEG exhibited a 61.9% reduction in thiol concentration, a 1:2 ratio resulted in a 22.6% reduction, indicating incomplete conversion of VPM into the PEG network. We next used trypsin as a model enzyme to confirm that hydrogels were successfully incorporated with VPM, as shown in Figure 3.2 (B), using a fluorescamine

assay to determine the presence of primary amines. Using an enzyme concentration of 2 μM, we observed an increase in fluorescent signal in both the 1:4 and the 1:2 formulation, indicating the presence of cleaved peptides present within the hydrogel when compared to a control hydrogel containing no VPM. As expected, we saw that the fluorescent signal for the 1:2 formulation was higher than that for the 1:4 formulation, due to the increase in peptide used for the 1:2 ratio. However, at the 24-hour mark, all hydrogel samples remained intact despite the cleavage of incorporated VPM. The plateau in fluorescent signal at the 24-hour mark also indicates that peptide cleavage was complete, thus resulting in incomplete degradation.

### *3.3.2 Synthesis Scheme 2 – Synthesis of PEG-VPM macromers for controlled Michael addition reactions*

We next adjusted our reaction scheme to more tightly control the reaction of the acrylate to thiol group, thus incorporating more peptide to increase the extent of degradation of the

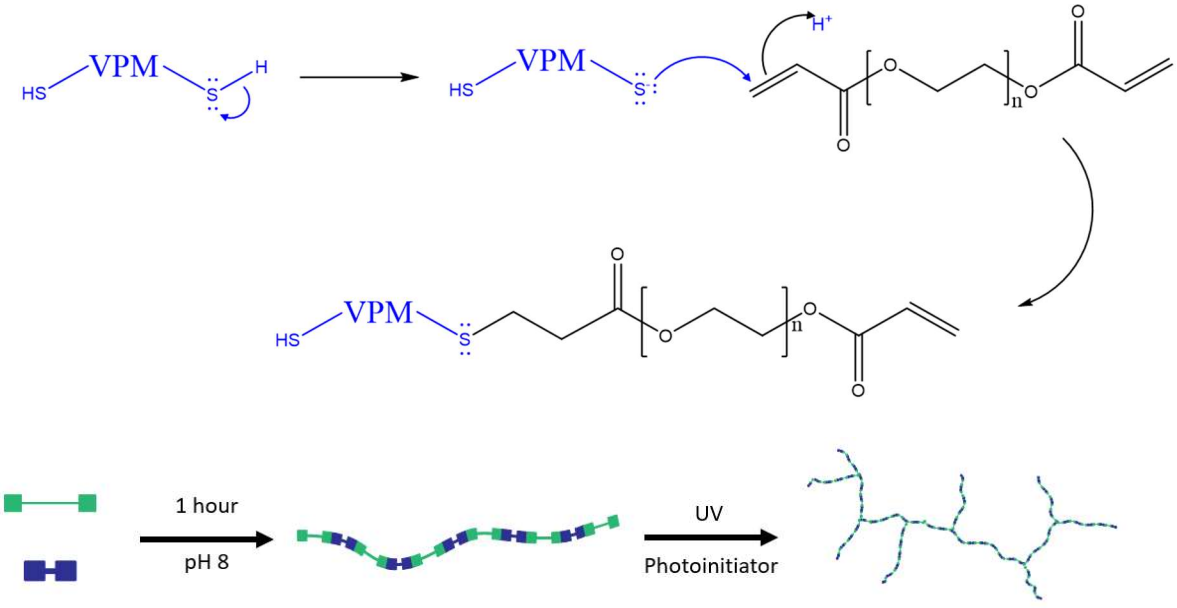


Figure 3.3: Reaction mechanism of thiol groups from VPM and acrylate groups on PEGDA. After deprotonation, of the thiol group, it reacts specifically to the alkene bond of acrylate in a Michael addition click reaction. A schematic of the synthesis and subsequent photocrosslinking of the PEG-VPM macromers is shown in the lower half of the figure.

hydrogel material. Here, in lieu of a photoinitator to drive the reaction of PEGDA and VPM, we mixed the two reagents and reacted them via a pH driven Michael addition, as described in Figure 3.3, circumventing the use of photoinitiator and avoiding side reactions of alkene chain propagation. Under basic conditions, the thiol group of VPM first becomes deprotonated, generating a negative charge on the nucleophilic sulfur atom. Next, the electrophilic alkene bond of the PEGDA undergoes nucleophilic attack by the thiol group, resulting in a conversion to stable thioether bonds, thus conjugating the VPM to the PEG molecule. Under these reaction conditions, the polymer undergoes a step growth mechanism with specific chemistry, generating larger macromers with alternating PEG and VPM units. Thus, the reaction proceeds with a higher conversion of the thiol functional groups and yields a more homogenous material with a higher degree of functionality. Finally, a slight excess of PEGDA ensures that the macromers are acrylate-terminated, which allows for crosslinking via radical polymerization.

We then quantified the conversion of VPM by performing an Ellman's assay on the PEG-VPM mixture over time. As shown in Figure 3.4 (A), the absorbance signal of the PEG-VPM mixture was observed to decrease by 15 minutes. The reaction was allowed to proceed for 1.5 hours, at which point we were able to achieve a 95% conversion of thiol groups, indicating near total incorporation of the VPM with PEG.

After fabrication of bulk hydrogels using the PEG-VPM macromers, we evaluated the bioactivity of the samples by exposing the bulk samples to 2 μm trypsin and monitoring degradation using a fluorescamine assay. Notably, a polymer concentration of 25 wt% was needed for gelation. By normalizing the data to the final fluorescent signal achieved by each sample, we represented the degradation profile of the PEG-VPM hydrogels as a percentage of

remaining sample. As shown in Figure 3.3 (B), all hydrogel samples were fully degraded by the

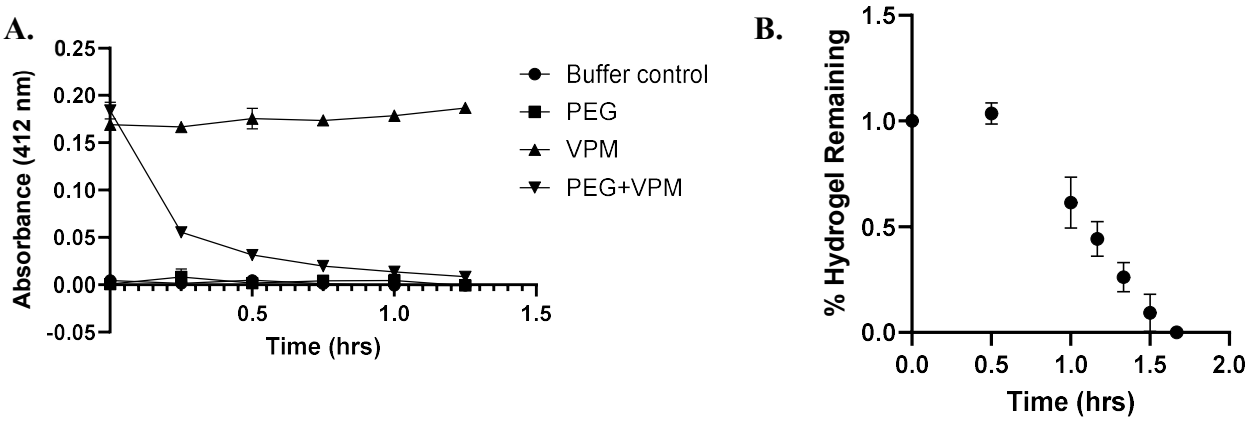


Figure 3.4: (A) Ellman's assay over 1.5 hours of a mixture of VPM and PEGDA. Absorbance of thiol groups decreased over time, indicating successful conjugation of the VPM to PEG. (B) Degradation profile of bulk 25 wt% hydrogel samples made from PEG-VPM macromers using 2 μM trypsin. Complete degradation was achieved by two hours.

2-hour time point, with no sample visible in solution.

After confirming that hydrogels can successfully degrade in the presence of a model enzyme, we assessed the feasibility of using this hydrogel material as a particle drug carrier. Specifically, because of the increased amount of material required for hydrogel fabrication, we measured the elastic modulus of this material to determine its usability for vascular delivery using an AR-G2 rheometer. Figure 3.5 shows the rheometry data of the PEG-VPM hydrogels,

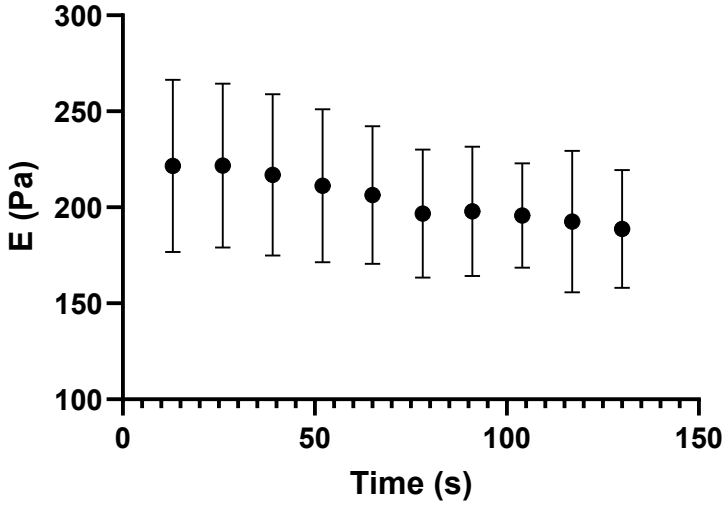


Figure 3.5: Rheometry data of PEG-VPM hydrogels to measure the Young's modulus, averaging about 225 Pa.

which have an average Young's modulus of 225 Pa. Based on a prior study looking at the effects of particle elasticity on adhesion to an inflamed endothelium, we determined that this material was too soft for vascular delivery because they would likely be unable to marginate as effectively to the wall and instead co-localize with RBCs in the center of the blood vessel[47].

### *3.3.3 Synthesis 3 – Use of multifunctional PEG for increased polymer network density*

Because hydrogel elasticity is largely dictated by crosslinking density[95], we next used a multifunctional, 4-armed PEG variant with vinyl sulfone groups, which more readily undergo Michael addition reactions with thiol groups than acrylate groups[96–98]. Figure 3.6 outlines the structure of the 4-armed PEG vinyl sulfone (PEGVS) and the reaction of PEGVS with VPM, which results in a highly branched network of alternating PEG and VPM units.

We again fabricated bulk hydrogels using PEGVS and degraded hydrogel samples in 2 μM trypsin solutions to confirm that VPM was successfully incorporated into the PEG hydrogel. Here, three different formulations were used to determine changes in degradation profile due to different polymer concentrations. As shown in Figure 3.7 (A), we observed similar degradation profiles for all PEG formulations, as evident by the time at which the fluorescamine signal plateaued indicating complete degradation. Indeed, all hydrogel samples were visually fully degraded by the 4-hour mark. Notably, the fluorescamine signal for both the 20% and 30% PEG were similar, while that for 40% PEG was higher, likely from the increase in degraded material. We next performed shear rheometry to measure the shear modulus, used to calculate the Young's modulus of these PEGVS hydrogels. Figure 3.7 (B) shows the calculated Young's modulus over the timespan of a rheometric assay, which demonstrates the increase in modulus with an increase

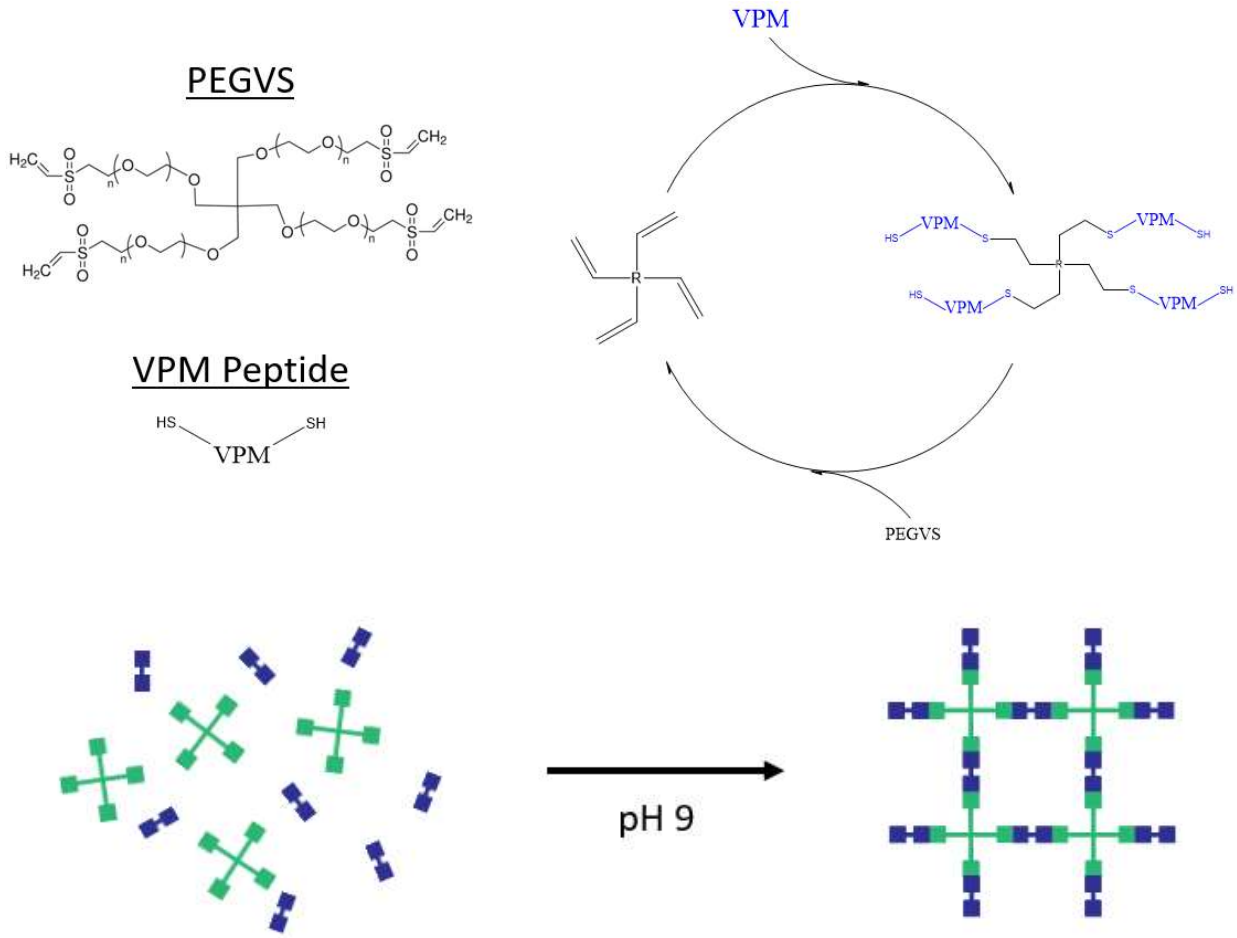


Figure 3.6: Reaction scheme of PEGVS and VPM. The terminal vinyl sulfone groups on PEGVS react with thiol groups from VPM via a Michael addition, which then undergo subsequent addition reactions to ultimately yield a highly branched network of PEG molecules connected by VPM units. A schematic of the reaction between PEGVS and VPM has shown on the lower half of the figure, outlining the network of PEG and VPM that is formed upon reaction of the vinyl sulfone groups with the thiol groups.

in polymer concentration. The average Young's modulus for each formulation was 14, 24, and 30 kPa for 20%, 30%, and 40% PEG respectively. While the Young's modulus of the 20% PEGVS was too low to be considered for vascular delivery, the modulus of both the 30% and 40% PEGVS were within the range of moduli demonstrated to bind to an inflamed endothelium in a flow chamber[48].

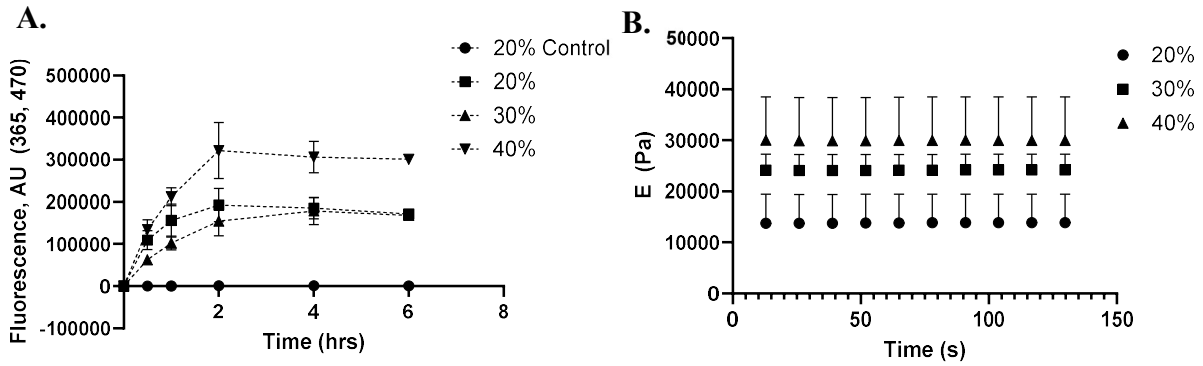


Figure 3.7: (A) Degradation profile of PEGVS hydrogels, fabricated with 20%, 30%, and 40% polymer concentrations, using 2 μM trypsin. The 20% control indicates hydrogels that were placed in buffer with no enzyme. (B) Rheometry data of different PEGVS formulations. The Young's modulus of the hydrogel increases with increasing PEG concentration.

Because of the similarities in modulus between the 30% and 40%, we chose to continue exploring the 30% formulation for its applications in vascular targeted drug delivery. We next used MMP-2 to degrade bulk hydrogel samples as a more physiologically relevant enzyme. As shown in Figure 3.8, hydrogels exposed to 20 nM MMP-2 were found to start degrading by the 2-hour mark and were visually completely degraded by 24 hours, though the fluorescamine signal continued to increase slightly until the 48-hour timepoint. The control samples, which were placed in buffer with no enzyme, did not show an increase in fluorescence over time, indicating that the hydrogels were hydrolytically stable.

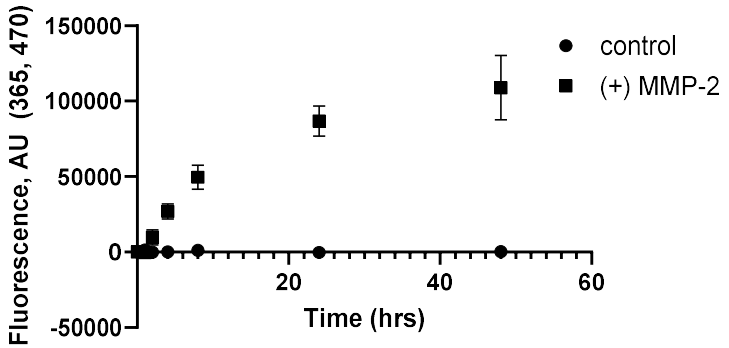


Figure 3.8: Degradation of 30% PEGVS hydrogels using 20 nM MMP-2. Hydrogels were visually shown to be fully degraded by the 24-hour time point, while fluorescent signal increased until the 48-hour time point.

### 3.4 Discussion

The use of vascular targeted carriers has gained increasing interest as a potential treatment alternative to current clinical standards, which typically include administration of statins, which come with side effects, and invasive surgeries, such as stents and bypass. However, current particle technologies need to address many obstacles to successful delivery, including the need for site-specific release of therapeutics from these carriers, which mitigates off-target effects and increases drug efficiency. Here, we have developed different reaction schemes to fabricate a peptide-incorporated hydrogel material that responds to MMP-2, an enzyme upregulated in areas of inflammation[51], yet is otherwise stable in physiologic conditions.

Building off previous work fabricating PEG-based hydrogel particles, we first used thiol-ene photoclick chemistry to conjugate the VPM peptide to PEGDA. Initially, we expected that because the PEGDA was in excess compared to VPM, we would be able to achieve a high degree of peptide incorporation due to the excess concentration of PEG radicals to link to VPM thiols. However, we were only able to achieve up to 60% conversion of thiols, suggesting that the crosslinking mechanism proceeds via radical propagation via the acrylate groups to a greater extent than the thiol-ene reaction. Upon generation of the sulfur radical, it can only undergo chain transfer with another thiol group, which yields another sulfur radical without forming a stable bond, or with an acrylate group, which yields a thioether bond and a carbon radical. However, the carbon radical can either undergo reaction with a thiol group or an acrylate group; thus, the reaction of the carbon radical to acrylate groups proceeds at a greater rate than reaction with thiol. Furthermore, the incomplete degradation of the resulting bulk hydrogels confirmed the lack of sufficient peptide incorporation. While this method was unable to yield the high degree of conversion needed for hydrogel degradation, this process is facile with a single, quick

reaction step and may instead be more applicable where high levels of conversion may not be needed, such as with the incorporation of cell signaling peptides such as RGD[99].

To develop a material to properly degrade under enzymatic conditions, we adjusted the reaction scheme to avoid any unwanted reactions other than the addition of acrylate to thiol groups, similar to other studies investigating MMP-sensitive hydrogels[88]. However, the higher concentration threshold needed for hydrogel gelation indicated that crosslinking density was greatly reduced compared to the thiol-ene photopolymerized hydrogels. Based on the molecular weight of the PEGDA used (700 Da), the spacing between each branch point of the resulting hydrogel was much lower than that of the PEG-VPM hydrogels, which were likely much greater because of the greatly increased molecular weight from the PEG-VPM macromers. The resulting softness of this material also indicates that PEG-VPM particles would likely be unable to reach the endothelium due to frequent inelastic collisions with red blood cells. A stiffer material, closer to the modulus of white blood cells, would instead participate in more elastic collisions driving them to the cell wall, which likely could be achieved using this method by increasing the ratio of PEG to VPM during the conjugation step to generate shorter macromers. However, the softness of this material, while not relevant for vascular targeted drug delivery, may still see use in tissue engineering, where softer materials are more desirable for their ability to act as tissue models and cell scaffolds.

PEGVS-based hydrogels exhibited an increase in Young's modulus, likely from the increased crosslinking density compared to that of the PEG-VPM hydrogels. Since the PEGVS has a 4-armed structure and a molecular weight of 20 kDa, the space between each branch point of the resulting hydrogel network would be composed of two PEG arms and one VPM molecule with a molecular weight of approximately 12 kDa. The increase in crosslinking density also

accounts for the increase in time needed for complete hydrogel degradation, and the facile one-step method to fabricate hydrogels using this click-chemistry method is more advantageous than the conjugation of linear PEG to VPM, which requires purification and rigorous characterization of the macromers prior to crosslinking. Furthermore, the degradation time of this material on a bulk scale is more relevant than with the PEG-VPM hydrogels, as it allows for sufficient time to traverse the vasculature and bind before being enzymatically degraded. Notably, the degradation time for hydrogels using 20 nM MMP-2 was much greater than with 2 μm trypsin, likely from differences in both enzyme concentration and enzyme kinetics. However, particles fabricated with this material would potentially degrade much more quickly than on a bulk scale as investigated in this chapter from the increased surface area to volume ratio.

### 3.5 Conclusion

In this work, we explored multiple synthesis schemes to conjugate and incorporate VPM peptides into PEG-based hydrogels and assessed their bioactivity using trypsin as a model enzyme and feasibility for vascular drug delivery using shear rheometry. The use of a photoinitiator to fabricate photopolymerized PEG hydrogels resulted in densely crosslinked hydrogels with limited VPM incorporation, further noted by their incomplete degradation in a trypsin solution. Instead, controlled conjugation of VPM to PEG molecules using both PEGDA and PEGVS resulted in hydrogels capable of degrading completely in trypsin, yet the differences in crosslinking density indicate that PEGDA-VPM hydrogels were not feasible for use in a vascular context. Overall, we have developed a method for fabricating bioactive hydrogels for the use of vascular targeted drug delivery and contributes to the information on developing materials responsive to biological stimuli. The next chapter of this dissertation will focus on the application of this material and assessing the functionality of PEGVS-based VTCs.

# Chapter 4 : Functional Assessment of Nanoparticle-Loaded Hydrogels for Vascular Targeted Drug Delivery

## 4.1 Abstract

The size mismatch between particles able to localize and bind to the vascular wall and those able to effectively enter the tissue space presents a dilemma in VTC design that does not properly address both of these transport phenomena. To address this gap in VTC design, we have designed a NP-loaded hydrogel MP to first facilitate the transport of NPs to the vascular wall, followed by MP degradation and NP release to the wall and finally into the tissue space. In this chapter, we outline the development and characterization of an NP-loaded hydrogel MP system that can degrade in the presence of MMP-2, an upregulated enzyme in areas of inflammation. We fabricated particles 2 – 4 μm in diameter and found that when incubated with MMP-2, particles were able to fully degrade within 4 – 8 hours. Next, we demonstrated that particles could be conjugated with avidin followed by biotinylated anti-ICAM1, and subsequently showed that these particles adhered to an inflamed endothelium. Finally, we performed adhesion-degradation assays and found that particles in flow could first bind to the endothelium, and upon perfusion of trypsin, showed that these particles could degrade while bound to the cells. The work in this chapter demonstrates the first degradable hydrogel particle to be used in the context of vascular drug delivery and showcases the utility of using hydrogels as a VTC as opposed to more rigid polymeric materials.

## 4.2 Introduction

Nano-sized carriers have long been of interest in the field of vascular drug delivery for the numerous advantages they possess over larger, micron-sized particles, including longer circulation time, ability to traverse the vasculature, and avoidance of immune cell clearance[31,33]. Furthermore, carrier size plays an integral role in a cell's ability to internalize them; indeed, numerous studies throughout the last two decades have reported that particles on the order of 100 nm or smaller are easily internalized by multiple cell types, such as endothelial cells and Caco-2 epithelial cells[34–36].

Aside from navigation of the vasculature and entry into the tissue space, however, VTCs must first reach the endothelium and adhere to enter the tissue space. From this perspective of VTC transport, research has shown that NPs are unable to navigate the complexity of blood flow and instead co-localize with red blood cells in the center of blood vessels, thus limiting their propensity for vascular wall adhesion[38]. In fact, the optimal size to facilitate particle adhesion to the vascular wall in human blood has been reported to be between 2 – 5 μm, well above the upper limit for intracellular delivery[27,37].

Considering the unique advantages and drawbacks of particle carriers on both the micro- and the nano-scale, we see that there is an apparent size mismatch in meeting the design criteria for transport of the carrier first to the vascular wall and then into the tissue space. Thus, to bridge the performance gap between these two size regimes, we have combined the two together by loading NPs into a hydrogel MP. Here, the MP material is made of PEG crosslinked with peptides sensitive to MMPs, similar to other studies developing hydrogel materials that degrade in the presence of trypsin and elastase[55,56]. Thus, by conferring enzyme sensitivity to the hydrogel material and functionalizing the surface with targeting ligands, we can achieve both

site-specific accumulation and degradation near areas of vascular inflammation via inflammation markers and upregulated MMP enzymes, respectively. While previous work has already demonstrated the concept of loading NPs into an MP to facilitate NP delivery to the wall, the PEG carrier used was non-degradable, and so it is yet to be seen whether NPs delivered via an MP will subsequently adhere to the vascular wall. In this chapter, we have characterized the degradation and adhesion of a degradable NP-loaded hydrogel MP as a dual delivery approach for facilitating the transport of NPs to the vascular wall.

### 4.3 Results

We first fabricated PEGVS hydrogel particles using a water-in-oil emulsion of polymer precursor in paraffin oil. Based on prior rheometry data on the PEGVS material, we selected the 30 wt% formulation to be most suitable in terms of material stiffness for our drug carrier applications. After particle formation and subsequent washing, we characterized the particles in terms of size and surface morphology using SEM imaging. As shown in Figure 4.1 (A), the

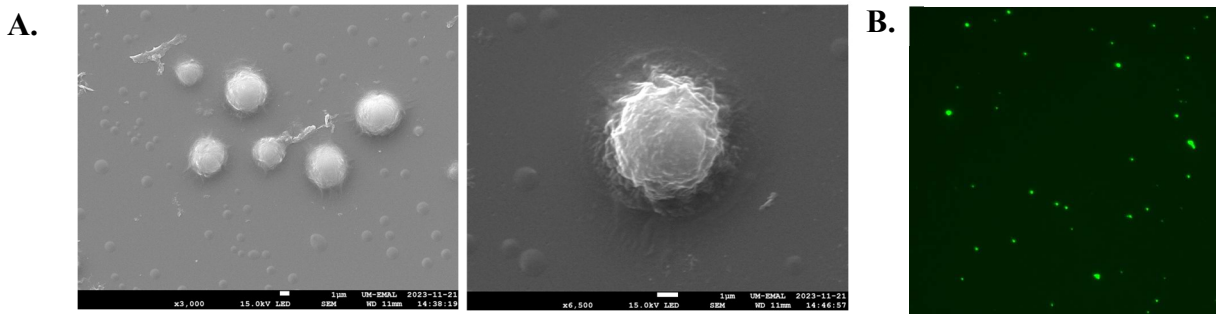


Figure 4.1: (A) SEM images of the 30 wt% PEGVS hydrogel particles (left) and a zoomed-in image (right) of a single particle to more closely visualize particle surface morphology. Scale bars for the SEM images were 1 μm. (B) Fluorescent microscopy image of 30 wt% hydrogels with PS NPs loaded inside.

PEGVS particles ranged between 2 – 4 μm, and the surface morphology of a single particle looks dimpled and collapsed, indicative of their deformable nature. We next measured the zeta potential of the hydrogels using a Malvern zetasizer; we determined that the particles were negatively charged, likely from charges present on the peptide residues as well as the charge of

the PEG backbone. Finally, we imaged the particles using fluorescent microscopy to visually confirm that NPs loaded into the aqueous phase during particle fabrication remained in the particles after washing. Here, PS NPs were loaded into the PEGVS hydrogels as a model NP. As shown in Figure 4.1 (C), particles loaded with FITC NPs fluoresced green, confirming that NPs were successfully loaded into the hydrogel particles.

Next, we confirmed that particles remained bioactive after the centrifugation and washing steps, especially after washing with organic solvents. First, we exposed unloaded particles to 20 nM MMP-2 to confirm that any incorporated peptide could be cleaved by enzymatic degradation when hydrogels were fabricated in particle form as opposed to bulk form. Particle degradation

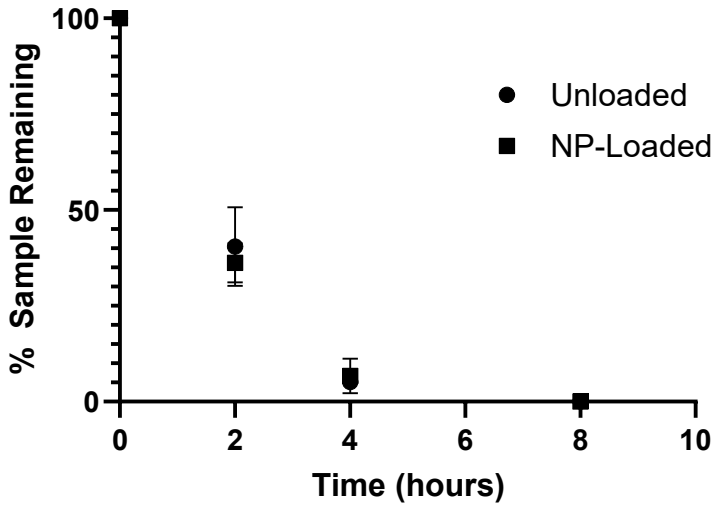


Figure 4.2: Degradation profile of 30 wt% hydrogels either unloaded or loaded with PS NPs. The particles were found to be fully degraded between the 4 – 8-hour timepoint.

was quantified using a fluorescamine reaction to detect the presence of degradation products, and complete degradation was set as the time at which the signal stopped increasing. As shown in Figure 4.2, unconjugated particles were able to degrade completely by the 8-hour mark, and particle degradation was able to be detected even at the 2-hour mark. We also confirmed visually that the particles had degraded due to the lack of an apparent pellet upon centrifugation of the

samples over time. Furthermore, the turbidity of the particle solutions slowly decreased across the timespan of the assay, indicating that particles had degraded into solution. We next incubated NP-loaded hydrogel MPs with 20 nM MMP-2 in tricine buffer to determine whether the addition of NPs would alter the degradation profile of the PEGVS. We found that there were no significant differences between the unloaded and loaded PEGVS particles at the 2- or 4-hour timepoint.

After confirming that our hydrogel particles retained their bioactivity to MMP-2, we next conjugated our particles with both avidin and targeting ligands for adhesion to an inflamed endothelium. Avidin conjugation was performed using a thiolated avidin molecule to react with

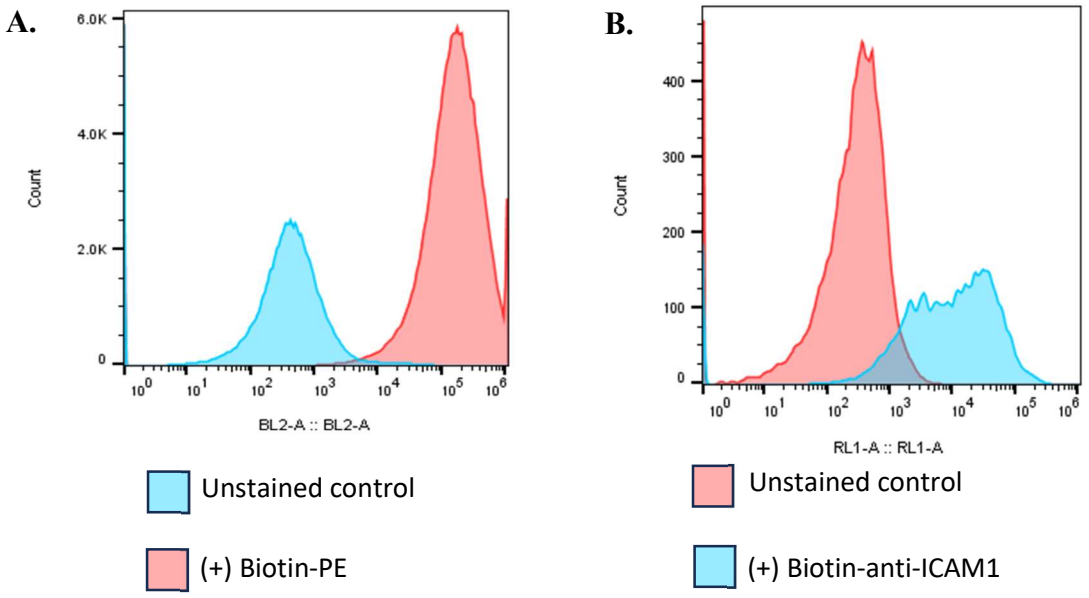


Figure 4.3: Flow cytometry data for the conjugation of (A) avidin and (B) biotinylated anti-ICAM1 to the surface of the hydrogel particles. Successful conjugation was indicated by the shift in the fluorescence peak of the conjugated samples as compared to an unstained control.

residual vinyl sulfone groups on the particle surface. We then confirmed that avidin was successfully attached to the surface via staining with a biotinylated fluorophore and analyzing particles with flow cytometry. As shown in Figure 4.3 (A), particles stained with biotin-PE exhibited a pronounced shift in fluorescence as compared to an unstained control, thus validating

our avidin reaction. Next, we attached targeting ligands to the surface avidin, specifically anti-ICAM1 to bind to ICAM1, respectively, which has been shown to be upregulated in inflamed endothelial cells. Here, we used biotinylated ligands to connect to the conjugated avidin protein on the particle surface, followed by a secondary fluorescent antibody stain to detect the presence of anti-ICAM1. As shown in Figure 4.3 (B), we again were able to detect a shift in the fluorescence peak of the anti-ICAM1-coated particles as opposed to an avidin particle control, thus confirming that our conjugation was successful. Thus, we were able to design a NP-loaded hydrogel MP with the potential to be used for vascular targeted drug delivery.

We then demonstrated that our conjugated microparticles could bind to an inflamed endothelium model by incubating targeted particles with a monolayer of HUVEC. Here, endothelial cells were either left unactivated or activated with a solution of IL-1β over 24 hours to induce maximal ICAM1 expression, followed by incubation of either targeted or untargeted

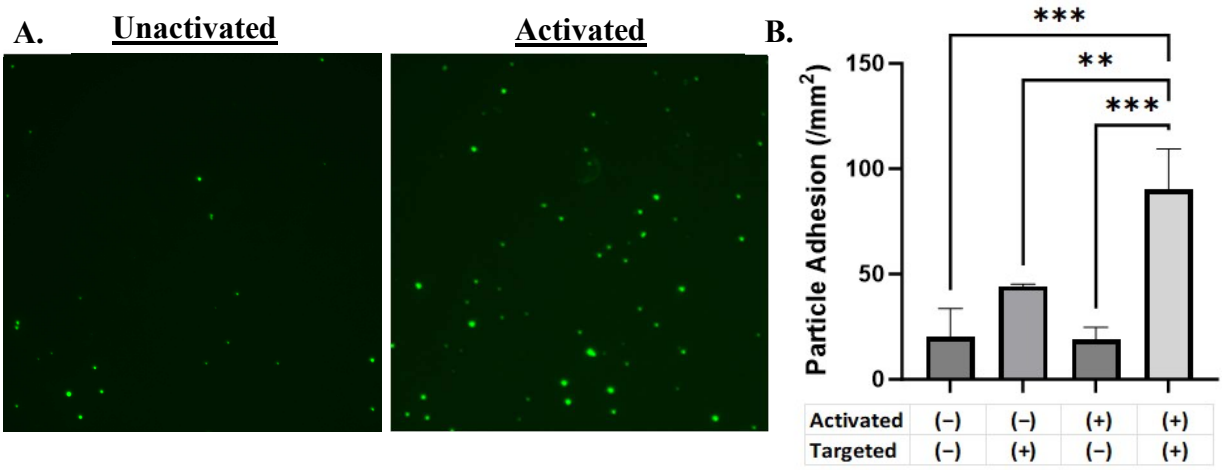


Figure 4.4: (A) Fluorescent microscopy images of 30 wt% hydrogel particles loaded with fluorescent green PS NPs adhered to either an unactivated (left) or activated (right) endothelium. (B) Quantification of the particle adhesion of either targeted or untargeted particles to both an activated and unactivated endothelium to determine nonspecific binding. Using activated particles over an activated endothelium resulted in significantly higher binding than all other cases, which were not significantly different from each other. Statistics were performed using one-way ANOVA with Tukey's multiple comparison test. (**, $P < 0.01$; ***, $P < 0.001$).

particles under static conditions to quantify both specific and nonspecific adhesion. As shown in

Figure 4.4 (A), we were visually able to see more targeted particles bound to an inflamed endothelium as opposed to an uninflamed endothelium. This was further confirmed by the quantification of adhesion density to the HUVEC; as shown in Figure 4.4 (B), untargeted particles had an adhesion density of nearly 20 particles per $mm^2$ for both activated and unactivated HUVEC, indicating minimal nonspecific adhesion. However, though not significant, we did observe a twofold increase in the particle adhesion for targeted particles incubated with an unactivated endothelium. Finally, when we incubated targeted particles to an activated endothelium, we saw a significant 4.5-fold increase in particle adhesion when compared to untargeted particles, and a significant twofold increase in adhesion compared to an uninflamed endothelium. The large increase in particle adhesion of anti-ICAM1-targeted particles to an activated endothelium confirmed that our particles were indeed functioning as vascular targeted carriers.

To finally demonstrate that our particles could improve the delivery of NPs to the vascular wall, we performed an adhesion-degradation assay by first perfusing anti-ICAM1 coated NP-loaded particles through a parallel-plate flow chamber with activated HUVEC, followed by trypsin as a model enzyme. Prior to performing these assays, we first determined

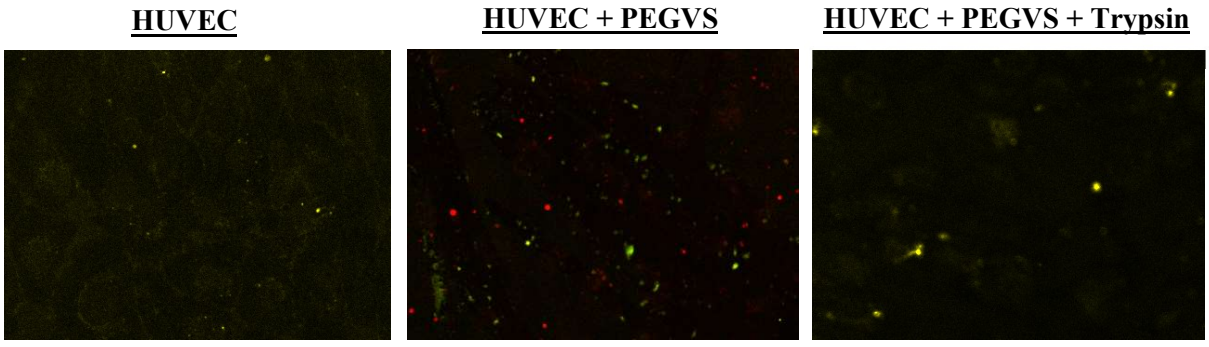


Figure 4.5: Confocal microscopy of a monolayer of fixed HUVEC (left), activated and fixed HUVEC with 30 wt% PEGVS hydrogel particles (center), or activated and fixed HUVEC with particles followed by trypsin enzyme. Hydrogel MPs were loaded with PE-coated PS NPs (red), and HUVEC were stained with wheat germ agglutinin (green). Particles successfully adhered to the endothelium and were found to be degraded when exposed to trypsin.

whether the enzyme buffer used for active MMP-2 would be cytotoxic to the HUVEC. We found that the Brij-35 surfactant used to keep the enzyme in solution was cytotoxic to the endothelial to be used in the adhesion assays. However, we also noticed that when MMP-2 was solubilized in buffer without Brij-35 surfactant, the enzyme tended to precipitate out of solution, as observed by the presence of turbidity in the enzyme solution, rendering it inactive. Thus, for these adhesion assays, we opted to first activate the HUVEC with IL-1β to induce ICAM1 expression followed by fixing of the cells to prevent cell death during the assay. Hydrogels were loaded with PE-stained NPs (red), and the HUVEC layer was stained with FITC conjugated wheat germ agglutinin (green). As shown in Figure 4.5, the HUVEC layer was easily visible, and when PEGVS particles were perfused across the fixed and activated HUVEC, we detected the presence of particles adhered to the cells. Furthermore, when we perfused trypsin through the channel afterwards, we were no longer able to detect the presence of the PEGVS particles, suggesting that they were successfully degraded after being bound to cells. However, we were unable to detect any changes in relative fluorescence of the HUVEC after particle degradation, and thus it remains unclear whether the NPs released from the hydrogel MPs successfully bound to the endothelium.

### 4.4 Discussion

While there have been numerous studies on the use of hydrogel particles in the context of vascular targeted drug delivery, they lack a degradation pathway that allows for site-specific release of any encapsulated cargo. While enzymatic degradable particles have been explored, they have mostly been limited to pulmonary applications and have yet to be used in a vascular context. Thus, in the work detailed in this chapter, we have developed an enzyme-degradable

hydrogel particle functionalized with targeting ligands as a VTC capable of site-specific accumulation and release.

Though the fabrication of the hydrogels follows a similar fabrication method to other peptide-linked hydrogel particle fabrication protocols, a critical step added to our fabrication included the use of hexanes to wash any residual oil on the particle surface that may interfere with enzyme degradation. However, it remains to be seen whether the use of these organic solvents will affect the bioactivity of any therapeutics loaded into the NPs of the hydrogels. During fabrication of the PS NP-loaded hydrogels, we found that the fluorophore encapsulated within the PS matrix leached out of the NPs upon washing with hexanes, likely from the expansion of the PS network in an organic environment. Thus, there is evidence that NPs loaded into the hydrogels, along with any loaded therapeutics, may be affected by the particle fabrication process.

The SEM images of the particles indicate a range of particle sizes between 2 – 4 μm, yet given their dehydrated state, they would likely swell to be larger in an aqueous environment. Thus, these particles may potentially be of a size that typically is associated with risks of capillary occlusion. However, because their deformability is very similar to that of RBCs, which are on the order of 8 – 10 μm and are capable of deforming to traverse capillaries, these particles may present significantly less risk of occlusive events compared to a typically rigid polymeric particle.

Particle degradation was shown to be complete at the 8-hour mark, though nearly all particles had degraded by the 4-hour mark, a significant reduction in degradation time when compared to bulk samples. The greatly shortened time for full degradation is likely due to the vastly increased surface area to volume ratio, since the degradation of the hydrogel material

occurs largely via surface erosion as opposed to bulk degradation. This 4-hour mark for nearly complete degradation is also advantageous because of the timespan at which deformable particles have been shown to be cleared from blood circulation, on the order of 4 – 8 hours[58]. We also hypothesized that NP encapsulation might affect the particle degradation time due to local effects of carboxylic acid groups attached to the NPs that could affect pH. However, the degradation profile of both loaded and unloaded particles was nearly identical, confirming that particle loading did not affect the kinetics of particle degradation.

Conjugation of the particles was performed using a thiolated avidin in place of typical diimide chemistry because the activation and chemical modification of both amine and carboxylic acid groups present on the VPM peptide would potentially render the modified peptide enzymatically inactive. Though each avidin site contains 4 avidin binding sites, we find that the peak shift of the biotin-anti-ICAM1 coated particle is not as pronounced as the shift observed with the biotin-PE particles, indicating that the amount of anti-ICAM1 conjugated to the particle was less than the amount of available avidin sites for biotin binding. Thus, despite saturating the particle surface with anti-ICAM1, we find that we are unable to access the full extent of avidin binding, potentially from steric effects from the size of the antibody compared to the PE fluorophore.

The greatly increased adhesion of the particles to an inflamed endothelium as opposed to an unactivated endothelium demonstrates that our particles were conjugated with active ligands capable of targeting inflammation. While there were only minimal levels of adhesion when using untargeted particles, the increased levels of adhesion when using targeted particles over an unactivated endothelium are likely due to the presence of basal levels of ICAM1 that are typically expressed on endothelial cells. Furthermore, because these assays were performed

under static conditions, the lower binding forces associated with an unactivated endothelium may be sufficient under static conditions. However, under flow, the greatly decreased ICAM1 on the HUVEC may also help to reduce nonspecific binding to off-target endothelium due to shear forces competing with adhesion forces.

For all enzymatic degradation experiments performed with MMP-2, we found that Brij-36 was a critical component to include in the enzyme buffer to retain enzyme activity. However, because of its cytotoxic effects even at lower concentrations, we fixed the HUVEC to avoid cell death. This tricine buffer is not as physiologically relevant as other types of media that could be used to mimic the enzyme environment more accurately, such as human plasma or even human whole blood. Notably, though typical blood anticoagulants include citrate and heparin, the use of citrate to prevent blood coagulation may also interfere with enzyme function due to its ability to chelate calcium ions, which are necessary to maintain enzyme activity. Using these more biologically relevant media would also allow for the use of live HUVEC, which would provide a more accurate model of the conditions under which particles would be adhering and degrading.

While the degradation-adhesion experiment was indeed able to confirm that hydrogel particles bound to the endothelium, we were still unable to visualize any changes in fluorescence of the endothelium after degradation via trypsin, either from a lack of NP adhesion or because the fluorescent signal of the NPs was too low to be detected at this concentration. While commercially available PS typically is quite fluorescent, the incompatibility of the encapsulated fluorophore and our fabrication protocol made fluorescent detection difficult, and even after the conjugation of additional biotin-PE, particles remained quite dim and thus quantification of bound NPs remained difficult. Detection could be made easier via encapsulation of NPs of materials that are either less or not affected by exposure to organic solvents during the wash step,

such as PLGA, silica, titania, or gold, but may also alter other characteristics of the particle, most notably density in the case of these materials listed. Aside from fluorescent detection, we might also employ the use of detection methods such as nanoindentation, which could be used to measure and detect significant spikes in elastic modulus from bound NPs, or imaging cells to visualize bound NPs on cells. Improved NP detection would help to provide more definitive evidence of the function of our NP-loaded MP delivery system.

After further characterization of our NP-loaded hydrogel system *in vitro*, we could then bring our particle system to an *in vivo* system instead, which would provide more insight on how these particles would perform in a more physiologically relevant model. Crucial parameters, such as circulation time, biodistribution, and *in vivo* degradation kinetics, would be necessary to assess the performance of these particles. Furthermore, we have yet to assess the potential therapeutic benefits of these particles, since we have only thus far explored the loading of PS particles. A more biocompatible and biodegradable material choice for NPs would be PLGA, which can be loaded with therapeutics and would degrade into biocompatible degradation products. A potential therapeutic that may hold great utility in the clinic for the treatment of is the use of anti-CD47, which binds to CD47, a marker of self in the body[100]. A previous study by Kojima *et al.* demonstrated the ability of CD47 blocking antibodies to block upregulated CD47 typically associated with atherogenesis, and thus it would be advantageous to delivery of this therapeutic to areas affected by atherosclerosis to improve plaque clearance[101]. While overall, we have successfully developed an NP-loaded hydrogel MP capable of binding to an inflamed endothelium and subsequently degrading enzymatically while bound, we recognize that there is much more work to be done to further characterize and optimize this particle delivery approach. However, if successful, this particle system would represent a flexible platform that could be

tuned by using different peptides and surface ligands to target different enzymes and diseases as well.

### 4.5 Conclusion

In this chapter, we have developed and characterized a hydrogel particle system based on the material developed in the previous chapter. We first characterized the particles after fabrication, followed by the degradation response to MMP-2, finding that the particles were approximately 2 – 4 μm in diameter in a dehydrated and fully degraded between 4 and 8 hours. We then successfully conjugated both avidin and anti-ICAM1 to the particle surface and confirmed that these particles were able to bind to an inflamed endothelium while exhibiting minimal nonspecific adhesion. Finally, when we performed adhesion-degradation assays, we found that particles that were bound to the endothelium degraded following perfusion of trypsin into the flow chamber, as evident by the lack of particles present after the degradation step. However, without confirmation of subsequent NP adhesion to the endothelium, it remains to be seen whether NPs released from the hydrogel particles can successfully be delivered to the wall at a greater rate than free NPs in flow. Though there is more characterization and optimization to be done, overall, we have developed a particle system that can bind to areas of inflammation and respond to inflammatory enzymes and degrade in a site-specific manner.

# Chapter 5 : Enhanced Phagocytosis of Elastic Particles by Primary Human Neutrophils

## 5.1 Abstract

Particle elasticity has widely been established to have a significant influence on immune cell clearance and circulation time of vascular targeted carriers (VTCs). However, the majority of studies in the literature have only investigated interactions with macrophages and monocytic cell lines along with *in vivo* murine models. Interactions between particles and human neutrophils remain largely unexplored yet represent a critical aspect of VTC performance within the context of vascular targeted drug delivery. Here, we explore the impact of particle elasticity on primary human neutrophil phagocytosis using polyethylene glycol (PEG) based particles of different elastic moduli. We found that neutrophils effectively phagocytose deformable particles irrespective of their modulus, indicating a departure from established phagocytosis trends seen with other types of immune cells. Furthermore, we explored potential interplay between particle elasticity and surface modifications, finding that phagocytosis of deformable particles was largely unaffected by altered zeta potential, though surface conjugation using diimide chemistry resulted in reduced particle uptake due to increased albumin adsorption. These findings highlight the observed phenotypic difference between different types of phagocytes and underscore the need for characterization of VTC performance using different cell types and animal models to more closely represent human systems.

## 5.2 Introduction

Vascular targeted carriers (VTCs) are a promising drug delivery approach for treating various conditions, including cancer and coronary artery disease[48,71]. However, a major issue that limits VTCs' *in vivo* efficacy is their rapid removal from circulation through filtration via RES organs and clearance by phagocytic leukocytes[59–61]. Over the years, researchers have explored ways to design VTCs to avoid phagocytic uptake and achieve longer circulation times. Most of these efforts have focused on non-fouling surface coatings such as polyethylene glycol (PEG), cell membrane-derived, and zwitterionic coatings[62–64]. Particle elasticity has emerged as an important factor in designing polymeric particles for intravenous drug delivery applications in recent years due to its favorable effects on phagocytosis.

In this work, we investigate the effects of particle elasticity on neutrophil phagocytosis. Deformable PEG hydrogel particles of varying Young's modulus were exposed to human neutrophils in whole blood, and neutrophil phagocytosis was quantified by flow cytometry as the percentage of particle-positive cells. Additional hydrogel materials were also explored to determine the potential interplay between surface physiochemistry and particle elasticity. Further understanding of interactions between particles and neutrophils will be invaluable in optimizing carrier design in vascular targeted delivery.

## 5.3 Results

### *5.3.1 Evaluation of neutrophil phagocytosis of PEG particles of two distinct elasticities*

We first evaluated the uptake of 2 μm and 500 nm spherical PEG particles by primary human neutrophils in whole blood from healthy donors relative to the uptake of rigid polystyrene particles. Fluorescent polystyrene (PS) particles were purchased from Polysciences, and

deformable PEG particles with embedded rhodamine dye were fabricated in-house, as previously described[47]. The moduli for the deformable PEG particles were determined to be 23 kPa and 500 kPa for the 15 and 50 wt% PEG, respectively[47]. Particles were incubated in fresh human blood for 2 hours, and cell-particle association was evaluated via flow cytometry, using double positive stains for CD11b and CD45 to identify neutrophils. Particle-positive cells were identified by either a positive signal for fluorescein for PS or rhodamine for PEG.

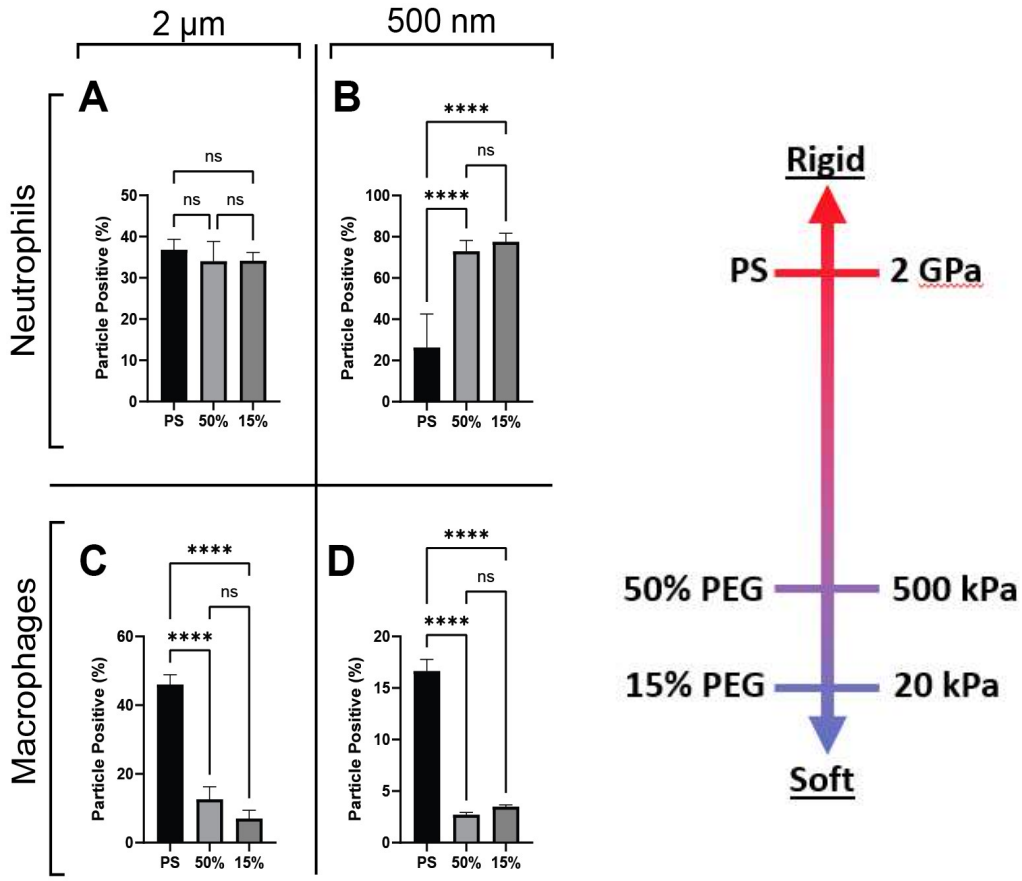


Figure 5.1: Phagocytosis of 2 µm and 500 nm sized PS and PEG particles by (A, B) primary human neutrophils in whole blood and (C, D) J774 macrophages in DMEM with 10% FBS. Samples were incubated with cells for 2 hours before staining, fixing, and analyzing with flow cytometry. Statistical analysis was performed using one-way ANOVA with Tukey's multiple comparisons test. (ns, $P > 0.05$; ****, $P < 0.0001$).

Figure 5.1a-b compares neutrophil uptake of PS and PEG nano- and microspheres in whole blood. Interestingly, all microparticle types exhibited similar uptake levels despite the wide range

of Young's moduli they encompassed, which contradicts previous research that suggests particles of different moduli exhibit different uptake levels[58,65,102]. Additionally, we saw increased neutrophil uptake of the PEG 500 nm nanoparticles compared to PS, where both deformable PEG nanoparticle types had nearly a 3-fold increase in neutrophil uptake compared to PS.

To compare these results to published literature, we repeated uptake assays using J774 macrophages – the most common cell line used in phagocytosis assays. Uptake of 2 μm microspheres by J774 macrophages resulted in a downward trend of phagocytosis levels with decreasing particle modulus, more typical of this cell line with respect to particle elasticity[58,71,103]. As shown in Figure 5.1c, there was a 3 and 6-fold decrease in uptake for the 50% and 15% PEG microspheres, respectively, when compared to PS. Although uptake was decreased by 2-fold for the 15% PEG microspheres as compared to their 50% counterpart, it was not significant. A similar trend was found for 500 nm nanosphere uptake by J774 macrophages, where 50% and 15% PEG nanospheres had a 4.7 and 6-fold decrease, respectively, in uptake compared to PS. We also observed the uptake of PS and PEG particles with mouse neutrophils in whole mouse blood, as shown in Figure 5.6. Mouse neutrophils phagocytosed 2 μm PEG particles at a greater rate than the PS control, with the 15% particle having a 1.7-fold increase in uptake and the 50% particle having a 1.2-fold increase, although the latter was not statistically significant.

### *5.3.2 Evaluation of impact of particle chemistry on neutrophil phagocytosis of deformable particles*

To determine if the differences in particle uptake between neutrophil and macrophage reported in Figure 5.1 are indeed due to deformability or could be attributed to changes in surface chemistry between PS and PEG, we next sought to fabricate hydrogel particles of a different material from PEG. For this purpose, we used hyaluronic acid methacrylate (HAMA) as an

analogous material to compare to PEG particles. HA is an extracellular matrix (ECM) component and recent studies have used chemically modified HA for numerous applications, including cell scaffolding and pulmonary and vascular delivery[90,104–108]. First, we characterized the elasticity of our HAMA hydrogel material using bulk hydrogel rheometry to confirm that their Young's modulus was comparable to the PEG hydrogels. As shown in Figure 5.2a, we obtained hydrogel samples with Young's moduli ranging from approximately 46 kPa up to 730 kPa, matching closely with the range of reported Young's moduli for the PEG material (23 kPa to 500 kPa)[47]. The 2.5% HAMA material was not explored further due to its similarities in modulus compared to the 5% HAMA formulation.

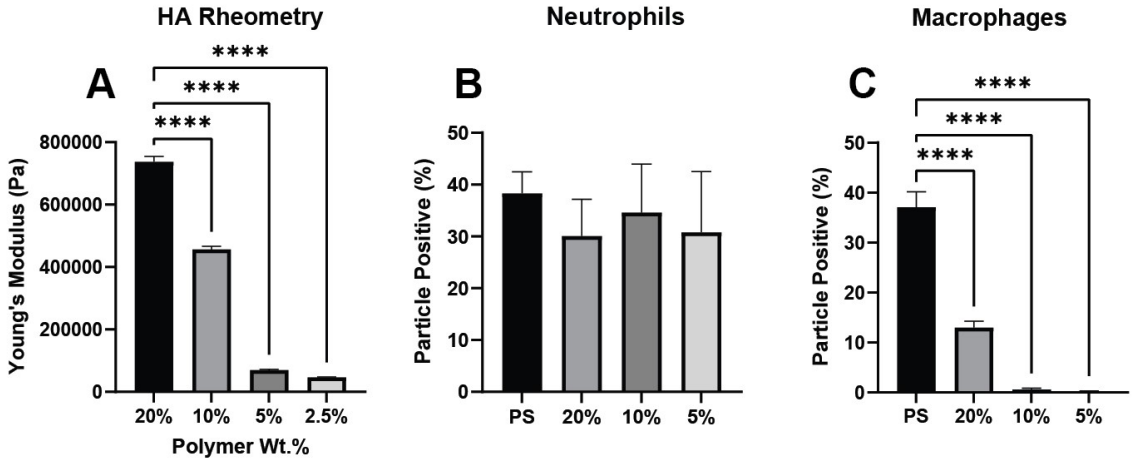


Figure 5.2: (A) Rheometry of bulk HA hydrogel samples, indicating a wide range of Young's moduli. Uptake of 2 µm sized HA-derived hydrogel particles in by (B) primary human neutrophils in whole blood and (C) J774 macrophages in DMEM media. Statistics for the phagocytosis assays were performed using one-way ANOVA with Dunnett's multiple comparisons test, while the rheometry data was analyzed with one-way ANOVA with Šídák's multiple comparisons test. Error bars represent standard deviation. All particle conditions were not significant in the case of neutrophils. (ns, $P > 0.05$; ****, $P < 0.0001$).

Figure 5.2b shows that neutrophils take up HAMA particles at nearly equal levels regardless of the particle modulus, similar to observation with PEG particles. Conversely, when HAMA particles were incubated with J774 macrophages, as in Figure 5.2c, we observed a significant decrease in uptake of HAMA particles with decreasing modulus. The uptake of 20% HAMA

particles was nearly 3-fold lower than the PS control, while the 10% and 5% HAMA particles exhibited a 60 and 150-fold decrease, respectively.

### *5.3.3 Visual observation of deformable PEG particles phagocytosis in optical tweezer assays*

While the phagocytosis assays performed using particles in whole blood allows for analysis of neutrophil behavior on a population level, we were interested in visualizing cell-particle interactions in real time to observe the behavior of single cells and any apparent effects of membrane wrapping on deformable particles. To achieve this, we used an optical tweezer system previously employed in similar studies for imaging engulfment of PS particles by neutrophils[109,110]. Microspheres 2 μm-sized and leukocytes were incubated in the presence of an optical tweezer, allowing for single particle manipulation. As shown in Figure 5.3, when a PS particle was placed in contact with a neutrophil, the neutrophil captures the particle on its membrane surface and begins engulfing the particle during the 5-minute window in which the cell was observed, and by the 2-minute mark, the PS particle is fully engulfed by the cell. Similarly, when a PEG particle was delivered to a neutrophil, it was visually fully inside the cell by the 3-minute mark. These observations are consistent with the previous assays with phagocytosis in whole blood in Figure 5.1.

When J774 macrophages were used instead of neutrophils, we observed differences in the particle-cell interactions. As shown in Figure 3, a macrophage was observed to engulf a 2 μm polystyrene particle within 2 minutes, similar to the timescale for phagocytosis of a particle by a neutrophil. However, when a PEG particle was in contact with a macrophage, the particle was not fully engulfed by the cell, even by the 5-minute mark. The particle instead stayed on the periphery of the cell membrane, and when the optical tweezers were moved off the particle after the assay, the

particle detached from the cell, indicating the particle was only weakly bound to the cell membrane.

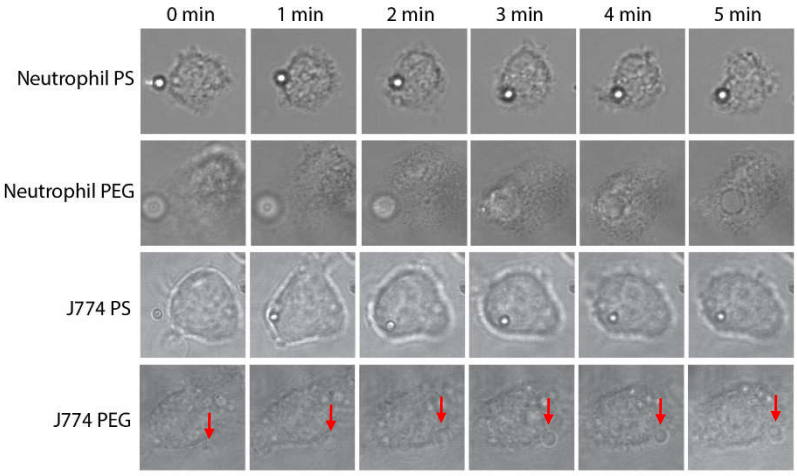


Figure 5.3: Optical tweezer images where a single 2 μm particle was brought into contact with a cell. Assays were carried out with either primary human neutrophils with (A) PS or (B) PEG or cultured J774 macrophages with (C) PS or (D) PEG. Frames were selected at one-minute intervals to visualize particles as they were engulfed by cells. The PEG particle was unable to be phagocytosed by the J774 macrophage, as indicated by the red arrow near the periphery of the cell.

As expected, when both neutrophils and J774 macrophages were brought into contact with a PS particle, the apparent shape of the particle remained unchanged throughout the engulfment process due to the rigidity of PS. However, we were still unable to detect any shape change when the cells engaged PEG particles, despite the particle modulus being well below the stiffness of other particle types shown to deform when engulfed by macrophages[111,112].

### *5.3.4 Evaluation of effects of zeta potential on neutrophil phagocytosis of PEG particles*

Particle surface charge as defined by the zeta potential has been shown to impact phagocytosis in macrophages[113,114]. Thus, we investigated the potential interplay between particle zeta potential and deformability and phagocytosis by neutrophils. To alter the zeta potential, we adjusted the polymer formulation to include an amino-containing linker, 2-aminoethyl methacrylate hydrochloride (AEM) in place of 2-carboxyethyl acrylate (CEA), resulting in

positively charged particles. To achieve near-neutrally charged particles, i.e., a zeta potential as close to zero, we used a mixture of AEM and CEA. We confirmed that the zeta potential was altered from the negative charge typically associated with the incorporation of the carboxylic acid-containing CEA and that a combination of CEA and AEM resulted in a roughly neutrally charged PEG particle, as shown in Figure 5.7.

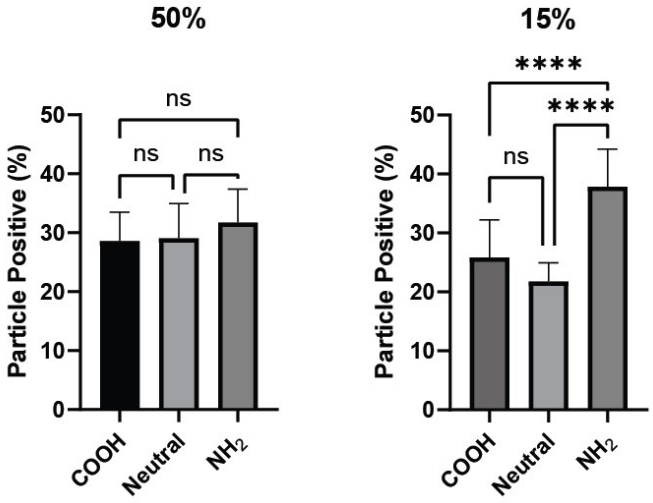


Figure 5.4: 2 µm sized PEG particles of varying zeta potentials (either positive, negative, or neutral) were incubated with primary human neutrophils in whole blood. Displayed zeta potentials confirmed successful surface modification of surface charge using an amino-group containing linker. Significance was determined using one-way ANOVA with Tukey's multiple comparisons test. Error bars represent standard deviation (ns, $P > 0.05$; ****, $P < 0.0001$)

Interestingly, when 50 wt% PEG particles of various surface charges were incubated with neutrophils in whole blood (Figure 5.4), we saw comparable uptake levels across all zeta potentials. For the 15 wt% PEG particles, negatively and neutrally charged particles exhibited nearly the same uptake levels. However, the uptake of the amino-coated 15% PEG particles was 1.5-fold and 1.7-fold greater than the carboxy-coated and neutral 15% particles, respectively.

We conducted phagocytosis assays with isolated neutrophils in RPMI media to see if the cells would differentially phagocytose particles of different surface charges in the absence of plasma proteins since zeta potential strongly affects the adsorption of opsonins that drives phagocytosis[115–117]. As shown in Figure 5.8, we again saw similar levels of uptake for both the

15% and 50% PEG particles across all zeta potentials tested, though the relative uptake of particles in media was notably lower than in whole blood, likely from the absence of opsonins that typically drive phagocytosis, such as immunoglobulins and apolipoproteins[68,118,119].

### *5.3.5 Evaluation of particle surface functionalization impact on particle neutrophil phagocytosis in whole blood*

Particle surface functionalization with targeting ligands is particularly relevant for those used as VTCs. Thus, we next used functionalized particles to elucidate any impacts of particle surface conjugation on neutrophil phagocytosis. We employed diimide (EDC) chemistry to activate carboxylic acid groups on the particle surface before linking avidin protein to the activated groups[27,47]. Surface-conjugated particles were incubated with neutrophils in whole blood and their uptake was compared to unconjugated particles. In Figure 5.5, neutrophil phagocytosis of PEG particles activated with EDC decreased significantly compared to unactivated ones for both the 50% and the 15% wt PEG formulations. The 50% particle type displayed a 25% reduction in uptake when comparing EDC-activated particles to an unconjugated control. We find the reduction of PEG particle uptake with EDC activation was not eliminated with the coupling of avidin protein to the activate groups on particles. The reduction in particle uptake was 33% when comparing an avidin-coated particle to an unconjugated control. Similarly, when comparing 15% EDC-activated and avidin-coated particles to an unconjugated control, we observed a reduction of 45% and 50%, respectively, in neutrophil phagocytosis. The dotted line in Figure 5.5 corresponds to the average uptake of the corresponding PEG particle by J774 macrophages shown previously, demonstrating that this reduction in neutrophil uptake due to conjugation is not as pronounced as the reduced uptake observed when macrophages engaged highly elastic particles relative to rigid PS.

Based on the data in the prior figures, we determined that these apparent differences in uptake were likely not linked to differences in particle deformability or altered zeta potential. Thus, to account for these differences in particle uptake, we next looked at any differences in protein adsorption, which have been strongly correlated with particle recognition and phagocytosis. Using SDS-PAGE to analyze the protein corona of the particles, we found that there were distinct bands present on both the EDC-activated and avidin-conjugated particles, which were not present on the unconjugated control, most notably at around 60 kDa, which was present for both EDC and avidin conditions. To determine if this differential protein adsorption with conjugation is linked to the EDC chemistry or due to surface morphology changes, we incubated PEG particles coated with avidin using thiol-ene click chemistry, circumventing the use of EDC. As shown in Figure 5.9, when EDC was removed from the coupling process, we did not observe any differences in

neutrophil uptake of avidin-coated particles compared to an unconjugated control. This data was further supported by the similarities in protein corona between the two particle types.

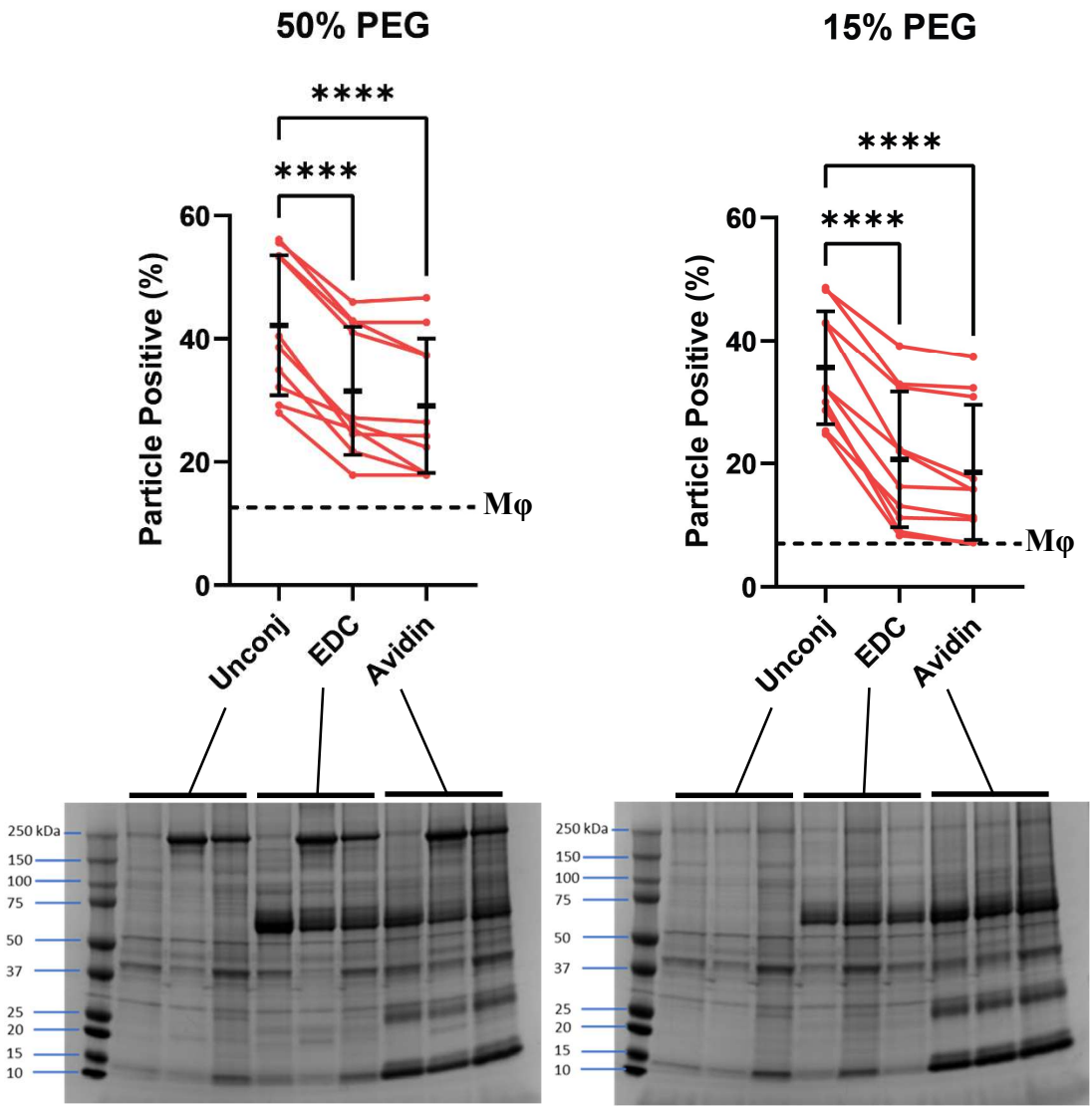


Figure 5.5: 2 µm sized PEG particles either unconjugated, activated with EDC, or covalently coated with Avidin were incubated with primary human neutrophils in whole blood. Data average is shown as horizontal check with error bars. For comparison, the dotted line on each graph represents the average uptake of each respective particle by J774 macrophages. The protein coronas of these particles were also visualized using SDS-PAGE and stained with Coomassie Blue. There were notable bands for both EDC activation and avidin coating around 60 kDa. Statistics for phagocytosis assays were performed using repeated measures one-way ANOVA with Dunnett's multiple comparisons test. Error bars represent standard deviation (ns, $P > 0.05$; ****, $P < 0.0001$)

## 5.4 Discussion

The current literature regarding phagocytosis of particles by immune cells has largely focused on macrophages and monocytes, with few papers exploring the use of neutrophils, likely due to difficulties in obtaining fresh neutrophils combined with a lack of a reliable neutrophil-like cell lines for culture. As more studies look at interactions between particles and neutrophils, differences in their phagocytic behavior relative to other immune cells have begun to arise. For example, a study by Kelley *et al*. showed that PEGylation of particles can cause enhanced phagocytosis by primary human neutrophils in human blood instead of reducing uptake as seen with THP-1 monocytes and bone marrow-derived macrophages from mice[73]. Similarly, a study by Safari *et al*. saw notably higher phagocytosis of rod-shaped particles by neutrophils than spheres compared to rat alveolar macrophages and primary human monocytes[74]. These studies emphasize the critical need for characterization of neutrophil interactions with particle carriers, which have to date been understudied. Thus, we sought to determine whether cell-particle interactions between neutrophils and particles of different elasticities would depart from accepted trends in the literature regarding phagocytosis by macrophages and monocytes.

Based on the vast amount of literature on interactions between immune cells and particles of varying moduli, we expected to see a reduction in uptake as we moved from a rigid polystyrene control to softer PEG-derived particles. Instead, neutrophils were as likely or more likely to phagocytose softer particles compared to the non-deformable polystyrene, suggesting that modulus may not be as effective of a parameter to leverage when designing particles to avoid clearance by neutrophils, most notably in vascular drug delivery, where they are likely the first phagocytes encountered by intravenously delivered particles. The data furthermore suggests that the mechanism by which deformable particles are more likely to be phagocytosed is exaggerated

when neutrophils encounter nanoparticles as opposed to microparticles. Given the relevance of nanoparticles compared to microparticles in current vascular delivery technologies, these results indicate there may in fact be a loss of efficacy by using more deformable particles, given the higher propensity for clearance by neutrophils. We hypothesize that these differences in uptake may arise from the deformation of the PEG particles as they undergo membrane wrapping by neutrophils, resulting in an enhanced phagocytosis effect due to an apparent elongated particle shape as the particle is engulfed[112]. Similarly, we see a reduction in uptake by J774 macrophages because of their reported inability to effectively phagocytose rod-like particles, which has been linked to a higher energy barrier of membrane wrapping[120,121]. The results with HA microparticles, with different hydrogel chemistry from PEG, support the hypothesis that the difference in uptake is due to neutrophils sensing the particle stiffness. Notably, the neutrophil uptake levels of HA particles were comparable to that seen with PEG particles, providing strong evidence that this enhanced phagocytosis effect is indeed linked to particle modulus.

Interestingly, we did not observe significant deformation of the PEG particles when engulfed by both neutrophils in our optical tweezer assay, though prior studies successfully imaged particle deformation with macrophages phagocytosing notably stiffer particles that used here – between two and three orders of magnitude higher[111]. Our inability to visualize any changes in particle shape during the engulfment process with our optical tweezer system may be due to the use of micron sized particles, because of instrument limitations, as opposed to nano-sized particles with prior studies. It is also possible that the lack of shape change with neutrophil phagocytosis may be linked to differences in forces exerted by macrophages and neutrophils. Considering that the PEG particle detached from the macrophage after the tweezer assay was complete, the lack of phagocytosis may also be linked to their inability to adhere to the particle as well as energetic

barriers to membrane wrapping of a deformable particle. One modification that may be employed in future imaging studies may come in the form of flipper dyes incorporated into the particle matrix, which would allow for more sensitive measurements of particle deformation than visual shape changes. Furthermore, the ability to image nanoparticles during phagocytosis would help to elucidate the mechanism by which we see this enhanced phagocytosis of deformable particles, as well as further characterization of the biomechanics of neutrophil phagocytosis.

Past literature has reported that both negatively and positively charged cellulose-derived particles were effectively taken up by mouse peritoneal macrophages, while a neutrally charged particle exhibited a sharp reduction in uptake[113]. Many studies in the literature have accordingly leveraged this phenomenon to modulate zeta potential, most notably with zwitterionic coatings, to either reduce or eliminate the protein corona and thereby avoid immune cell recognition[61,62,122]. Given the implications of zeta potential on plasma protein adsorption and observed behavior with macrophages, we predicted a similar reduction in uptake at a neutral charge as well with neutrophils in whole blood. However, the surprisingly equal uptake of 50% PEG particles observed across all charges suggests that there may be competing forces affecting neutrophil uptake. While a neutral charge typically lowers phagocytosis, our findings indicate that a deformable particle is also more likely to be taken up by neutrophils, which may explain the lack of reduced uptake. The only significantly different particle type was the increase in uptake of positively charged 15% PEG particles, which was likely due to the greater positive charge on the 15% particle compared to the 50% particle, which drives phagocytosis to a greater extent than a stronger negative charge[113]. Similar results obtained when using isolated neutrophils in media support our hypothesis that these observations are indeed linked to deformability as opposed to any differences in protein corona.

Because VTCs typically are functionalized with targeting ligands for adhesion to cellular markers, we also investigated the effects of surface modification on neutrophil phagocytosis. Previous studies have indicated that surface functionalization enhances phagocytosis, yet the decrease in uptake by neutrophils suggests that these modifications to the particle surface may help in evading immune cell clearance when delivered intravenously[123,124]. After running SDS-PAGE, we saw a distinct band at the 60 kDa mark that was not present on unconjugated particles. This protein is likely albumin, a highly prevalent plasma protein given the molecular weight. Albumin, a dysopsonin, has been shown to protect particles from immune cell recognition and clearance, and may be the cause for the reduced phagocytosis observed in neutrophils[125–128]. Compared to SDS-PAGE gels of particles activated with EDC, we did not see an increase in band intensity at the 60 kDa mark corresponding to albumin, thus confirming that the reduced uptake was indeed linked to the EDC causing an increased adsorption of proteins on the particle surface. Given the more drastic decrease in macrophage uptake of deformable particles, we find that there may still be concerns with enhanced phagocytosis of deformable particles by neutrophils despite the reduction in uptake upon conjugation.

Our work seeks to advance our understanding of interactions between particle drug carriers and neutrophils, which historically have not been as well characterized as macrophages and monocytes, especially in the context of vascular drug delivery. Our results here suggest that the reported benefits of deformable particles, including longer circulation times and more effective avoidance of clearance by tissue-resident macrophages and monocytes, may not hold true with respect to neutrophils. We find that a deformable particle instead exhibits an enhanced phagocytic effect, which might instead undermine efforts to improve vascular-targeted drug delivery. Indeed, work in this space will need to further explore potential interplay between deformability and other

design parameters, such as density and shape. Our results here also highlight the potential shortcomings of mouse models and cell lines, which may be less physiologically relevant with respect to neutrophils and vascular drug delivery, along with a need for greater characterization of neutrophils and their interactions with particle drug carriers.

## 5.5 Supplementary Figures

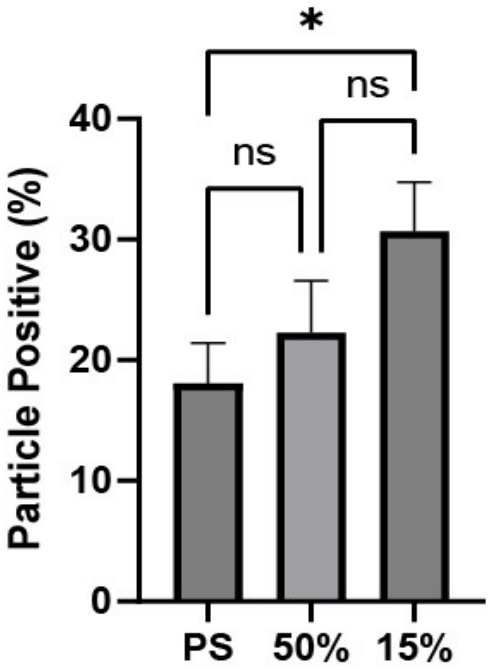


Figure 5.6: Uptake of 2 μm PS and PEG particles by BalbC mouse neutrophils in whole mouse blood. Particle uptake was increased when going from a stiffer to softer particle, with the 15% PEG particle being significantly higher than the PS particle. Statistics were performed using one-way ANOVA with Tukey's multiple comparisons test. Error bars represent standard deviation. (ns, $P > 0.05$; *, $P < 0.05$)

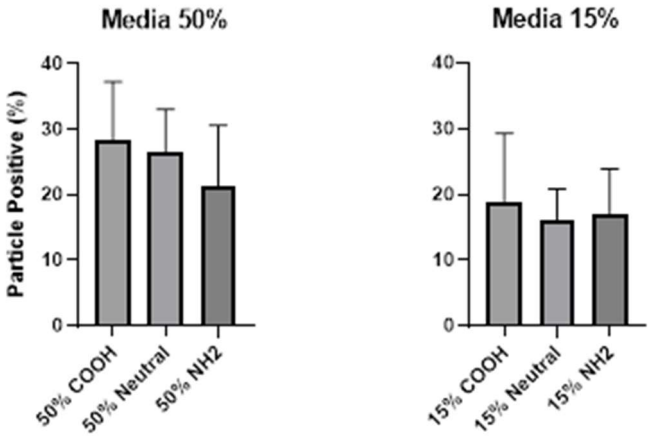


Figure 5.7: Uptake of particles of varying surface charges by isolated neutrophils in RPMI media. No significant differences in particle uptake were seen for either particle types. Statistics were performed using one-way ANOVA with Tukey's multiple comparisons test.

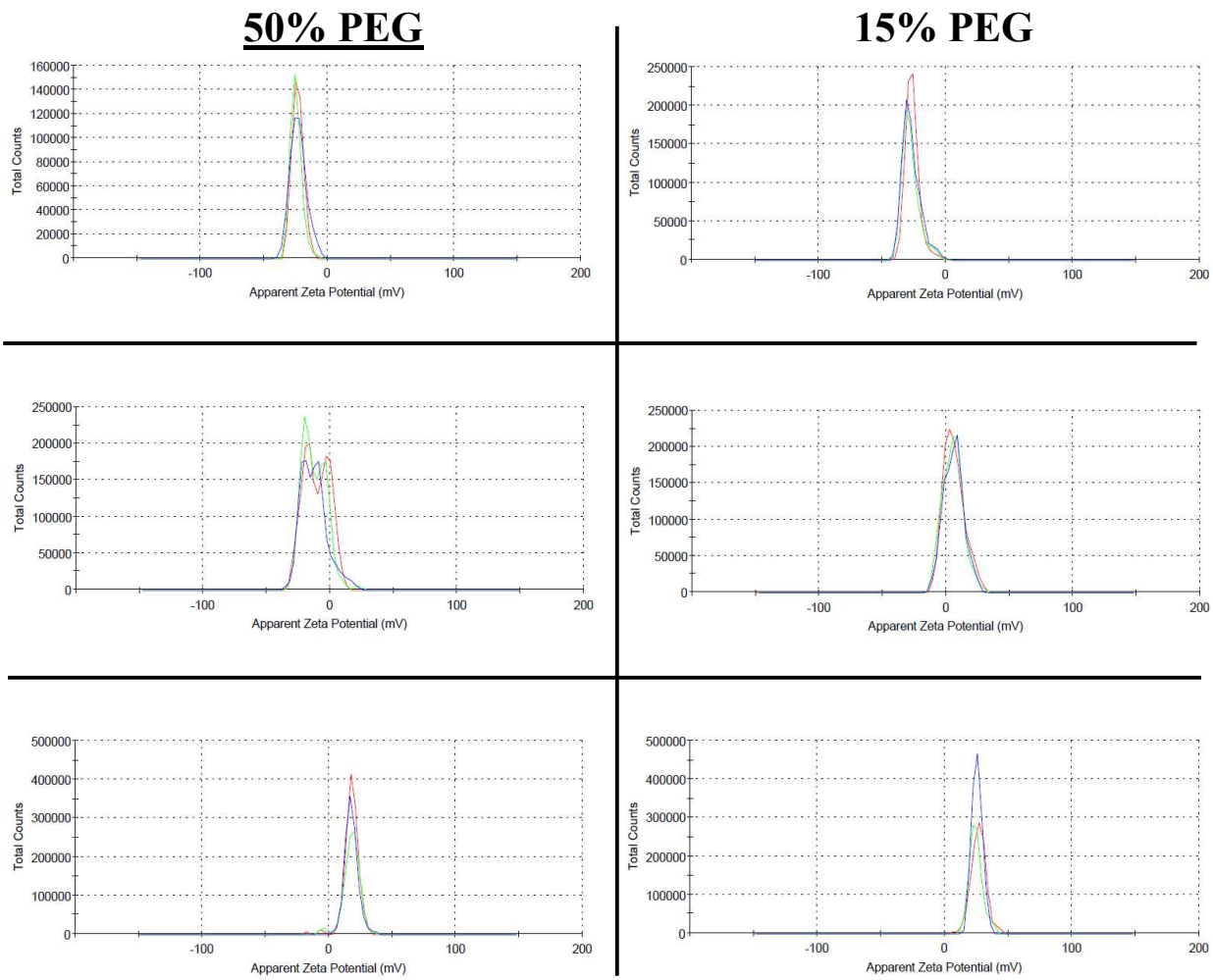


Figure 5.8: Zeta potential measurements for both 50% and 15% PEG particles with varying ratios of – COOH and – NH2 surface functional groups. Particle formulations were designed to either have a negative (top), neutral (middle), or positive charge (bottom).

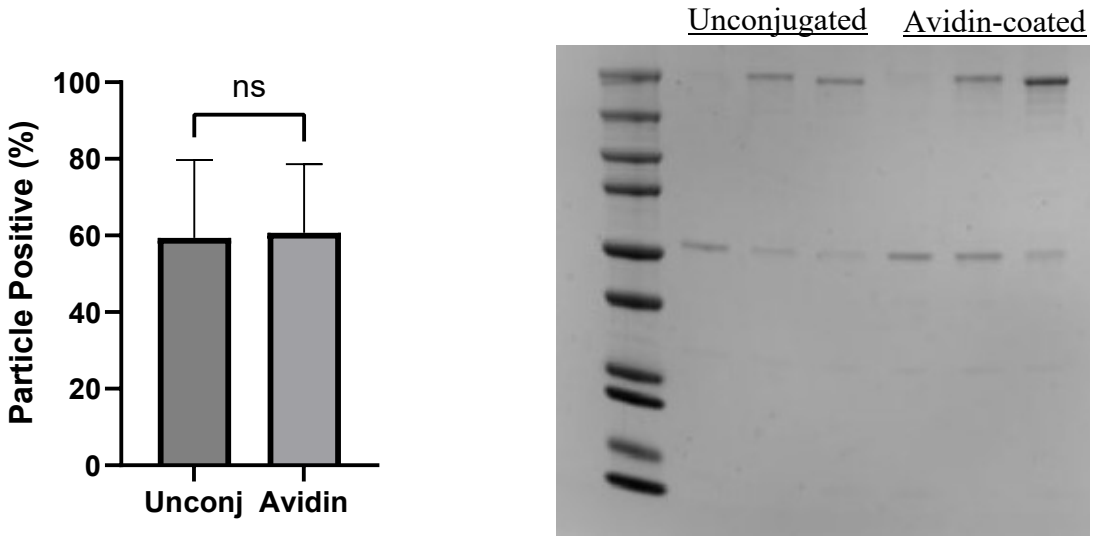


Figure 5.9: Uptake of unconjugated and avidin-coated PEG particles by neutrophils and corresponding protein coronas using SDS-PAGE. Particles were conjugated with avidin using thiol-ene click chemistry, and there were no significant differences in neutrophil uptake between unconjugated particles and avidin-coated particles. No notable differences were seen for the protein corona of these particle types. Statistics were performed using an unpaired t test.

# Chapter 6 : Rod-shaped Hydrogels for Biological Applications

## 6.1 Abstract

Elongated particles, including rods and fibers, have utility for their unique interactions in various biological contexts, yet are not as well studied as spherical particles, in part due to more complicated fabrication processes. The work in this chapter outlines the development of a novel process for deforming polymer droplets in shear and crosslinking those particles in that deformed state. We explored both cup-and-bob and cone-and-plate geometries for their ability to generate simple shear profiles, yet only achieved limited stretching. These rotational-driven shear systems also had the disadvantage of needing rigorous alignment of geometry, which was difficult to achieve and resulted in significant debris generation and fragmentation of any generated particles. We found a tube shear system instead generated stretched particles at a greater proportion, yet because of the inherent deformation gradient of a pipe, a portion of the particles remained spherical. Population analysis of particles fabricated at different shear rates indicated that predeformation particle size was relatively unchanging at an average of 5 μm, but AR increased from 1 – 3.5 as shear rate increased from 0 – 1400 $s^{-1}$. Centrifugal separation of the particles allowed for isolation of increasingly smaller ESD and AR particles. Finally, HAMA was used in place of PEG to expand on the types of materials that can be stretched using this method, and we were able to achieve limited success, fabricating a minor amount of stretched HA particles. However, the majority of particles were fragmented. Overall, this work demonstrates the feasibility of droplet shear as a method for the fabrication of hydrogel rods and fibers in a scalable, continuous process.

## 6.2 Introduction

While spherical particles have been heavily studied, in part due to their facile production as compared to other, more complex geometries, shape is a significant factor to consider in the context of particle-based technologies[129–132]. Many studies investigating particle shape have found that target geometry can affect how these particles interact with various biological processes, particularly rod-shaped and fibrous particles[120,133,134]. Rod-like particles have exhibited improved ability to reach the endothelial wall in the context of vascular drug delivery and reduced immune cell uptake and clearance by macrophages[120,135]. Furthermore, the anisotropic properties and propensity for alignment of fibrous hydrogels are also useful for providing effective scaffolding for skeletal muscle tissue[120,135–137].

There are numerous traditional fabrication strategies for generating hydrogel fibers, including electrospinning, use of microfluidic devices, and extrusion processes[137,138]. The electrospinning process involves pumping out polymer solution onto a needle tip and subjecting it to a high voltage to form polymer fibers that can then be processed further. This process is useful for producing fibrous hydrogel on the microscale, yet lacks the flexibility of other techniques due to the limiting types of hydrogel materials that can be used to generate defect-free fibers. Microfluidic devices are similarly useful for producing consistent fibers, yet lack scalability, typically needing complex production methods to build the devices. Finally, extrusion-based processes involve pumping polymer solution into extruders, such as needles or tubing, and subsequently crosslinking them, but processing steps render this method unfeasible for biological applications. This process typically involves the use of UV crosslinking that is not suitable for cell-encapsulation and viability, though cell adhesion post-processing may still have potential for UV crosslinked hydrogels. Overall, these processes are also unable to produce rod-

like particles on the micro- or nanoscale needed for drug carrier applications. For the purpose of vascular targeted drug delivery, rods are typically around 2 μm in ESD with an AR of up to 6, based on previous work[74]. Conversely, fibrous hydrogels are typically larger and more elongated, with an AR > 10[137].

Within the context of vascular targeted drug delivery, fabrication of rod-shaped particle drug carriers includes microfluidic devices, templating, and heat stretching of spherical particles[60,120,134]. Microfluidic devices and templating processes typically require complicated setups; while they can precisely fabricate uniform particles, they lack scalability and high throughput. Furthermore, the temperatures required for heat stretching likely would result in degradation of the loaded therapeutic and limit potential carrier materials (thermal stability, no crosslinked materials). Emulsion based fabrication methods are effective at generating micron-sized spherical particles with both high yield and scalability. However, they have not yet thoroughly been explored due to difficulties in attaining rod-shaped polymer droplets.

The elongation of polymer droplets in an emulsion is largely dictated by competing forces of interfacial tension between the oil and water phases promoting a spherical droplet and viscous shear forces imparted on the droplets promoting deformation. This phenomenon is captured by the Capillary number Ca, which can be represented as:

$$Ca = \frac{\mu r \dot{\gamma}}{\sigma}$$

where $\mu$ represents the viscosity of the bulk fluid, $r$ is the radius of the droplet, $\dot{\gamma}$ is the shear rate, and $\sigma$ is the interfacial tension[139–141]. In order for droplet elongation to occur, this parameter needs to be above 1, where the viscous shear forces are able to overcome interfacial tension forces that retain a spherical shape. Thus, to achieve an increased capillary number, we can

increase shear rate, viscosity of the carrier fluid, and droplet radius. Additionally, we can lower surface tension, which can be achieved via use of surfactants.

In this chapter, we explore various types of shear geometry to develop a high-throughput method for generation of rod-shaped hydrogel particles. The resulting particles were characterized by size and shape, and particles were then separated by size for potential use in applications such as phagocytosis assays, margination studies, and drug release profiles. The methodologies described in this chapter provide useful insights on developing a scalable method of fabricating particles on a usable size scale for vascular targeted drug delivery, as well as generation of larger, fibrous hydrogels that may see applications in skeletal muscle tissue regeneration.

### 6.3 Results

The generation of shear forces for production of elongated hydrogel rods was initially modelled after various rheometers to generate simple shear. We first used a cup and bob geometry to mimic the type of shear that would be seen in a typical Couette rheometer, as shown in Figure 6.1 (A). The polymer emulsion was placed between the gap, and rotational shear was

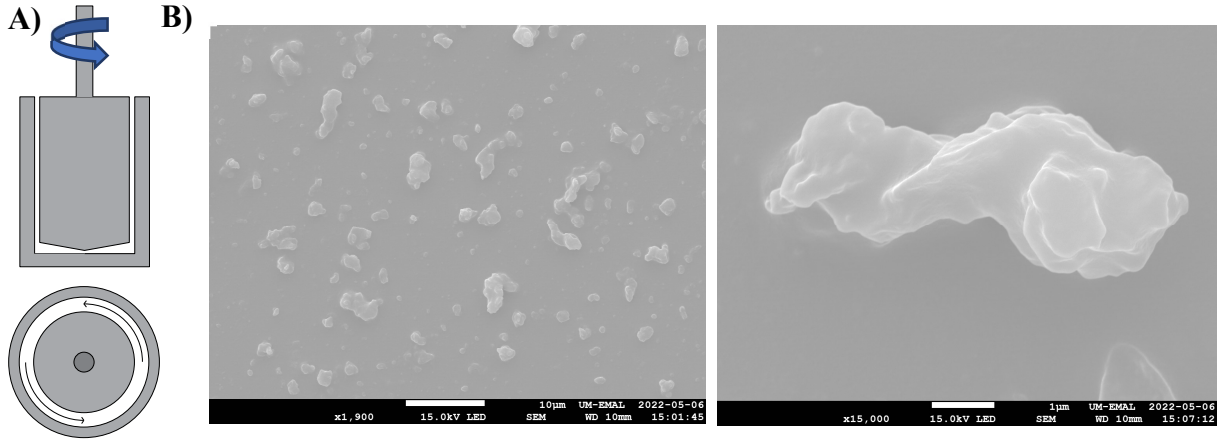


Figure 6.1: (A) schematic of the cup-and-bob geometry used to shear PEG polymer droplets. (B) SEM images of the resulting particles. Scale bar: 10 µm (left) and 1 µm (right)

applied to first deform the polymer droplets and subsequently crosslink them with UV. These particles were then imaged using both light microscopy and SEM, as shown in Figure 6.1 (B). The size of these particles ranged between 1 – 5 μm and were mostly nonspherical. The granularity of the particles indicated that these particle shapes were not due to droplet stretching, and instead, the polymer droplets were likely being destroyed or fragmented on formation. This could be due to multiple causes, such as the heat generated during fabrication or misalignment between the stationary and rotating sections of the shear geometries. Furthermore, the generation of resin debris in the sample indicated that this geometry would not be feasible for rod production on a lab scale without a significant investment in precise geometry and alignment.

We next modified our geometry to a cone and plate, which reduced the required precision on geometry alignment while retaining a similar shear profile to that of the cup and bob. However, with this geometry, we had better control over the shear forces generated by the rotational plate by adjusting the cone angle as well as the speed of rotation. A general schematic of the cone and plate is demonstrated in Figure 6.2 (A). After rod fabrication, particles were

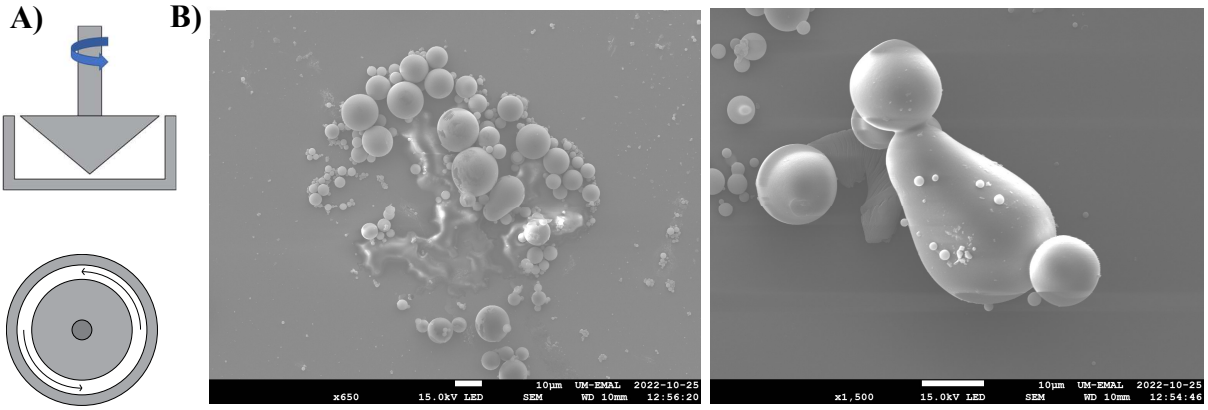


Figure 6.2: (A) Schematic of the cone-and-plate geometry. (B) SEM images of particles fabricated using the cone-and-plate. The asymmetrical shape of the particles indicates they were undergoing breakoff when crosslinked, and the majority of the particles remained spherical.

imaged on SEM to determine both particle shape and surface morphology, as shown in Figure 6.2 (B). We found that the surface morphology of these particles was quite smooth, indicating

that particles were formed properly in the emulsion process, with a particle size between 2 – 20 μm, which was larger than particle generated with the cup and bob. However, we saw that particles were inconsistently generated, with a significant portion of them being spherical, yet a small portion of generated particles were elongated, confirming that particles could indeed be stretched while in polymer solution and crosslinked in an elongated state. The heterogeneity of the particles indicated that the shear force generated by this cone and plate setup were not consistent throughout the fabrication process, likely due to small deviations in alignment between the rotating cone and the stationary plate along with potential bending of the 3D printed cone. Another design issue with the rotational driven setups is the potential loss in material that can be ejected out of the sides, especially in the case of the cone-and plate geometry.

To next improve on our fabrication geometry, we sought to design a system that would generate more consistent shear forces without the need for rigorous. We used displacement driven flow instead of rotational driven flow to generate shear forces. A polymer emulsion was pumped through a 1 mm diameter transparent tube across a bespoke UV array to induce crosslinking. A schematic of this pipe flow geometry can be seen in Figure 6.3 (A); the shear generated by the bulk oil moving across the pipe walls causes polymer droplets to elongate. After fabrication, particles were imaged using SEM, as done previously with other shear geometries shown in Figure 6.3 (B). Here, a significant portion of the particles were deformed from a spherical to a rod shape, indicating successful shearing of the polymer droplets. Notably, the size of the particles varied greatly, with some particles having a major axis under 10 μm, while others were similar to hydrogel fibers instead, having a major axis closer to 150 μm. Furthermore, we saw that again, not all particles were successfully deformed into a rod shape, suggesting particle yield would need to be optimized further. This method of rod hydrogel fabrication demonstrates

that we are able to generate rod-shaped hydrogels using a high-throughput method on a size scale relevant to vascular targeted drug delivery.

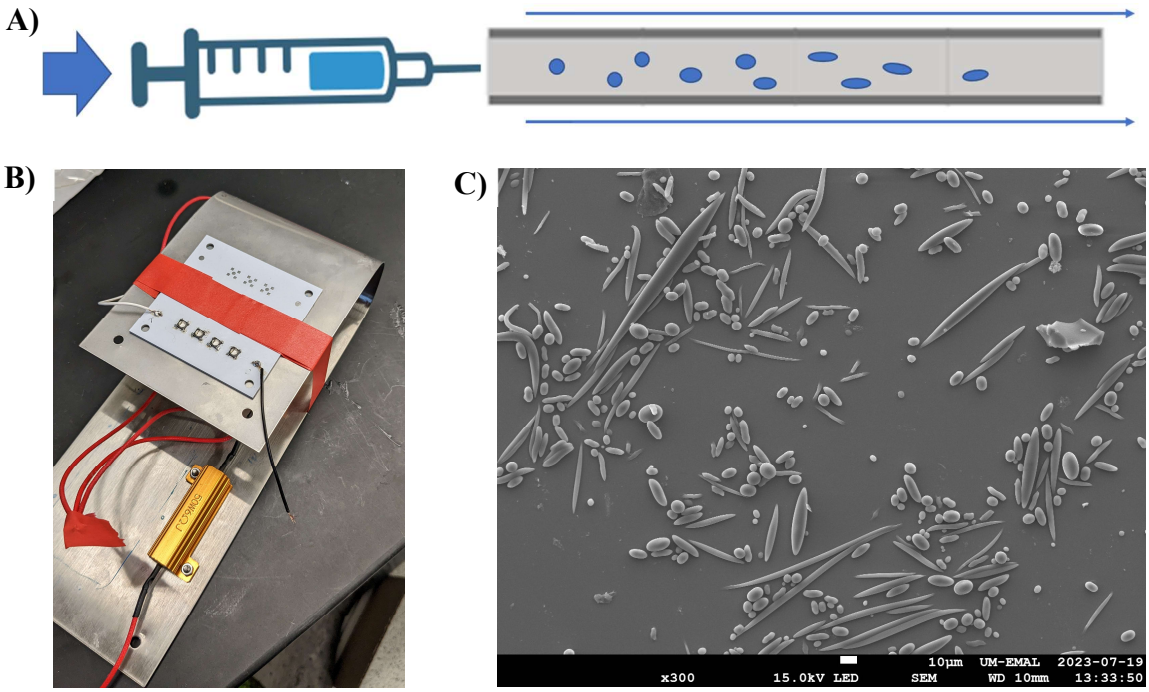


Figure 6.3: (A) Schematic of the tube shear system, where a PEG emulsion in silicone oil is injected into a small tube to generate shear for droplet deformation. (B) An image of the UV array used to crosslink PEG particles. (C) A representative SEM image of particles fabricated at a shear rate of 1000 $s^{-1}$. Most of the particles were stretched to varying degrees, though spheres were still present. Scale bar: 10 µm

We next characterized this hydrogel fabrication process by adjusting the volumetric flow rate, and thus the shear rate, to determine its effects on rod size and shape. Particles were fabricated using a range of flow rates and were then imaged using light microscopy to measure major and minor axes of particles, which were then used to calculate equivalent spherical diameter (ESD) and aspect ratio (AR). ESD was calculated according to the following equation:

$$ESD = (a * b^2)^{\frac{1}{3}}$$

where $a$ is the major axis length of the rod and $b$ is the minor axis length of the rod. This calculation assumes that the cross-sectional area of the rod is circular.

Figure 6.4 shows the AR of particle populations as a function of shear rate. As the shear rate increases from 0 to 1400 $s^{-1}$, the ESD stays relatively constant between 5 – 6 µm. The unchanging ESD indicates that the polymer size of the droplets is constant across all shear, indicating that any effects of coalescence during the fabrication and shearing processes are minimal. Conversely, the AR increases from a spherical particle, where AR is equal to one, up to

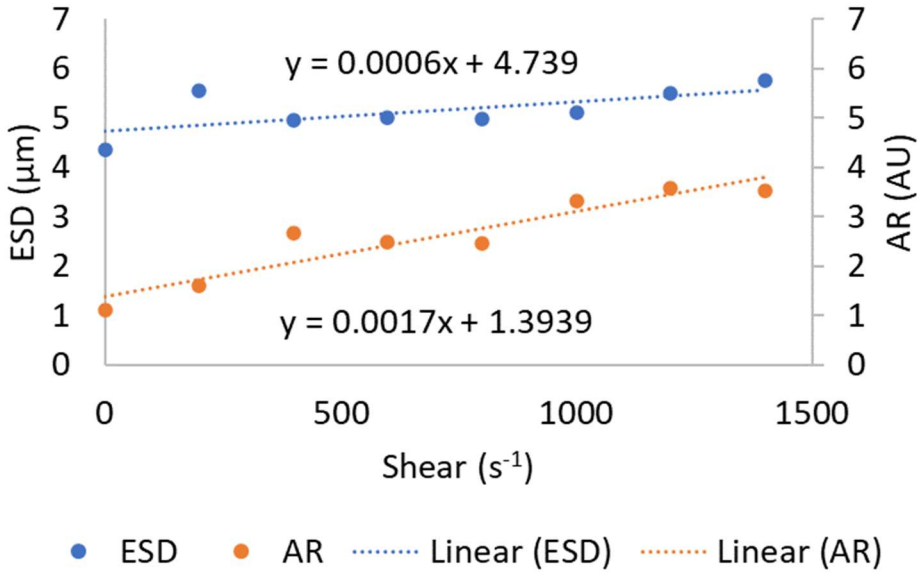


Figure 6.4: Population analysis of the ESD and AR of particles fabricated at varying shear rates. The ESD of the particles remained unchanged across all shear rates. However, the AR of the particles increased with increasing shear, which is consistent with the expected increase in capillary number.

about 3.5 at the highest shear rate tested. As expected, an increase in shear force results in increased elongation of the polymer droplets prior to particle formation. Thus, by modulating the flow rate at which the system is operated at, we are able to selectively fabricate particles of a given AR. Furthermore, given the control over the shear rate that this system provides, we can also increase the size of the polymer droplets by adjusting the emulsification step to generate a greater fraction of fibrous hydrogel particles, which may instead be useful for future studies in regeneration of skeletal muscle tissue.

Next, we performed a series of centrifugations at increasing speeds to separate particles by size and AR. Whole particle population samples were subject to centrifugation at incremental speeds from 50 – 3000 x g for 5 minutes, and particle fractions were collected for SEM imaging. A representative sample of particle fractions collected for particles fabricated using 1000 $s^{-1}$ is shown in Figure 6.5. Image analysis of the rod hydrogels indicates that increasing centrifugation speed allows for isolation of smaller particles with a lower ESD and AR. The average ESD of the rod particles decreased from 5.81 μm at a centrifugation speed of 50 x g down to 2.16 μm at 1500 x g. The AR of the particles decreased from 3.22 to 1.58, though each fraction of rods contained significantly elongated particles compared to the mean of each group, as indicated by the tail on each group of AR measurements. However, the overall trend confirms that particles can be separated by size and AR using centrifugation.

Though all fabrication studies up to this point have been done using PEG, we also explored the use of other hydrogel materials to demonstrate the flexibility of this system. Thus, we selected a functionalized hyaluronic acid (HA) to fabricate rod shaped hydrogel particles in a similar manner as previously done above. Unlike PEG, HA is a naturally occurring macromolecule in the body, produced as a component of the ECM. A major advantage of fabricating HA-based particles as opposed to PEG particles lies in native cell-adhesion motifs that are present on the HA molecule, whereas PEG is a synthetic polymer and thus would need additional conjugation steps to incorporate cell adhesion functionalities. Commercial HA was functionalized with methacrylate groups to form HA-methacrylate (HAMA) and placed in oil to form an emulsion, which was then pumped through the shear geometry. Particles were imaged using SEM, as shown in Figure 6.6. Here, the granularity of the particles varied greatly, indicating that some particles were fragmented during processing steps. The size of these

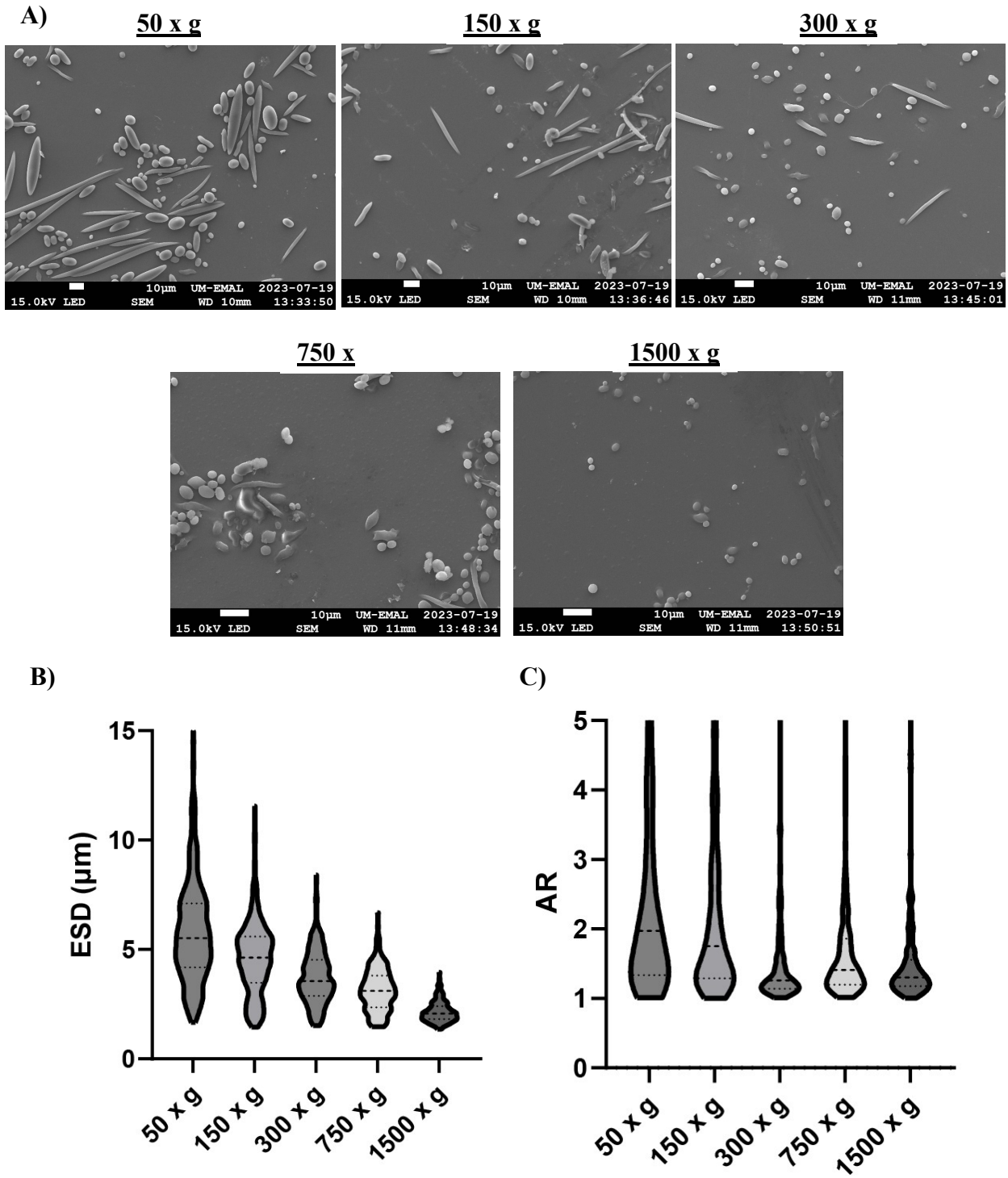


Figure 6.5: (A) SEM images of particles collected via centrifugation speeds from 50 – 1500 x g. As the speed increases, the particle population visually becomes smaller in size and length. (B) Violin plot of the ESD of the PEG particles for the 1000 $s^{-1}$ shear condition, where the size of the particles decreases from an average of 5.81 to 2.16 µm from 50 to 1500 x g respectively. (C) Violin plot of the AR of the PEG particles for the 1000 $s_{.1}$ shear condition, where the AR decreases from an average of 3.22 to 1.58 from 50 to 1500 x g respectively. Larger, stretched particles with an AR > 5 were still present for all samples.

particles ranged from 1 to 4 μm, though some particles may be smaller because of particle fragmentation. However, the presence of smooth, elongated particles in the sample also demonstrates that there is potential for the fabrication of HA-based rod hydrogels. Though the

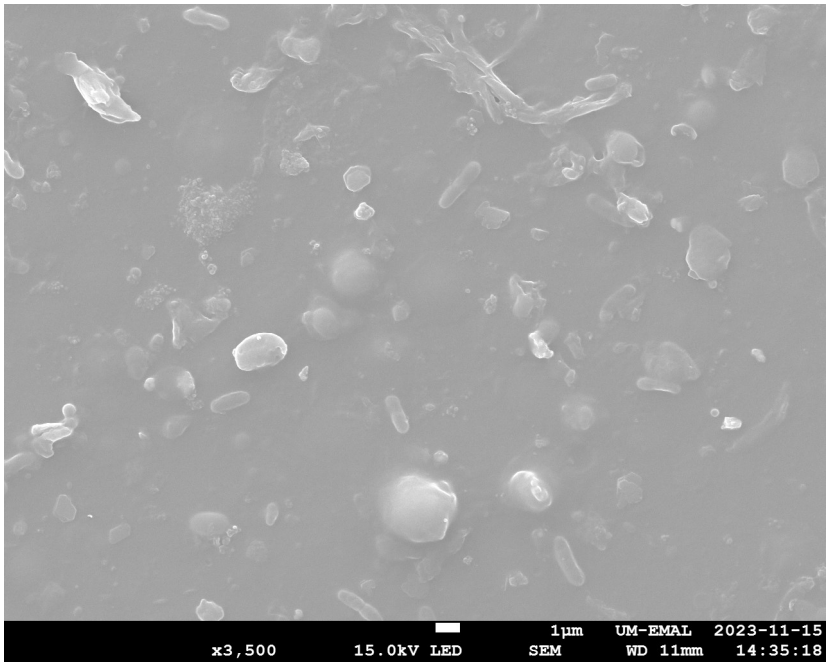


Figure 6.6: SEM image of HA particles fabricated using the tube shear system. While a majority of particles appear granular, some particles had a smooth surface morphology and appeared to be elongated.

yield of rod-shaped particles was low using HAMA, the successful fabrication of these rods indicates the flexibility of this process, where emulsified polymer solutions can be sheared and crosslinked *in situ* to generate elongated particles using various materials.

## 6.4 Discussion

Elongated particles have been demonstrated to provide additional utility compared to spherical particles, yet current fabrication techniques lack some combination of scalability, feasibility for biological applications, and particularly producibility of nano-sized rods as drug carriers. Here, we have shown that a water-in oil emulsion of polymer droplets can be placed in shear flow and crosslinked in a deformed state. This fabrication method demonstrates a novel

technique to produce both rod and fibrous hydrogels in a reproducible, scalable, and continuous manner.

The cup-and-bob and the cone-and-plate geometry were both chosen for their similar design to Couette and cone-and-plate rheometers, which create simple shear profiles in which the shear is uniform across the two moving surfaces. However, the difficulty in alignment of the rotational components resulted in both generation of significant debris and likely fragmentation of particles, which negated any advantages of consistent shear across the geometry gap. Thus, instead of generating uniform particles, we were only able to fabricate very polydisperse and heterogeneous particles, of which only a small proportion were slightly stretched. Furthermore, of the deformed particles, we see that they are also asymmetrical and not ellipsoidal, indicating that polymer droplets prior to crosslinking were undergoing breakoff.

While the biggest advantage of the rotational geometries is the potential for uniform shear and thus uniform deformation of polymer droplets, we were limited by the precision of our equipment. Thus, we shifted to a pipe model to generate shear instead, which circumvented the need for strict geometry alignment. Here, we were now able to generate elongated particles, of which a large portion of particles were deformed from a spherical shape. However, we still see a significant population of spheres, which is likely due to the shear profile in a pipe, which is greatest at the center and near-zero at the wall. These shear differences likely account for both the variation in particle elongation as well as the presence of spherical particles even at higher shear rates. Thus, while this technique demonstrates the concept of applying shear to deform polymer droplets prior to crosslinking, improvements to the shear system to generate a simple shear profile similar to the aforementioned rotational geometries would facilitate the fabrication of uniform particles.

The consistent ESD of the rods across shear rate indicated that increasing shear rate did not significantly change the relative size of the droplets, either from coalescence of the polymer droplets or from breakoff, which would have shifted the population ESD to be larger or smaller, respectively. However, we do see that there is a small amount of coalescence, as indicated by the comparatively large particles generated that are 100 μm or greater in length. Conversely, we also see that AR increases with increasing shear rate, as expected based on the increasing capillary number, thus successfully demonstrating that our shear system can modulate the level of particle deformation by adjusting shear rate. We can also control the size of the droplets in the emulsion by adjusting the mixing process by which the emulsion is generated. By adjusting the speed at the emulsion is made using the overhead mixer, the average diameter of the droplets prior to shearing and crosslinking can be made larger with less rotational speed and vice versa. Therefore, there is also potential for the fabrication of larger fibrous hydrogel particles in a scalable, reproducible, and consistent manner as well, which would be advantageous for skeletal muscle tissue regeneration.

By separating different sized particles using centrifugation, we wanted to isolate specific sizes for potential further applications. We were successfully able to separate particles by ESD as expected, and though the AR of each respective particle fraction also decreased with increasing centrifugation speed, the distribution of AR is quite large. Because of the propensity for rods to align in the same axis of movement, we are likely separating particles by minor axis as opposed to strictly by ESD, though larger particles are also likelier to have a larger minor axis. While this separation process allows us to isolate particles of various ESD and AR, we also see that spherical particles still remain in each fraction. Thus, to isolate a more uniform population of elongated particles, a method such as filtration may help to separate particles strictly based on

their shape. During filtration, spheres of a given diameter are more likely to pass through the filter than rods whose major axes may be larger than the pore size of the filter. There is also the potential for rod particles to pass through if their minor axis is smaller than the pore size, since rods can also align in the direction of flow. However, it is more likely that rods will not be able to pass through the entirety of the filter and thus after capturing the rods, flow can be reversed to recover the rods while removing spheres from the particle population.

Though PEG has utility as a highly tunable material, its synthetic nature does not allow it to interact with biological systems as easily as other naturally derived materials without further functionalization, such as with cell-signaling groups such as RGD peptide or antibodies. The use of HA as a cell scaffold for tissue engineering has been highly characterized, and because of its ability to be functionalized to participate in photopolymerization, we selected HAMA as an analogous material to demonstrate the flexibility of our shear system. Notably, the viscosity of the HAMA solution was much greater than the PEG solution, likely from the greatly increased molecular weight of the HAMA, allowing for entanglement of the polymer chains. The SEM images of the HA-based particles indicate that many of the particles were granular and nonuniform, suggesting that the particles were fragmenting. Furthermore, unlike with the PEG particles, we did not see any larger, elongated particles, which could be from a lack of coalescence of the HAMA solution, or breakoff of any larger particles contributing to the particle fragmentation. However, we were still able to visualize smaller particles with smooth surface morphologies, indicating limited success with HA rod fabrication. Because HA is a biocompatible molecule with native cell-signaling functionality, it is a highly attractive material for drug carrier applications as well as tissue regeneration. Though there is more optimization

required to further improve the HA rod fabrication process, we have shown that the shear system is robust and capable of using various materials for different applications.

The future work for this project will include improvements to the shear geometry to facilitate fabrication of more uniformly stretched particles, likely with a simple shear profile as opposed to a pipe shear profile. Additionally, characterization of the PEG and HA material will give further insight on the shear system, especially measurements of interfacial tension, which can be used to more rigorously calculate capillary numbers to target specific ESD and AR. Finally, improved separations will allow for the isolation of rods of a particular ESD and AR, which could be used to explore interplay between particle shape and deformability in various contexts of particle drug delivery, e.g. immune cell phagocytosis, drug release, and margination propensity.

### 6.5 Conclusions

In this chapter, we have developed a high-throughput, continuous method of fabricating both rod-shaped particles and fibrous hydrogels, demonstrating an improved method over other traditional fabrication processes. Though we were unable to consistently fabricate rods using rotational shear systems, we successfully generated elongated particles using a pipe shear system and shown that particle AR can be modulated using shear rate. Furthermore, by applying increasing centrifugation speeds, we are able to separate rods by ESD and to a lesser extent, AR. Finally, we functionalized HAMA and used it as an analogous material to PEG, indicating the flexibility of the system to be used for fabrication of particles of a variety of materials. Further development of this system to fabricate rods and fibers of specific sizes will greatly improve the utility of rods and fibers for drug delivery and tissue regeneration contexts.

# Chapter 7 : Conclusions and Future Directions

## 7.1 Dissertation Conclusions and Summary

Hydrogel-based materials continue to be of interest in tissue engineering because of the high degree of biocompatibility from their high water composition and general deformability allowing them to mimic various types of cells and tissues. Within the context of vascular targeted drug delivery, particle formulations remain largely underutilized in the clinic because of design obstacles to VTC success, especially the size mismatch between particles capable of adhering to the vascular wall and entering the tissue space. However, hydrogel microparticles have great potential because of their propensity for enhanced margination to the vascular wall on the micron scale, a crucial transport step for VTC success. Furthermore, because of their deformability, they present a greatly lowered risk of capillary occlusion than their rigid polymeric counterparts and thus may see utility as a carrier for NPs to enter the tissue space.

Another aspect of hydrogel VTC design that has yet to be well characterized is their interactions with neutrophils, the predominant immune cell present in circulation. While numerous studies have previously looked at impacts of particle elasticity on circulation time and immune cell phagocytosis, these studies were largely limited to macrophages and monocytic cell lines along with murine models that may not fully represent drug carrier performance in a human system. Furthermore, because of particle fabrication limitations currently in the literature, interplay between deformability and particle shape also remain largely unexplored.

The work detailed in this dissertation seeks to first develop a hydrogel material suitable for the fabrication of MPs that can degrade enzymatically while retaining other properties suitable for a VTC, especially the ability to conjugate targeting ligands and a Young's modulus shown to benefit from enhanced margination effects. We next developed a NP-loaded hydrogel system that properly addressed the shortcomings of both NPs and MPs in the context of VTC design and brings together the advantages of particles of each size regime. Furthermore, we performed in-depth characterization of the interactions between deformable particles and human neutrophils to determine how particle elasticity will impact VTC performance from the perspective of circulation time and immune cell clearance. Finally, we developed a scalable, high-throughput, and continuous method for the production of fibrous and rod-shaped particles that could have greater utility than spherical particles.

In chapter 3, we explored various reaction schemes to fabricate a peptide-conjugated hydrogel capable of degrading in the presence of trypsin, a model enzyme, and MMP-2, a physiologically relevant enzyme overexpressed in areas of inflamed and diseased vascular tissue. When using PEGDA and VPM in thiol-ene photopolymerization reaction, we found that the degree of VPM incorporation into the PEG matrix was lower than required for complete enzymatic degradation, likely from a lack of reaction selectivity of the thiol group to the acrylate group. While this reaction scheme was found to be infeasible for the fabrication of an enzyme degradable material, it remains useful as a facile one-step reaction that could be utilized for the incorporation of other thiolated molecules that does not require high conversions for usability, such as the conjugation of signaling or adhesion molecules like the cellular adhesion peptide RGD. When we instead shifted to a nucleophilic Michael addition reaction instead, we were able to achieve high degrees of VPM incorporation, as indicated by an Ellman's reaction and

supported by the resulting hydrogel material's ability to completely degrade in the presence of trypsin. However, the extremely low Young's modulus of this material indicated that it was not usable as a VTC, likely from the decreased crosslinking density from the formation of large molecular weight macromers. Despite this, materials made from this material may instead see use as cell scaffolding, where a lower Young's modulus allows for greater viability of encapsulated cells, and built-in enzyme degradation would allow for eventual biodegradation of this material[53,54,75]. When we shifted to a highly branched PEGVS polymer instead, we were able to increase the crosslinking density to a Young's modulus that has been demonstrated to benefit from enhanced particle margination in blood flow. Furthermore, this material retained the ability to fully degrade in the presence of trypsin as well as MMP-2.

Building off the work on material development in chapter 3, we first fabricated particles using the PEGVS hydrogel material using a water-in-oil emulsion, yielding particles within a size range of 2 – 4 μm. These particles were used in degradation assays with MMP-2 and were found to degrade completely within 8 hours. Furthermore, successful conjugation of avidin and subsequent biotinylated ligands to the particle surface were confirmed via flow cytometry. Finally, we demonstrated that these particles could bind to an inflamed endothelium, and additionally, appeared to successfully degrade in the presence of trypsin while bound. While NP loading into the hydrogel particles was successful, based on fluorescent imaging, we found that exposure of the hydrogels to hexanes used to remove residual oil had the unexpected drawback of dye leaching from the PS NPs, complicating NP detection, especially during adhesion-degradation assays. A current limitation to the data presented in this chapter is the lack of adequate NP detection upon release from the hydrogel MP, since the lack of hydrogel particles in the flow channel after perfusion of trypsin does not necessarily indicate particle degradation.

Indeed, while this circumstantial evidence suggests that particle degradation occurred, without proper detection of released NPs, it remains unclear whether the NP-loaded MP system is working as designed. However, the development of this particle system marks a step towards a viable micron-sized VTC that bridges together the ability to marginate and bind to the vascular endothelium as well as the propensity for intracellular transport into the tissue space.

While the previous two chapters focused on the transport of VTCs from bulk blood flow to the endothelium and entry into the tissue space, chapter 5 instead looks at the interactions between deformable particles and primary human neutrophils. These interactions typically account for immune cell clearance of circulating particles preventing them from reaching their targeted tissue. When we incubated 2 μm PEG and PS particles, we observed relatively equal uptake across all particle types, and when we used 500 nm particles, we observed an enhanced phagocytic effect on PEG particles as compared to PS. However, when these assays were repeated with J774 macrophages, we instead saw decreasing uptake with decreasing elastic modulus, as reported by numerous studies in the literature. When we incubated HA particles with neutrophils, we again saw equal uptake across all particle types, indicating that these trends seen with PEG particles were unrelated to particle composition and likely linked to particle elasticity. Similarly, with J774 macrophages, we again saw decreasing uptake with decreasing elastic modulus. We visually confirmed these trends by using an optical tweezer system, where 2 μm PS particles were shown to be engulfed by neutrophils and J774 macrophages within 5 minutes, but PEG particles were only successfully internalized by neutrophils. Altering the zeta potential of the particles largely did not affect the level of internalization of 2 μm PEG particles by neutrophils, though we saw an increase in the positively charged 15% PEG particle, likely from the greater positive charge on the 15% particle compared to the 50% particles. After EDC

activation and avidin conjugation, we observed a reduction in uptake by neutrophils, and based on SDS-PAGE analysis, this reduction was likely due to the increased adsorption of albumin on the particle surface preventing phagocytosis. Though we have explored interactions between deformable particles in detail, this data would benefit from further exploration of the HA material and whether modifications to zeta potential and surface charge would yield similar trends to those seen with PEG. However, after the COVID-19 pandemic, the supplier was unable to manufacture more of this specific chemical, and so these limitations restricted our ability to explore this material further. Additionally, though the optical tweezer experiments visually demonstrated that neutrophils can phagocytose PEG particles, we also expected to see a shape change during membrane wrapping of the particle. It remains unclear why deformable NPs can deform when phagocytosed by other cells, yet MPs, which are larger, were visually unchanged. Further investigation into the biomechanics of neutrophil phagocytosis would provide greater insight on why neutrophils are able to more effectively uptake deformable particles than macrophages. Additionally, there is more to be explored regarding the types of proteins that may affect neutrophil phagocytosis of elastic particles. For example, conjugating albumin without the use of EDC would support our hypothesis that albumin adsorption reduced neutrophil uptake. Conversely, the conjugation or adsorption of opsonins such as IgG may instead result in an enhanced phagocytic effect. The work detailed in this chapter represents the first study on the effects of particle elasticity on human neutrophil uptake, which is critically important within the context of vascular targeted drug delivery.

Because we hypothesized that the enhanced phagocytosis of deformable particles by neutrophils was due to particle deformation, we next explored the potential of fabrication rod-shaped hydrogels to determine if the phagocytosis of deformable particles could be further

enhanced by shape. Though we initially explored rotational shear systems, including a cup-and-bob and a cone-and-plate geometry, we shifted to a tube shear system to circumvent the need for geometry alignment. This system allowed us to fabricate stretched hydrogels at various shear rates, and shape analysis of the particles indicated that particle AR could be modulated via flow rate, though ESD remained relatively unchanged. We were able to separate the particles by ESD and AR using increasing centrifugation speeds, though particles were likely separated based on minor axis due to the propensity of rods to align during centrifugation. Though we also fabricated HA-based rods as well, these particles were largely granular and inconsistent. The data in this chapter showcases a novel fabrication method for continuous, high-throughput generation of rod-shaped particles, and improves on already existing methods for rod fabrication that typically suffer from a lack of either scalability or ability to generate micron-sized rods.

### 7.2 Future Directions

The work in this thesis represents significant advances towards the use of hydrogels as VTCs and overall, we have demonstrated their utility for a variety of biological applications. Based on the data detailed in the previous chapters, there are multiple directions in which these projects can go to further develop our knowledge of hydrogels for the treatment of various diseases, which are outlined below.

1. Further development of the NP-loaded hydrogel MP system to demonstrate clinical viability. While significant progress has been made in this area and a NP-loaded MP system has successfully been developed, there is more work to be done to demonstrate viability of the system. Specifically, NPs need to successfully adhere to the vascular wall, and the loading of therapeutics such as anti-CD47 to facilitate efferocytosis of atherosclerotic plaques would provide substantial evidence of the

success of this dual delivery approach. One specific obstacle to the effective treatment of atherosclerosis is the lack of treatments capable of halting and reversing the accumulation of lipids, macrophages, and foam cells that contribute to plaque formation. The inability of the body's immune system to recognize and remove this apoptotic cell debris has been shown to be linked to an upregulation of CD47, an anti-phagocytic marker of self, rendering macrophages largely unable to clear these plaques[101]. While the administration of anti-CD47 antibodies would allow for the blocking of this "don't eat me" signal, a significant barrier to using these antibodies is the presence of RBCs circulating in blood flow that natively express CD47. Thus, the majority of anti-CD47 administered intravenously would largely be diverted to these RBCs instead of to the atherosclerotic plaque. In our NP-loaded MP system, the anti-CD47 would instead be loaded into a biodegradable PLGA NP first, followed by loading into an enzyme degradable hydrogel microparticle. This system would allow for a more controlled delivery of the anti-CD47 therapeutic to the plaque as opposed to the RBC sink.

2. Modulation of the enzyme-degradable hydrogel to other relevant diseases. Significant work has been done with similar materials targeting enzymes such as elastase in a pulmonary context, and the flexibility of the NP-loaded MP system lends itself to being used for various disease contexts. The peptide of choice can be adjusted to the enzyme of interest, since thiol functionality can easily be incorporated by flanking the peptide with cysteine residues[56]. Furthermore, the use of avidin as a foundation for other targeting ligands allows for the use of a wide variety of ligands that can be biotinylated to bind to the surface of particles. One potential application of this

system is their use in specifically targeting neutrophils, which have been linked to ARDS and sepsis, where neutrophils typically undergo feedback loops that do not result in resolution of immune reactions[142]. Because of their role in exacerbating these pro-inflammatory states, a potential solution to help ameliorate this condition could be the diversion of neutrophils from the lungs combined with administration of an anti-inflammatory compound (such as aspirin). Previous work in our lab that has yet to be published suggests a poly-anhydride ester composed of salicylic acid (PolyA) has the ability to reduce the inflammation and activation of neutrophils. Combined with our findings that neutrophils can phagocytose deformable particles at equal or greater rates than rigid particles, there is the potential of preferentially targeting the neutrophil immune cell population using deformable particles that have been crosslinked with peptides sensitive to neutrophil elastase instead of MMP-2 for the targeted delivery of polyA NPs to help mitigate excessive inflammation and neutrophil infiltration into the lungs.

3. Mechanobiology testing of neutrophil membrane wrapping. Though we have observed that neutrophils phagocytose deformable particles indiscriminately of particle modulus, it is still unclear why this phenomenon is observed only with this cell type and not with other phagocytes such as macrophages and monocytes. The work detailed in chapter 5 strongly suggests that it may be due to the mechanics of engulfment; a deeper understanding of the biomechanics of neutrophil phagocytosis will help to elucidate the role of particle deformability in the phagocytosis process. Our current working hypothesis regarding the enhanced phagocytosis of spherical deformable particles by human neutrophils is their apparent deformation during the

engulfment process. Forces exerted on the particle by the cell during membrane wrapping have been shown to cause the particle shape to change from a sphere to an ellipsoid[112]. Because these neutrophils now see an apparent rod-shaped particle instead of a spherical particle, we hypothesize that these particles may experience an enhanced level of phagocytosis similar to previous studies with rigid rod-shaped particles. Thus, further experiments to investigate and quantify the forces exerted on the particle by the cell during phagocytosis may help to elucidate the mechanism by which these deformable particles are engulfed by neutrophils. The cortical tension and cytoplasmic viscosity of neutrophils has been reported to be an order of magnitude lower than that of macrophages, which indicates that the mechanics of cell membrane deformation are different between these types of phagocytes[143,144]. The lowered tension and viscosity associated with neutrophils may be associated with a lower energy barrier to restructuring of the cell membrane that occurs during phagocytosis. Overall, there are still many questions about the mechanisms of neutrophil phagocytosis that have yet to be explored and sufficiently answered, and understanding these interactions between particles and neutrophils are critical to informed VTC design and accurate assessment of carrier performance.

4. Investigation of deformable particles with neutrophils in other animal contexts. The trends seen with deformable particles and neutrophils have largely been in a human context, and a thorough investigation of neutrophil-particle interactions in other contexts would provide a basis for comparison with other work in the literature. By looking at these particle interactions in animal models, we can determine if these trends are specific to human neutrophils and may provide insight into why we see

trends that are inconsistent with those reported for other immune cells. Mouse models continue to be relevant for modeling various diseases, and thus it is critically important that we understand the similarities and differences between a mouse and human system to properly assess the translatability of animal models to the clinic. Other large animal models to consider could potentially include pigs, which have been known to have a more similar immune system than the typical murine model[145].

5. Improved rod fabrication and isolation for characterization of rod-shaped hydrogels as VTCs. While we have successfully developed a system to fabricate rod-shaped hydrogels, these particles display a large amount of heterogeneity, due to the pipe shear profile in the tube shear system as opposed to simple shear, which would generate more uniform particles. This could be achieved by using a more rigorous rotational shear system with proper geometry alignment. Furthermore, improved isolation of rods using techniques such as filtration will yield rods of more uniform ESD and AR, which could then be used for further applications, especially phagocytosis and margination assays to begin exploring potential interplay between particle shape and deformability.
6. Optimization of fibrous hydrogel fabrication and functionalization for skeletal muscle regeneration. While most of the work in this thesis has focused on fabricating and characterizing micron-sized particles as VTCs, the potential for fibrous hydrogel fabrication in our shear system has potential utility as a cell scaffold for muscle tissue regrowth. By incorporating cell adhesion ligands to PEG particles, we can facilitate interactions between PEG fibers as a scaffold and smooth muscle cells. Additionally, the use of HA as a hydrogel material instead is very attractive because it is a native

ECM component and possesses native adhesion motifs without the need for further chemical modification.

### 7.3 Closing Thoughts and Research Outlook

Treatment of CVD remains a significant medical and economic burden, and the work in this thesis aims to advance VTC design as an improved alternative to current treatments. While there definitely remains significant work in this space to bring these technologies to the clinic, I am optimistic that this work will lay a strong foundation for the development of successful particle-based platforms for the treatment of a wide variety of disease, not limited to CVD. The emergence of increasingly complex materials allows for improved environmental responses from a biological context. I have spent a significant amount of time characterizing hydrogel materials for the treatment of CVD, and I look forward to seeing the demonstrated utility of hydrogels that has been explored here in this thesis.

## References


1. Benjamin, E.J., Blaha, M.J., Chiuve, S.E., Cushman, M., Das, S.R., Deo, R., de Ferranti, S.D., Floyd, J., Fornage, M., Gillespie, C., et al. (2017). Heart Disease and Stroke Statistics—2017 Update: A Report From the American Heart Association. Circulation. 10.1161/CIR.0000000000000485.

2. Tsao, C.W., Aday, A.W., Almarzooq, Z.I., Anderson, C.A.M., Arora, P., Avery, C.L., Baker-Smith, C.M., Beaton, A.Z., Boehme, A.K., Buxton, A.E., et al. (2023). Heart Disease and Stroke Statistics-2023 Update: A Report From the American Heart Association. Circulation *147*, e93–e621. 10.1161/CIR.0000000000001123.

3. Rafieian-Kopaei, M., Setorki, M., Doudi, M., Baradaran, A., and Nasri, H. (2014). Atherosclerosis: Process, Indicators, Risk Factors and New Hopes. Int J Prev Med *5*, 927–946.

4. Crowther, M.A. (2005). Pathogenesis of Atherosclerosis. Hematology *2005*, 436–441. 10.1182/asheducation-2005.1.436.

5. Parang, P., and Arora, R. (2009). Coronary vein graft disease: Pathogenesis and prevention. Can J Cardiol *25*, e57–e62.

6. Pal, N., Din, J., and O'Kane, P. (2019). Contemporary Management of Stent Failure: Part One. Interv Cardiol *14*, 10–16. 10.15420/icr.2018.39.1.

7. Ramkumar, S., Raghunath, A., and Raghunath, S. (2016). Statin Therapy: Review of Safety and Potential Side Effects. Acta Cardiol Sin *32*, 631–639. 10.6515/ACS20160611A.

8. Koren, E., and Torchilin, V.P. (2011). Drug carriers for vascular drug delivery. IUBMB Life *63*, 586–595. 10.1002/iub.496.

9. Kelley, W.J., Safari, H., Lopez-Cazares, G., and Eniola-Adefeso, O. (2016). Vascular-targeted nanocarriers: design considerations and strategies for successful treatment of atherosclerosis and other vascular diseases. Wiley Interdiscip Rev Nanomed Nanobiotechnol *8*, 909–926. 10.1002/wnan.1414.

10. Park, J.W. (2002). Liposome-based drug delivery in breast cancer treatment. Breast Cancer Res *4*, 95–99. 10.1186/bcr432.

11. Ripple, D.C., and Dimitrova, M.N. (2012). Protein particles: What we know and what we do not know. Journal of Pharmaceutical Sciences *101*, 3568–3579. 10.1002/jps.23242.

12. Tabatabaei Mirakabad, F.S., Nejati-Koshki, K., Akbarzadeh, A., Yamchi, M.R., Milani, M., Zarghami, N., Zeighamian, V., Rahimzadeh, A., Alimohammadi, S., Hanifehpour, Y., et al. (2014). PLGA-Based Nanoparticles as Cancer Drug Delivery Systems. Asian Pacific Journal of Cancer Prevention *15*, 517–535. 10.7314/APJCP.2014.15.2.517.

13. Barenholz, Y. (Chezy) (2012). Doxil® — The first FDA-approved nano-drug: Lessons learned. Journal of Controlled Release *160*, 117–134. 10.1016/j.jconrel.2012.03.020.

14. Niu, G., Cogburn, B., and Hughes, J. (2010). Preparation and characterization of doxorubicin liposomes. Methods Mol Biol *624*, 211–219. 10.1007/978-1-60761-609-2_14.

15. Sercombe, L., Veerati, T., Moheimani, F., Wu, S.Y., Sood, A.K., and Hua, S. (2015). Advances and Challenges of Liposome Assisted Drug Delivery. Front Pharmacol *6*. 10.3389/fphar.2015.00286.

16. Petrou, G., and Crouzier, T. (2018). Mucins as multifunctional building blocks of biomaterials. Biomater. Sci. *6*, 2282–2297. 10.1039/C8BM00471D.

17. Fukui, Y., Fukuda, M., and Fujimoto, K. (2018). Generation of mucin gel particles with self-degradable and -releasable properties. Journal of Materials Chemistry B *6*, 781–788. 10.1039/C7TB02663C.

18. Swaminathan, R., Ravi, V.K., Kumar, S., Kumar, M.V.S., and Chandra, N. (2011). Lysozyme: A model protein for amyloid research. In Advances in Protein Chemistry and Structural Biology, R. Donev, ed. (Academic Press), pp. 63–111. 10.1016/B978-0-12-386483-3.00003-3.

19. Aganyants, H.A., Nikohosyan, G., and Danielyan, K.E. (2016). Albumin microparticles as the carriers for allopurinol and applicable for the treatment of ischemic stroke. Int Nano Lett *6*, 35–40. 10.1007/s40089-015-0169-0.

20. Watcharin, W., Schmithals, C., Pleli, T., Köberle, V., Korkusuz, H., Huebner, F., Zeuzem, S., Korf, H.W., Vogl, T.J., Rittmeyer, C., et al. (2014). Biodegradable human serum albumin nanoparticles as contrast agents for the detection of hepatocellular carcinoma by magnetic resonance imaging. European Journal of Pharmaceutics and Biopharmaceutics *87*, 132–141. 10.1016/j.ejpb.2013.12.010.

21. Mohammed, M.A., Syeda, J.T.M., Wasan, K.M., and Wasan, E.K. (2017). An Overview of Chitosan Nanoparticles and Its Application in Non-Parenteral Drug Delivery. Pharmaceutics *9*. 10.3390/pharmaceutics9040053.

22. Ekici, S., Ilgin, P., Butun, S., and Sahiner, N. (2011). Hyaluronic acid hydrogel particles with tunable charges as potential drug delivery devices. Carbohydrate Polymers *84*, 1306–1313. 10.1016/j.carbpol.2011.01.028.

23. Ching, S.H., Bansal, N., and Bhandari, B. (2017). Alginate gel particles–A review of production techniques and physical properties. Critical Reviews in Food Science and Nutrition *57*, 1133–1152. 10.1080/10408398.2014.965773.

24. Sosnik, A. (2014). Alginate Particles as Platform for Drug Delivery by the Oral Route: State-of-the-Art. International Scholarly Research Notices. 10.1155/2014/926157.

25. Danhier, F., Ansorena, E., Silva, J.M., Coco, R., Le Breton, A., and Préat, V. (2012). PLGA-based nanoparticles: An overview of biomedical applications. Journal of Controlled Release *161*, 505–522. 10.1016/j.jconrel.2012.01.043.

26. Khan, F., Valere, S., Fuhrmann, S., Arrighi, V., and Bradley, M. (2013). Synthesis and cellular compatibility of multi-block biodegradable poly(ε-caprolactone)-based polyurethanes. J. Mater. Chem. B *1*, 2590–2600. 10.1039/C3TB00358B.

27. Charoenphol, P., Huang, R.B., and Eniola-Adefeso, O. (2010). Potential role of size and hemodynamics in the efficacy of vascular-targeted spherical drug carriers. Biomaterials *31*, 1392–1402. 10.1016/j.biomaterials.2009.11.007.

28. Galkina, E., and Ley, K. (2007). Vascular Adhesion Molecules in Atherosclerosis. Arteriosclerosis, Thrombosis, and Vascular Biology *27*, 2292–2301. 10.1161/ATVBAHA.107.149179.

29. Hubbard, A.K., and Rothlein, R. (2000). Intercellular adhesion molecule-1 (ICAM-1) expression and cell signaling cascades. Free Radical Biology and Medicine *28*, 1379–1386. 10.1016/S0891-5849(00)00223-9.

30. Bendas, G., Krause, A., Schmidt, R., Vogel, J., and Rothe, U. (1998). Selectins as new targets for immunoliposome-mediated drug delivery A potential way of anti-inflammatory therapy. 8.

31. Alexis, F., Pridgen, E., Molnar, L.K., and Farokhzad, O.C. (2008). Factors Affecting the Clearance and Biodistribution of Polymeric Nanoparticles. Molecular Pharmaceutics *5*, 505–515. 10.1021/mp800051m.

32. Potter, R.F., and Groom, A.C. (1983). Capillary diameter and geometry in cardiac and skeletal muscle studied by means of corrosion casts. Microvasc Res *25*, 68–84. 10.1016/0026-2862(83)90044-4.

33. Fang, C., Shi, B., Pei, Y.-Y., Hong, M.-H., Wu, J., and Chen, H.-Z. (2006). In vivo tumor targeting of tumor necrosis factor-α-loaded stealth nanoparticles: Effect of MePEG molecular weight and particle size. European Journal of Pharmaceutical Sciences *27*, 27–36. 10.1016/j.ejps.2005.08.002.

34. Desai, M.P., Labhasetwar, V., Walter, E., Levy, R.J., and Amidon, G.L. (1997). The Mechanism of Uptake of Biodegradable Microparticles in Caco-2 Cells Is Size Dependent. Pharm Res *14*, 1568–1573. 10.1023/A:1012126301290.

35. Garnacho, C. (2016). Intracellular Drug Delivery: Mechanisms for Cell Entry. Current Pharmaceutical Design *22*, 1210–1226. 10.2174/1381612822666151216151021.

36. Lin, A., Sabnis, A., Kona, S., Nattama, S., Patel, H., Dong, J.-F., and Nguyen, K.T. (2010). Shear-regulated Uptake of Nanoparticles by Endothelial Cells and Development of Endothelial-targeting Nanoparticles. J Biomed Mater Res A *93*, 833–842. 10.1002/jbm.a.32592.

37. Charoenphol, P., Onyskiw, P., Carrasco-Teja, M., and Eniola-Adefeso, L. Particle-cell dynamics in human blood flow: implications for vascular-targeted drug delivery. - PubMed - NCBI. https://www.ncbi.nlm.nih.gov/pubmed/23010218.

38. Carboni, E.J., Bognet, B.H., Bouchillon, G.M., Kadilak, A.L., Shor, L.M., Ward, M.D., and Ma, A.W.K. (2016). Direct Tracking of Particles and Quantification of Margination in Blood Flow. Biophys J *111*, 1487–1495. 10.1016/j.bpj.2016.08.026.

39. Champion, J.A., Walker, A., and Mitragotri, S. (2008). Role of Particle Size in Phagocytosis of Polymeric Microspheres. Pharm Res *25*, 1815–1821. 10.1007/s11095-008-9562-y.

40. Doerschuk, C.M., Beyers, N., Coxson, H.O., Wiggs, B., and Hogg, J.C. (1993). Comparison of neutrophil and capillary diameters and their relation to neutrophil sequestration in the lung. Journal of Applied Physiology *74*, 3040–3045. 10.1152/jappl.1993.74.6.3040.

41. Jay, A.W. (1975). Geometry of the human erythrocyte. I. Effect of albumin on cell geometry. Biophysical Journal *15*, 205–222. 10.1016/S0006-3495(75)85812-7.

42. Zhou, C., Yue, P., and Feng, J.J. (2007). Simulation of Neutrophil Deformation and Transport in Capillaries using Newtonian and Viscoelastic Drop Models. Ann Biomed Eng *35*, 766–780. 10.1007/s10439-007-9286-x.

43. Tsutsui, J.M., Xie, F., and Porter, R.T. (2004). The use of microbubbles to target drug delivery. Cardiovasc Ultrasound *2*, 23. 10.1186/1476-7120-2-23.

44. Sabın, J., Prieto, G., Ruso, J.M., Hidalgo-Álvarez, R., and Sarmiento, F. (2006). Size and stability of liposomes: A possible role of hydration and osmotic forces. Eur. Phys. J. E *20*, 401–408. 10.1140/epje/i2006-10029-9.

45. Winterhalter, M., and Lasic, D.D. (1993). Liposome stability and formation: Experimental parameters and theories on the size distribution. Chemistry and Physics of Lipids *64*, 35–43. 10.1016/0009-3084(93)90056-9.

46. Wichterle, O., and Lím, D. (1960). Hydrophilic Gels for Biological Use. Nature *185*, 117–118. 10.1038/185117a0.

47. Fish, M.B., Fromen, C.A., Lopez-Cazares, G., Golinski, A.W., Scott, T.F., Adili, R., Holinstat, M., and Eniola-Adefeso, O. (2017). Exploring deformable particles in vascular-targeted drug delivery: Softer is only sometimes better. Biomaterials *124*, 169–179. 10.1016/j.biomaterials.2017.02.002.

48. Fish, M.B., Banka, A.L., Braunreuther, M., Fromen, C.A., Kelley, W.J., Lee, J., Adili, R., Holinstat, M., and Eniola-Adefeso, O. (2021). Deformable microparticles for shuttling nanoparticles to the vascular wall. Sci Adv *7*, eabe0143. 10.1126/sciadv.abe0143.

49. Ozcelik, B. (2016). 7 - Degradable hydrogel systems for biomedical applications. In Biosynthetic Polymers for Medical Applications Woodhead Publishing Series in Biomaterials., L. Poole-Warren, P. Martens, and R. Green, eds. (Woodhead Publishing), pp. 173–188. 10.1016/B978-1-78242-105-4.00007-9.

50. Halade, G.V., Jin, Y.-F., and Lindsey, M.L. (2013). Matrix metalloproteinase (MMP)-9: A proximal biomarker for cardiac remodeling and a distal biomarker for inflammation. Pharmacology & Therapeutics *139*, 32–40. 10.1016/j.pharmthera.2013.03.009.

51. Galis, Z.S., Sukhova, G.K., Lark, M.W., and Libby, P. (1994). Increased expression of matrix metalloproteinases and matrix degrading activity in vulnerable regions of human atherosclerotic plaques. J. Clin. Invest. *94*, 2493–2503. 10.1172/JCI117619.

52. Ezhov, M., Safarova, M., Afanasieva, O., Mitroshkin, M., Matchin, Y., and Pokrovsky, S. (2019). Matrix Metalloproteinase 9 as a Predictor of Coronary Atherosclerotic Plaque Instability in Stable Coronary Heart Disease Patients with Elevated Lipoprotein(a) Levels. Biomolecules *9*, 129. 10.3390/biom9040129.

53. Patterson, J., and Hubbell, J.A. (2010). Enhanced proteolytic degradation of molecularly engineered PEG hydrogels in response to MMP-1 and MMP-2. Biomaterials *31*, 7836–7845. 10.1016/j.biomaterials.2010.06.061.

54. Salimath, A.S., Phelps, E.A., Boopathy, A.V., Che, P., Brown, M., García, A.J., and Davis, M.E. (2012). Dual Delivery of Hepatocyte and Vascular Endothelial Growth Factors via a Protease-Degradable Hydrogel Improves Cardiac Function in Rats. PLoS ONE *7*, e50980. 10.1371/journal.pone.0050980.

55. Wanakule, P., Liu, G.W., Fleury, A.T., and Roy, K. (2012). Nano-inside-micro: Disease-responsive microgels with encapsulated nanoparticles for intracellular drug delivery to the deep lung. Journal of Controlled Release *162*, 429–437. 10.1016/j.jconrel.2012.07.026.

56. Mejías, J.C., Forrest, O.A., Margaroli, C., Frey Rubio, D.A., Viera, L., Li, J., Xu, X., Gaggar, A., Tirouvanziam, R., and Roy, K. Neutrophil-targeted, protease-activated pulmonary drug delivery blocks airway and systemic inflammation. JCI Insight *4*. 10.1172/jci.insight.131468.

57. Turk, B.E., Huang, L.L., Piro, E.T., and Cantley, L.C. (2001). Determination of protease cleavage site motifs using mixture-based oriented peptide libraries. Nature Biotechnology *19*, 661. 10.1038/90273.

58. Anselmo, A.C., Zhang, M., Kumar, S., Vogus, D.R., Menegatti, S., Helgeson, M.E., and Mitragotri, S. (2015). Elasticity of Nanoparticles Influences Their Blood Circulation, Phagocytosis, Endocytosis, and Targeting. ACS Nano *9*, 3169–3177. 10.1021/acsnano.5b00147.

59. Merkel, T.J., Chen, K., Jones, S.W., Pandya, A.A., Tian, S., Napier, M.E., Zamboni, W.E., and DeSimone, J.M. (2012). The effect of particle size on the biodistribution of low-

modulus hydrogel PRINT particles. Journal of Controlled Release *162*, 37–44. 10.1016/j.jconrel.2012.06.009.

60. Merkel, T.J., Jones, S.W., Herlihy, K.P., Kersey, F.R., Shields, A.R., Napier, M., Luft, J.C., Wu, H., Zamboni, W.C., Wang, A.Z., et al. (2011). Using mechanobiological mimicry of red blood cells to extend circulation times of hydrogel microparticles. PNAS *108*, 586–591. 10.1073/pnas.1010013108.

61. Zhang, L., Cao, Z., Li, Y., Ella-Menye, J.-R., Bai, T., and Jiang, S. (2012). Softer Zwitterionic Nanogels for Longer Circulation and Lower Splenic Accumulation. ACS Nano *6*, 6681–6686. 10.1021/nn301159a.

62. Pombo García, K., Zarschler, K., Barbaro, L., Barreto, J.A., O'Malley, W., Spiccia, L., Stephan, H., and Graham, B. (2014). Zwitterionic-coated "stealth" nanoparticles for biomedical applications: recent advances in countering biomolecular corona formation and uptake by the mononuclear phagocyte system. Small *10*, 2516–2529. 10.1002/smll.201303540.

63. Hu, C.-M.J., Zhang, L., Aryal, S., Cheung, C., Fang, R.H., and Zhang, L. (2011). Erythrocyte membrane-camouflaged polymeric nanoparticles as a biomimetic delivery platform. Proceedings of the National Academy of Sciences *108*, 10980–10985. 10.1073/pnas.1106634108.

64. Fang, R.H., Kroll, A.V., Gao, W., and Zhang, L. (2018). Cell Membrane Coating Nanotechnology. Adv Mater *30*, e1706759. 10.1002/adma.201706759.

65. Anselmo, A.C., and Mitragotri, S. (2017). Impact of particle elasticity on particle-based drug delivery systems. Advanced Drug Delivery Reviews *108*, 51–67. 10.1016/j.addr.2016.01.007.

66. Yildirim, M., Weiss, A.-V., and Schneider, M. (2023). The Effect of Elasticity of Gelatin Nanoparticles on the Interaction with Macrophages. Pharmaceutics *15*, 199. 10.3390/pharmaceutics15010199.

67. Beningo, K.A., and Wang, Y.-L. (2002). Fc-receptor-mediated phagocytosis is regulated by mechanical properties of the target. Journal of Cell Science *115*, 849–856.

68. Li, M., Jin, X., Liu, T., Fan, F., Gao, F., Chai, S., and Yang, L. (2022). Nanoparticle elasticity affects systemic circulation lifetime by modulating adsorption of apolipoprotein A-I in corona formation. Nat Commun *13*, 4137. 10.1038/s41467-022-31882-4.

69. Tao, J., Shi, W., Chen, K., Lu, W., Elbourne, A.J., Bao, L., Weng, L., Zheng, X., Su, X., Teng, Z., et al. (2023). Elasticity of mesoporous nanocapsules regulates cellular uptake, blood circulation, and intratumoral distribution. Biomater. Sci. *11*, 822–827. 10.1039/D2BM01701F.

70. Müllner, M., Dodds, S.J., Nguyen, T.-H., Senyschyn, D., Porter, C.J.H., Boyd, B.J., and Caruso, F. (2015). Size and Rigidity of Cylindrical Polymer Brushes Dictate Long Circulating Properties In Vivo. ACS Nano *9*, 1294–1304. 10.1021/nn505125f.

71. Key, J., Palange, A.L., Gentile, F., Aryal, S., Stigliano, C., Di Mascolo, D., De Rosa, E., Cho, M., Lee, Y., Singh, J., et al. (2015). Soft Discoidal Polymeric Nanoconstructs Resist Macrophage Uptake and Enhance Vascular Targeting in Tumors. ACS Nano *9*, 11628–11641. 10.1021/acsnano.5b04866.

72. Wu, C.-H., Wang, T.-D., Hsieh, C.-H., Huang, S.-H., Lin, J.-W., Hsu, S.-C., Wu, H.-T., Wu, Y.-M., and Liu, T.-M. (2016). Imaging Cytometry of Human Leukocytes with Third Harmonic Generation Microscopy. Scientific Reports *6*, 37210. 10.1038/srep37210.

73. Kelley, W.J., Fromen, C.A., Lopez-Cazares, G., and Eniola-Adefeso, O. (2018). PEGylation of model drug carriers enhances phagocytosis by primary human neutrophils. Acta Biomaterialia *79*, 283–293. 10.1016/j.actbio.2018.09.001.

74. Safari, H., Kelley, W.J., Saito, E., Kaczorowski, N., Carethers, L., Shea, L.D., and Eniola-Adefeso, O. (2020). Neutrophils preferentially phagocytose elongated particles—An opportunity for selective targeting in acute inflammatory diseases. Science Advances *6*, eaba1474. 10.1126/sciadv.aba1474.

75. Miller, J.S., Shen, C.J., Legant, W.R., Baranski, J.D., Blakely, B.L., and Chen, C.S. (2010). Bioactive Hydrogels Made from Step-Growth Derived PEG-Peptide Macromers. Biomaterials *31*, 3736–3743. 10.1016/j.biomaterials.2010.01.058.

76. Huang, R.B., and Eniola-Adefeso, O. (2012). Shear stress modulation of IL-1β-induced E-selectin expression in human endothelial cells. PLoS One *7*, e31874. 10.1371/journal.pone.0031874.

77. Fromen, C.A., Fish, M.B., Zimmerman, A., Adili, R., Holinstat, M., and Eniola-Adefeso, O. (2016). Evaluation of receptor-ligand mechanisms of dual-targeted particles to an inflamed endothelium. Bioengineering & Translational Medicine *1*, 103–115. 10.1002/btm2.10008.

78. Khan, F., and Tanaka, M. (2017). Designing Smart Biomaterials for Tissue Engineering. Int J Mol Sci *19*, 17. 10.3390/ijms19010017.

79. Lim, F., and Sun, A.M. (1980). Microencapsulated islets as bioartificial endocrine pancreas. Science *210*, 908–910. 10.1126/science.6776628.

80. Khan, F., and Ahmad, S.R. (2013). Polysaccharides and their derivatives for versatile tissue engineering application. Macromol Biosci *13*, 395–421. 10.1002/mabi.201200409.

81. Giovanna Pitarresi, *, Paola Pierro, Fabio S. Palumbo, Giuseppe Tripodo, and, and Giammona, G. (2006). Photo-Cross-Linked Hydrogels with Polysaccharide−Poly(amino acid) Structure: New Biomaterials for Pharmaceutical Applications. ACS Publications. 10.1021/bm050697m.

82. Shi, C., Zhu, Y., Ran, X., Wang, M., Su, Y., and Cheng, T. (2006). Therapeutic potential of chitosan and its derivatives in regenerative medicine. J Surg Res *133*, 185–192. 10.1016/j.jss.2005.12.013.

83. Lee, C.H., Singla, A., and Lee, Y. (2001). Biomedical applications of collagen. Int J Pharm *221*, 1–22. 10.1016/s0378-5173(01)00691-3.

84. Liu, W., Griffith, M., and Li, F. (2008). Alginate microsphere-collagen composite hydrogel for ocular drug delivery and implantation. J Mater Sci Mater Med *19*, 3365–3371. 10.1007/s10856-008-3486-2.

85. Suri, S., and Schmidt, C.E. (2009). Photopatterned collagen–hyaluronic acid interpenetrating polymer network hydrogels. Acta Biomaterialia *5*, 2385–2397. 10.1016/j.actbio.2009.05.004.

86. Gentile, P., Chiono, V., Carmagnola, I., and Hatton, P.V. (2014). An Overview of Poly(lactic-co-glycolic) Acid (PLGA)-Based Biomaterials for Bone Tissue Engineering. Int J Mol Sci *15*, 3640–3659. 10.3390/ijms15033640.

87. Hoffman, A.S. (2002). Hydrogels for biomedical applications. Advanced Drug Delivery Reviews *54*, 3–12. 10.1016/S0169-409X(01)00239-3.

88. Zhu, J. (2010). Bioactive Modification of Poly(ethylene glycol) Hydrogels for Tissue Engineering. Biomaterials *31*, 4639–4656. 10.1016/j.biomaterials.2010.02.044.

89. Lin, L., Zhu, J., Kottke-Marchant, K., and Marchant, R.E. (2014). Biomimetic-Engineered Poly (Ethylene Glycol) Hydrogel for Smooth Muscle Cell Migration. Tissue Eng Part A *20*, 864–873. 10.1089/ten.tea.2013.0050.

90. Beldman, T.J., Senders, M.L., Alaarg, A., Pérez-Medina, C., Tang, J., Zhao, Y., Fay, F., Deichmöller, J., Born, B., Desclos, E., et al. (2017). Hyaluronan Nanoparticles Selectively Target Plaque-Associated Macrophages and Improve Plaque Stability in Atherosclerosis. ACS Nano *11*, 5785–5799. 10.1021/acsnano.7b01385.

91. Hachet, E., Van Den Berghe, H., Bayma, E., Block, M.R., and Auzély-Velty, R. (2012). Design of Biomimetic Cell-Interactive Substrates Using Hyaluronic Acid Hydrogels with Tunable Mechanical Properties. Biomacromolecules *13*, 1818–1827. 10.1021/bm300324m.

92. Lin, C.-C., and Anseth, K.S. (2009). PEG hydrogels for the controlled release of biomolecules in regenerative medicine. Pharm Res *26*, 631–643. 10.1007/s11095-008-9801-2.

93. Csucs, G., Michel, R., Lussi, J.W., Textor, M., and Danuser, G. (2003). Microcontact printing of novel co-polymers in combination with proteins for cell-biological applications. Biomaterials *24*, 1713–1720. 10.1016/S0142-9612(02)00568-9.

94. Weber, L.M., Hayda, K.N., Haskins, K., and Anseth, K.S. (2007). The effects of cell–matrix interactions on encapsulated β-cell function within hydrogels functionalized with matrix-derived adhesive peptides. Biomaterials *28*, 3004–3011. 10.1016/j.biomaterials.2007.03.005.

95. Stenekes, R.J.H., De Smedt, S.C., Demeester, J., Sun, G., Zhang, Z., and Hennink, W.E. (2000). Pore Sizes in Hydrated Dextran Microspheres. Biomacromolecules *1*, 696–703. 10.1021/bm005574a.

96. Northrop, B.H., and Coffey, R.N. (2012). Thiol–Ene Click Chemistry: Computational and Kinetic Analysis of the Influence of Alkene Functionality. J. Am. Chem. Soc. *134*, 13804–13817. 10.1021/ja305441d.

97. Chan, J.W., Hoyle, C.E., Lowe, A.B., and Bowman, M. (2010). Nucleophile-Initiated Thiol-Michael Reactions: Effect of Organocatalyst, Thiol, and Ene. Macromolecules *43*, 6381–6388. 10.1021/ma101069c.

98. Nair, D.P., Podgórski, M., Chatani, S., Gong, T., Xi, W., Fenoli, C.R., and Bowman, C.N. (2014). The Thiol-Michael Addition Click Reaction: A Powerful and Widely Used Tool in Materials Chemistry. Chem. Mater. *26*, 724–744. 10.1021/cm402180t.

99. Yang, F., Williams, C.G., Wang, D.-A., Lee, H., Manson, P.N., and Elisseeff, J. (2005). The effect of incorporating RGD adhesive peptide in polyethylene glycol diacrylate hydrogel on osteogenesis of bone marrow stromal cells. Biomaterials *26*, 5991–5998. 10.1016/j.biomaterials.2005.03.018.

100. Huang, Y., Ma, Y., Gao, P., and Yao, Z. (2017). Targeting CD47: the achievements and concerns of current studies on cancer immunotherapy. J Thorac Dis *9*, E168–E174. 10.21037/jtd.2017.02.30.

101. Kojima, Y., Volkmer, J.-P., McKenna, K., Civelek, M., Lusis, A.J., Miller, C.L., Direnzo, D., Nanda, V., Ye, J., Connolly, A.J., et al. (2016). CD47-blocking antibodies restore phagocytosis and prevent atherosclerosis. Nature *536*, 86.

102. Yi, X., Shi, X., and Gao, H. (2011). Cellular Uptake of Elastic Nanoparticles. Physical Review Letters *107*. 10.1103/PhysRevLett.107.098101.

103. Alexander, J.F., Kozlovskaya, V., Chen, J., Kuncewicz, T., Kharlampieva, E., and Godin, B. (2015). Cubical Shape Enhances the Interaction of Layer-by-Layer Polymeric Particles with Breast Cancer Cells. Advanced Healthcare Materials *4*, 2657–2666. 10.1002/adhm.201500537.

104. Messager, L., Portecop, N., Hachet, E., Lapeyre, V., Pignot-Paintrand, I., Catargi, B., Auzély-Velty, R., and Ravaine, V. (2013). Photochemical crosslinking of hyaluronic acid confined in nanoemulsions: towards nanogels with a controlled structure. J. Mater. Chem. B *1*, 3369–3379. 10.1039/C3TB20300J.

105. Nikjoo, D., van der Zwaan, I., Brülls, M., Tehler, U., and Frenning, G. (2021). Hyaluronic Acid Hydrogels for Controlled Pulmonary Drug Delivery—A Particle Engineering Approach. Pharmaceutics *13*, 1878. 10.3390/pharmaceutics13111878.

106. Seidlits, S.K., Khaing, Z.Z., Petersen, R.R., Nickels, J.D., Vanscoy, J.E., Shear, J.B., and Schmidt, C.E. (2010). The effects of hyaluronic acid hydrogels with tunable mechanical properties on neural progenitor cell differentiation. Biomaterials *31*, 3930–3940. 10.1016/j.biomaterials.2010.01.125.

107. Spearman, B.S., Agrawal, N.K., Rubiano, A., Simmons, C.S., Mobini, S., and Schmidt, C.E. (2020). Tunable methacrylated hyaluronic acid-based hydrogels as scaffolds for soft tissue engineering applications. J Biomed Mater Res A *108*, 279–291. 10.1002/jbm.a.36814.

108. Garantziotis, S., and Savani, R.C. (2019). Hyaluronan biology: A complex balancing act of structure, function, location and context. Matrix Biol *78–79*, 1–10. 10.1016/j.matbio.2019.02.002.

109. Richards, D.M., and Endres, R.G. (2014). The Mechanism of Phagocytosis: Two Stages of Engulfment. Biophys J *107*, 1542–1553. 10.1016/j.bpj.2014.07.070.

110. Herant, M., Heinrich, V., and Dembo, M. (2006). Mechanics of neutrophil phagocytosis: experiments and quantitative models. Journal of Cell Science *119*, 1903–1913. 10.1242/jcs.02876.

111. Hui, Y., Yi, X., Wibowo, D., Yang, G., Middelberg, A.P.J., Gao, H., and Zhao, C.-X. (2020). Nanoparticle elasticity regulates phagocytosis and cancer cell uptake. Sci Adv *6*, eaaz4316. 10.1126/sciadv.aaz4316.

112. Sun, J., Zhang, L., Wang, J., Feng, Q., Liu, D., Yin, Q., Xu, D., Wei, Y., Ding, B., Shi, X., et al. (2015). Tunable Rigidity of (Polymeric Core)–(Lipid Shell) Nanoparticles for Regulated Cellular Uptake. Advanced Materials *27*, 1402–1407. 10.1002/adma.201404788.

113. Tabata, Y., and Ikada, Y. (1988). Effect of the size and surface charge of polymer microspheres on their phagocytosis by macrophage. Biomaterials *9*, 356–362. 10.1016/0142-9612(88)90033-6.

114. Lopez-Cazares, G., and Eniola-Adefeso, O. (2022). Dual Coating of Chitosan and Albumin Negates the Protein Corona-Induced Reduced Vascular Adhesion of Targeted PLGA Microparticles in Human Blood. Pharmaceutics *14*, 1018. 10.3390/pharmaceutics14051018.

115. Cui, M., Liu, R., Deng, Z., Ge, G., Liu, Y., and Xie, L. (2014). Quantitative study of protein coronas on gold nanoparticles with different surface modifications. Nano Res. *7*, 345–352. 10.1007/s12274-013-0400-0.

116. Honary, S., and Zahir, F. (2013). Effect of Zeta Potential on the Properties of Nano-Drug Delivery Systems - A Review (Part 1). Tropical Journal of Pharmaceutical Research *12*, 255–264. 10.4314/tjpr.v12i2.19.

117. Lundqvist, M., Stigler, J., Elia, G., Lynch, I., Cedervall, T., and Dawson, K.A. (2008). Nanoparticle size and surface properties determine the protein corona with possible implications

for biological impacts. Proceedings of the National Academy of Sciences *105*, 14265–14270. 10.1073/pnas.0805135105.

118. Kozel, T.R., and McGaw, T.G. (1979). Opsonization of Cryptococcus neoformans by human immunoglobulin G: role of immunoglobulin G in phagocytosis by macrophages. Infect Immun *25*, 255–261.

119. Papini, E., Tavano, R., and Mancin, F. (2020). Opsonins and Dysopsonins of Nanoparticles: Facts, Concepts, and Methodological Guidelines. Frontiers in Immunology *11*.

120. Champion, J.A., and Mitragotri, S. (2006). Role of target geometry in phagocytosis. Proceedings of the National Academy of Sciences *103*, 4930–4934. 10.1073/pnas.0600997103.

121. Garapaty, A., and Champion, J.A. (2017). Tunable particles alter macrophage uptake based on combinatorial effects of physical properties. Bioeng Transl Med *2*, 92–101. 10.1002/btm2.10047.

122. Arvizo, R.R., Miranda, O.R., Moyano, D.F., Walden, C.A., Giri, K., Bhattacharya, R., Robertson, J.D., Rotello, V.M., Reid, J.M., and Mukherjee, P. (2011). Modulating Pharmacokinetics, Tumor Uptake and Biodistribution by Engineered Nanoparticles. PLoS One *6*, e24374. 10.1371/journal.pone.0024374.

123. Zhong, H., Lin, H., Pang, Q., Zhuang, J., Liu, X., Li, X., Liu, J., and Tang, J. (2021). Macrophage ICAM-1 functions as a regulator of phagocytosis in LPS induced endotoxemia. Inflamm Res *70*, 193–203. 10.1007/s00011-021-01437-2.

124. Magenau, A., Benzing, C., Proschogo, N., Don, A.S., Hejazi, L., Karunakaran, D., Jessup, W., and Gaus, K. (2011). Phagocytosis of IgG-Coated Polystyrene Beads by Macrophages Induces and Requires High Membrane Order. Traffic *12*, 1730–1743. 10.1111/j.1600-0854.2011.01272.x.

125. Beukers, H., Deierkauf, F.A., Blom, C.P., Deierkauf, M., and Riemersma, J.C. (1978). Effects of albumin on the phagocytosis of polysterene spherules by rabbit polymorphonuclear leucocytes. Journal of Cellular Physiology *97*, 29–36. 10.1002/jcp.1040970105.

126. Furumoto, K., Yokoe, J.-I., Ogawara, K., Amano, S., Takaguchi, M., Higaki, K., Kai, T., and Kimura, T. (2007). Effect of coupling of albumin onto surface of PEG liposome on its in vivo disposition. International Journal of Pharmaceutics *329*, 110–116. 10.1016/j.ijpharm.2006.08.026.

127. Peng, Q., Zhang, S., Yang, Q., Zhang, T., Wei, X.-Q., Jiang, L., Zhang, C.-L., Chen, Q.-M., Zhang, Z.-R., and Lin, Y.-F. (2013). Preformed albumin corona, a protective coating for nanoparticles based drug delivery system. Biomaterials *34*, 8521–8530. 10.1016/j.biomaterials.2013.07.102.

128. Sobczynski, D.J., and Eniola-Adefeso, O. (2017). IgA and IgM protein primarily drive plasma corona-induced adhesion reduction of PLGA nanoparticles in human blood flow. Bioeng Transl Med *2*, 180–190. 10.1002/btm2.10064.

129. Karandikar, S., Mirani, A., Waybhase, V., Patravale, V.B., and Patankar, S. (2017). Chapter 10 - Nanovaccines for oral delivery-formulation strategies and challenges. In Nanostructures for Oral Medicine Micro and Nano Technologies., E. Andronescu and A. M. Grumezescu, eds. (Elsevier), pp. 263–293. 10.1016/B978-0-323-47720-8.00011-0.

130. Pednekar, P.P., Godiyal, S.C., Jadhav, K.R., and Kadam, V.J. (2017). Chapter 23 - Mesoporous silica nanoparticles: a promising multifunctional drug delivery system. In Nanostructures for Cancer Therapy Micro and Nano Technologies., A. Ficai and A. M. Grumezescu, eds. (Elsevier), pp. 593–621. 10.1016/B978-0-323-46144-3.00023-4.

131. Safari, H., Kin-Hun Lee, J., and Eniola-Adefeso, O. (2020). Chapter 5 - Effects of shape, rigidity, size, and flow on targeting. In Nanoparticles for Biomedical Applications Micro and Nano Technologies., E. J. Chung, L. Leon, and C. Rinaldi, eds. (Elsevier), pp. 55–66. 10.1016/B978-0-12-816662-8.00005-9.

132. Fish, M.B., Thompson, A.J., Fromen, C.A., and Eniola-Adefeso, O. (2015). Emergence and Utility of Nonspherical Particles in Biomedicine. Ind. Eng. Chem. Res. *54*, 4043–4059. 10.1021/ie504452j.

133. Decuzzi, P., Lee, S., Bhushan, B., and Ferrari, M. (2005). A Theoretical Model for the Margination of Particles within Blood Vessels. Annals of Biomedical Engineering *33*, 179–190. 10.1007/s10439-005-8976-5.

134. Champion, J.A., Katare, Y.K., and Mitragotri, S. (2007). Making polymeric micro- and nanoparticles of complex shapes. Proceedings of the National Academy of Sciences *104*, 11901–11904. 10.1073/pnas.0705326104.

135. Ye, H., Shen, Z., Yu, L., Wei, M., and Li, Y. (2018). Anomalous Vascular Dynamics of Nanoworms within Blood Flow. ACS Biomater. Sci. Eng. *4*, 66–77. 10.1021/acsbiomaterials.7b00434.

136. Thompson, A.J., Mastria, E.M., and Eniola-Adefeso, O. (2013). The margination propensity of ellipsoidal micro/nanoparticles to the endothelium in human blood flow. Biomaterials *34*, 5863–5871. 10.1016/j.biomaterials.2013.04.011.

137. Volpi, M., Paradiso, A., Costantini, M., and Święszkowski, W. (2022). Hydrogel-Based Fiber Biofabrication Techniques for Skeletal Muscle Tissue Engineering. ACS Biomater. Sci. Eng. *8*, 379–405. 10.1021/acsbiomaterials.1c01145.

138. Jana, S., Lan Levengood, S.K., and Zhang, M. (2016). Anisotropic materials for skeletal muscle tissue engineering. Adv Mater *28*, 10588–10612. 10.1002/adma.201600240.

139. Müller-Fischer, N., Tobler, P., Dressler, M., Fischer, P., and Windhab, E.J. (2008). Single bubble deformation and breakup in simple shear flow. Exp Fluids *45*, 917–926. 10.1007/s00348-008-0509-1.

140. Gupta, A., and Sbragaglia, M. (2015). Deformation and break-up of Viscoelastic Droplets Using Lattice Boltzmann Models. Procedia IUTAM *15*, 215–227. 10.1016/j.piutam.2015.04.030.

141. Heslinga, M.J., Mastria, E.M., and Eniola-Adefeso, O. (2009). Fabrication of biodegradable spheroidal microparticles for drug delivery applications. J Control Release *138*, 235–242. 10.1016/j.jconrel.2009.05.020.

142. Yang, S.-C., Tsai, Y.-F., Pan, Y.-L., and Hwang, T.-L. (2021). Understanding the role of neutrophils in acute respiratory distress syndrome. Biomedical Journal *44*, 439–446. 10.1016/j.bj.2020.09.001.

143. Heinrich, V. (2015). Controlled One-on-One Encounters between Immune Cells and Microbes Reveal Mechanisms of Phagocytosis. Biophys J *109*, 469–476. 10.1016/j.bpj.2015.06.042.

144. Herant, M., Heinrich, V., and Dembo, M. (2005). Mechanics of neutrophil phagocytosis: behavior of the cortical tension. Journal of Cell Science *118*, 1789–1797. 10.1242/jcs.02275.

145. Mair, K.H., Sedlak, C., Käser, T., Pasternak, A., Levast, B., Gerner, W., Saalmüller, A., Summerfield, A., Gerdts, V., Wilson, H.L., et al. (2014). The porcine innate immune system: An update. Dev Comp Immunol *45*, 321–343. 10.1016/j.dci.2014.03.022.